PROGRAMA DE PÓS-GRADUAÇÃO EM ENGENHARIA MECÂNICA
CENTRO TECNOLÓGICO
PRÓ-REITORIA DE PESQUISA E PÓS-GRADUAÇÃO
UNIVERSIDADE FEDERAL DO ESPÍRITO SANTO

RUAN SCHULTZ RIGUETTI

DIMENSIONLESS GENERAL TRANSIENT MODELING FOR SMOLDERING COMBUSTION REACTORS

Vitória, ES
2025

PROGRAMA DE PÓS-GRADUAÇÃO EM ENGENHARIA MECÂNICA
CENTRO TECNOLÓGICO
PRÓ-REITORIA DE PESQUISA E PÓS-GRADUAÇÃO
UNIVERSIDADE FEDERAL DO ESPÍRITO SANTO

RUAN SCHULTZ RIGUETTI

DIMENSIONLESS GENERAL TRANSIENT MODELING FOR SMOLDERING COMBUSTION REACTORS

Dissertação apresentada ao Programa de Pós-Graduação em Engenharia Mecânica da Universidade Federal do Espírito Santo, como requisito parcial para obtenção do Grau de Mestre em Engenharia Mecânica.

Orientador: Prof. Dr. Márcio Ferreira Martins.
Coorientador: Prof. Dr. Flávio Lopes Francisco Bittencourt.

Vitória, ES
2025

Ficha catalográfica disponibilizada pelo Sistema Integrado de Bibliotecas - SIBI/UFES e elaborada pelo autor

---

Schultz Riguetti, Ruan, 1999-
S387d Dimensionless general transient modeling for smoldering combustion reactors / Ruan Schultz Riguetti. - 2025.
136 p.

Orientador: Márcio Ferreira Martins.
Coorientador: Flávio Lopes Francisco Bittencourt.
Tese (Mestrado em Engenharia Mecânica) - Universidade Federal do Espírito Santo, Centro Tecnológico.

1. Combustão. 2. Simulação (Computadores). 3. Calor - Transmissão. 4. Termoquímica. 5. Materiais porosos. I. Ferreira Martins, Márcio. II. Lopes Francisco Bittencourt, Flávio. III. Universidade Federal do Espírito Santo. Centro Tecnológico. IV. Título.

CDU: 621

PROGRAMA DE PÓS-GRADUAÇÃO EM ENGENHARIA MECÂNICA
CENTRO TECNOLÓGICO
UNIVERSIDADE FEDERAL DO ESPÍRITO SANTO

MODELAGEM TRANSIENTE GERAL ADIMENSIONAL PARA REATORES DE COMBUSTÃO SMOLDERING

RUAN SCHULTZ RIGUETTI

COMISSÃO EXAMINADORA

_____
Prof. Dr. Márcio Ferreira Martins
(Orientador – PPGEM/UFES)

_____
Prof. Dr. Flávio Lopes Francisco Bittencourt
(Coorientador – IFES)

_____
Prof. Dr. Marcelo Risso Errera
(Examinador Externo – UFPR)

_____
Dr. Marco Aurelio Bazelatto Zanoni
(Examinador Externo – Canadian Nuclear Laboratories)

_____
Dra. Miriam Suely Klippel
(Examinadora Interna – PPGEM/UFES)

Dissertação apresentada ao Programa de Pós-Graduação em Engenharia Mecânica da Universidade Federal do Espírito Santo como parte dos requisitos necessários à obtenção do título de Mestre em Engenharia Mecânica.

Vitória/ES, 28 de novembro de

Datas e horários baseados em Brasília, Brasil
Sincronizado com o NTP.br e Observatório Nacional (ON) em 03/12/2025 às 16:41:57

Folha aprovação - RUAN SCHULTZ RIGUETTI

Data e Hora de Criação: 03/12/2025 às 16:24:06

Documentos que originaram esse envelope:
- Folha aprovação - RUAN SCHULTZ RIGUETTI.pdf (Arquivo PDF) - 1 página(s)

Hashs únicas referente à esse envelope de documentos

[SHA256]: 21b173eeca10c21faf2916606b1ae4469b1076bd1e196c6ed165c4d6a36c9bef
[SHA512]: 925fade62072d6a0b40bf556ceecd5e02959c65f8a290d63b6a95e562a13d2da62112b30556a3dcf1cb3a09d3e022539e8ef8ed220442e68bb09e56ca64d8786

Lista de assinaturas solicitadas e associadas à esse envelope

ASSINADO - Flávio Lopes Francisco Bittencourt (flavio.lopes@ifes.edu.br)
Data/Hora: 03/12/2025 - 16:30:27, IP: 200.137.83.3, Geolocalização: [-20.8375, -40.7271]
[SHA256]: 770a279c80a9b6ff440a107bf5286cc8115002d22f153b74a67f9b00f679a768
Assinatura Eletrônica Avançada (Conforme Lei nº 14.063/20, art. 4º, II)

ASSINADO - Márcio Ferreira Martins (marcio.martins@ufes.br)
Data/Hora: 03/12/2025 - 16:33:52, IP: 200.137.65.104
[SHA256]: e29e6cc1068b66d329acac1da0a7fa1976988963c1cedbe5c8a5f31ff20159d0
Assinatura Eletrônica Avançada (Conforme Lei nº 14.063/20, art. 4º, II)

ASSINADO - Marco Aurelio Bazelatto Zanoni (marco.bazelattozanoni@cnl.ca)
Data/Hora: 03/12/2025 - 16:38:18, IP: 206.47.148.202
[SHA256]: 7bb7b1abd70dfc3944352774a07a8f01d37fca27d9e1c5408c4148598fe0e63c
Assinatura Eletrônica Avançada (Conforme Lei nº 14.063/20, art. 4º, II)

ASSINADO - Marcelo Risso Errera (merrera@gmail.com)
Data/Hora: 03/12/2025 - 16:26:45, IP: 177.220.182.178, Geolocalização: [-25.465972, -49.225563]
[SHA256]: 9eac6e3cb434a7408698c656e9b5f9fd9bc371dfa13e9a02c2c379577d09829e
Assinatura Eletrônica Avançada (Conforme Lei nº 14.063/20, art. 4º, II)

ASSINADO - Miriam Suely Klippel (miriam.klippel@edu.ufes.br)
Data/Hora: 03/12/2025 - 16:41:57, IP: 200.137.67.20
[SHA256]: 0db810ea4537754e60a57a03d24a48a42ac9d7e07b95c8533b1526bb73450533
Assinatura Eletrônica Avançada (Conforme Lei nº 14.063/20, art. 4º, II)

Histórico de eventos registrados neste envelope

03/12/2025 16:41:57 - Envelope finalizado por miriam.klippel@edu.ufes.br, IP 200.137.67.20
03/12/2025 16:41:57 - Assinatura realizada por miriam.klippel@edu.ufes.br, IP 200.137.67.20
03/12/2025 16:38:18 - Assinatura realizada por marco.bazelattozanoni@cnl.ca, IP 206.47.148.202
03/12/2025 16:33:52 - Assinatura realizada por marcio.martins@ufes.br, IP 200.137.65.104
03/12/2025 16:30:27 - Assinatura realizada por flavio.lopes@ifes.edu.br, IP 200.137.83.3
03/12/2025 16:30:22 - Envelope visualizado por flavio.lopes@ifes.edu.br, IP 200.137.83.3
03/12/2025 16:26:45 - Assinatura realizada por merrera@gmail.com, IP 177.220.182.178
03/12/2025 16:26:42 - Envelope visualizado por merrera@gmail.com, IP 177.220.182.178
03/12/2025 16:25:30 - Envelope registrado na Blockchain por andreia.eyng@ufes.br, IP 200.137.65.106
03/12/2025 16:25:30 - Envelope encaminhado para assinaturas por andreia.eyng@ufes.br, IP 200.137.65.106
03/12/2025 16:24:06 - Envelope criado por andreia.eyng@ufes.br, IP 200.137.65.106

Abstract

Smoldering combustion is a slow, flameless process that occurs at relatively low temperatures and reaction rates, typically under limited oxygen conditions. Beyond its scientific interest, this process offers environmental, technological, and social benefits, which make it relevant for both industrial applications and sustainable development. In this context, the present research develops and applies a general dimensionless numerical model for smoldering combustion reactors, aiming to simulate the phenomenon on a small scale. The approach relies on a 2D axisymmetric model implemented in COMSOL Multiphysics (v5.4) using the Local Thermal Non-Equilibrium (LTNE) consideration, which allows separate treatment of the solid and fluid phases. Conservation equations for mass, momentum, energy, and species transport were implemented in a dimensionless form and enable a comprehensive and generalized analysis of the physical and chemical processes involved. Novel dimensional and dimensionless groups emerged during the non-dimensionalization process, associated with the effects of particle-bed burning and the interstitial chemical kinetic dynamics. Classical numbers such as Prandtl, Grashof, Darcy, Schmidt, and Peclet numbers also appeared. The model proposed in the methodology was validated through three case studies. The first involved combustion at the fluid–porous interface, highlighting the influence of natural convection. In this case, the model reproduced the same recirculation patterns reported in the reference study and also allowed

investigation of how the velocity profile was distorted by these recirculations. The second case addressed the cooling of a porous bed and was used to calibrate convective heat transfer under transient conditions. The results showed that the model is capable of simulating studies without a reactive porous bed, although a maximum discrepancy of 25% was observed in the temperature profiles when comparing the simulations with the experimental data. The third case consisted of a full simulation of smoldering combustion, which included the ignition process through a heat source, propagation of the combustion front, and coupled interactions between heat and mass. This case allows analysis of solid fuel consumption over time and comparison of temperature profiles with experimental data obtained at different axial positions of the reactor. In general, the results demonstrate that the model created is capable of capturing the main behaviors with good agreement compared to the experimental data and the results from the literature. Therefore, the proposed methodology provides a reliable model that allows one to understand smoldering dynamics.

Keywords: combustion; dimensionless; 2D axisymmetric model; temperature profiles; smoldering dynamics.

Author's Declaration

The contributions of others are clearly stated in my dissertation.

Márcio Ferreira Martins: initiated the research topic, provided guidance on methodology development and numerical simulations, assisted in the development of dimensionless analysis with the mathematical equations governing the physics present in the model, contributed with the implementation in COMSOL Multiphysics, assisted in data interpretation.

Flávio Lopes Francisco Bittencourt: Assisted in the development of the dimensionless analysis with the mathematical equations governing the physics present in the model, and provided data from previous numerical simulations that contributed to comparison between the results obtained.

Gabriel Gusmão Almeida: provided guidance on the numerical simulation structure and contributed to the implementation in COMSOL Multiphysics.

Tarek L. Rashwan: provided guidance on the numerical simulation structure and assisted in the development of the dimensionless analysis with the mathematical equations governing the physics present in the model.

During the Master's degree period (2023–2025), the author participated in various academic, technical, and scientific activities. The main activities included attending mandatory and elective courses in the pos graduated program, participating in scientific events and submitting and publishing articles. Among the main technical and scientific contributions during the course, the following stand out:

- Participation and presentation in a workshop on smoldering combustion called NanoSymp, held on April 3, 2024. The event was organized by MMLABS at UFES and featured renowned authors in the smoldering combustion field, such as Tarek Rashwan and Marco Zanoni.

- Publication of the article "A Two-Dimensional Modeling of a Permeable Fluid–Porous Interface in COMSOL Multiphysics" for the 20th Brazilian Congress of Thermal Sciences and Engineering (ENCIT), in November 2024, as described in Appendix A1.

- Participation in a technical-scientific visit to The Open University, in Milton Keynes, England, from 30 April to 9 May, 2025, to meet and collaborate with the team of students led by Professor Dr. Tarek Rashwan, discussing the parameters that govern smoldering combustion, the optimization the computational simulation model developed by MM LABS (UFES), as well as to foster future partnerships and support the production of scientific articles, as described in Appendix A3.

- Publication of the work "Calibration of a Numerical Model for Cooling Simulation in a Porous Bed" to the 28th International Congress of Mechanical Engineering (COBEM), in November 2025, as described in Appendix A2.

- Development of the computational model described in this dissertation, focusing on the transient and dimensionless simulation of smoldering combustion in porous beds.

These activities contributed significantly to the consolidation of the author's academic and scientific training, as reflected in the results presented in this work.

Acknowledgments

It was an impressive period of about two years of development and learning. On 8 February, 2023, my best friend and a great researcher joined me on a car trip to the Federal University of Espírito Santo in Goiabeiras, Vitória–ES, to take the entrance test for the Master's degree in Mechanical Engineering. Since we lived in São Mateus–ES, we faced an exhausting 450-kilometer round trip on the same day. A few days later, the results were released, and it was confirmed that both, my friend and I, had been accepted into the program. After that, we took this long trip countless times, always happy and confident that we were doing what we loved and that our future was taking shape in academic life. That day, I met my advisor, Prof. Márcio Ferreira Martins, who administered the exam to all the candidates. Months later, we developed friendship and mutual trust. I am grateful for his guidance and for sharing his knowledge. I would also like to commend his humanity in understanding the different contexts in which his students are immersed, as well as his energy to collaborate with them regardless of the day of the week or the time of day. That is striking!

I would like to thank God for giving me the strength to face the challenges of the course, guidance in the trips from São Mateus to Vitória, and for opening my mind during the development of my dissertation. I am grateful to my parents, Elaine and Advaldo, who have been my constant support every week. To my fiancée, Daniela, I thank you for your wise advice and for all your patience during my less joyful moments, always striving to make each

day happier. To my best friend, Gabriel, thank you for all your support and assistance during the mathematical modeling of the equations used in my numerical simulation. Your shared knowledge of fluid mechanics was very important to my development. I thank the Federal University of Espírito Santo (UFES). I'm very proud to have coursed my Master's degree at such a respected institution. I am also grateful to the Federal Institute of Espírito Santo (IFES), where I studied for almost nine years (2014-2022), including four years in the Mining Technician program and almost five years in the undergraduate program in Mechanical Engineering. This institution was my second home throughout that time, where I made many friends and met outstanding professors who remain my friends to this day.

I thank my co-advisor, Prof. Dr Flávio Lopes Francisco Bittencourt, whom I had the privilege of knowing and being mentored by during this time. I am grateful for sharing his knowledge in the area of smoldering combustion. I thank the team MMLABS, especially André, Míriam, Bruno Lourenço, Cleyton, Bruno Gobi, João Victor, Marciellyo, Julio, Eron, Mateus, Eduardo, Alexandre, João Freitas and Prof Ramon, for the companionship during the routine in the laboratory. I thank SENAI (National Industrial Learning Service) and Multivix College, where I worked during my Master's degree. These institutions allowed me to develop my teaching skills and grow into a better professor.

Table of Contents

List of Tables

List of Figures

Nomenclature

Latin letter

$\dot{R}_f^{oxi}$	Fluid generation reaction rate
$\dot{R}_s$	General reaction rate
$\dot{R}_s^{oxi}$	Solid consumption reaction rate
A_s	Pre-exponential factor
Arr	Arrhenius number
b	Stoichiometric coefficient
Be	Bejan number
Bi	Biot number
c_p	Specific heat
D	Mass diffusivity
d	Diameter
Da_f	Darcy number

Da_s Damköhler number

E_f Activation energy for fluid phase

E_s Activation energy for solid phase

g Gravity

GF Dimensionless geometric factor

Gr Grashof number

H Enthalpy

h Height

K Intrinsic permeability

L Reactor's length

m Mass

m^*_{part} Particle mass fraction

Nu Nusselt number

P Power

p Pressure

Pe Peclet number

Pr Prandtl number

Q Heat Storage

q Radiation heat source

R Ideal gas constant

r Radial coordinates

Sc Schmidt number

T Temperature

t Time

u, U Velocity

u_z^* Dimensionless longitudinal velocity of fluid

Y Mass fraction

z Longitudinal coordinates

$\dot{v}_f$ Variation rate specific volume of the fluid phase

Greek symbols

α Thermal diffusivity

β Thermal expansion coefficient

Γ Convection heat transfer coefficient

λ Thermal conductivity

μ Dynamic viscosity

ν Kinematic viscosity

ρ Specific mass

σ Stefan-Boltzmann constant

τ Time scale

ε Surface emissivity

φ Porosity

Subscripts/superscripts

0 Initial

∞ Referrer to the ambient

* Dimensionless variable

abs Absolute

ext Refer an external parameter

f Fluid

fr Front propagation

h hot

i Index variable for solid phase

ig Ignition

in Inlet

int Refer an interstitial parameter

k	Index variable for fluid phase
m	Porous medium
$o2$	Referrer to the oxygen
out	Outlet
oxi	Oxidation
p	Porous bed
$part$	Particle
r	Radial direction
rad	Radiation
s	Solid
sg	Between solid and fluid phase
stg	Storage
w	Wall
$w1$	Wall in the fluid domain
$w2$	Wall in the solid domain
z	Longitudinal direction

Chapter 1

Introduction

1.1 Smoldering Combustion

Smoldering combustion is a process characterized by low temperatures and low reaction rates that occur without visible flames. Its difference from flaming combustion can be observed in Figure 1.1 [1].

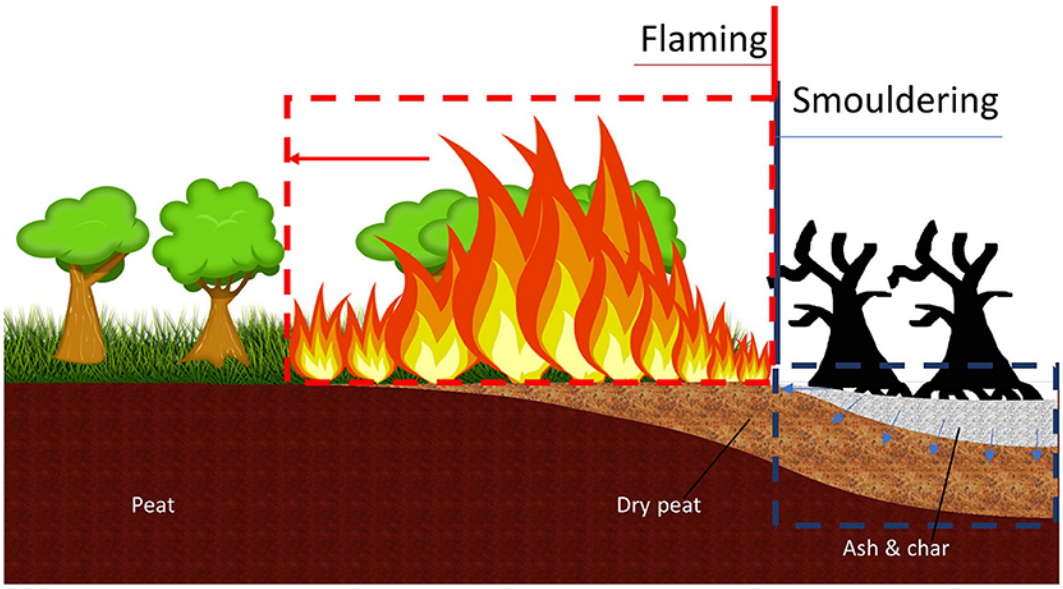

Figure 1.1: Difference between flaming and smoldering combustion and their residues. Developed by Santoso (2019).

The main difference between flaming and smoldering combustion is that the flaming occurs in the gas phase, with high temperatures and rapid propagation, while smoldering is a heterogeneous combustion in the solid phase, slow and with low heat release. In wildfires, flaming typically occurs in the initial phase and smoldering in the final phase, when less volatile fuels remain. In the environment scenario, smoldering combustion is the predominant combustion phenomenon in megafires that occur in natural deposits of peat and coal [2]. In addition, smoldering combustion is one of the primary causes of residential fires and is associated with significant safety concerns in industrial facilities. Although it may be undesirable in certain scenarios, such as forest fires, this mechanism can be used effectively in heating systems. This process offers high efficiency in converting the energy stored in the fuel into thermal energy while producing relatively low emissions [3], compared to other forms of combustion.

There are many examples of applied smoldering in the desired way. In some industrial processes, smoldering combustion can be used to generate heat, an example is in situ combustion, this process works with a local controlled burn of petroleum inside the reservatory to reduce viscosity and consequently to increase API gravity, facilities the recovery of crude oil [4]. Another example is the recovery of oil sludge-contaminated soil (OSS) [5, 6], after all, smoldering combustion is a new approach to organic waste treatment in which organic waste is efficiently destroyed with minimal energy input. For this case application, the influence of four key parameters was observed: the moisture content of the oil sludge, the filling ratio, the grain

size, and the airflow rate on the smoldering [7]. In addition to contributions to environmental causes, the smoldering combustion process can be used to achieve a relevant social impact. Recently, it was shown that this process can be applied as an energy efficient destruction technique for human feces [3] and a continuous device was created to perform pyrolysis in this type of material using smoldering combustion. This proposal can be utilized to address the sanitation challenges in some countries.

An important concept related to the phenomena of smoldering combustion is pyrolysis. When a coal particle or any type of material is placed inside a hot environment, without oxygen, it passes through a process called pyrolysis. This process leads to the release of combustion gases and a solid carbon-rich material, called 'char' [8]. This endothermic process converts materials into valuable products such as biochar, oil, and gas. This phenomenon helps to create new sources of energy, making it an important technology for sustainable waste management. To work effectively, pyrolysis needs a steady and controlled heat supply, which can be achieved through smoldering combustion. Smoldering combustion operates with low chemical reactions and does not need a continuous fuel supply, making it a controllable and efficient way to execute pyrolysis.

Considering the physics involved in smoldering combustion or other processes that occur during burn materials, it is important to mention that the characteristics of these combustion are governed by a complex interaction of chemical phenomena that occur close at the level of the particle scale. Within this type of context, there exist devolatilization, phase changes, and

heterogeneous chemical reactions, which are responsible for controlling crucial functionalities, from ignition behavior up to complete combustion of the material [9]. Devolatilization is the thermal decomposition of a fuel particle by heating, which releases volatile gases, and represents the initial phase of thermal conversion and is especially influenced by factors such as the heating rate, final temperature, and particle size [9]. After the devolatilization process, the char undergoes heterogeneous chemical reactions that appear in this type of system as slower processes, occurring throughout the entire combustion time of the particle. To understand the transition between the different combustion regimes, it is necessary to model the burn rate and the total fuel conversion time with precision [8, 9].

Following these concepts, the processes of phase change and mass transport are also present in smoldering combustion systems, especially in combustion with moisture. For example, the drying process is frequently controlled by heat transport through an evaporation front, where liquid water is converted to steam. This steam diffuses through the porous medium to colder areas and can condense, releasing latent heat and influencing the internal temperature profile of the particle [8]. The diffusion of mass is not restricted only to water vapor, for example, the gases generated in pyrolysis or devolatization and the oxidation products of char also move through the porous structure by diffusion and convection. The interaction between volatile gases and the diffusion of oxidants at the particle surface determines whether ignition occurs in the gaseous phase, called homogeneous, or on the char surface, in this case named heterogeneous [10]. Therefore, it is evident that the smoldering combustion

process has the highest complexity, the number of physical and chemical processes in smoldering is larger and demanded a thorough analysis of scales and parameters. The application of smoldering simulations should understand in detail the process to optimize operational conditions, for example, since fuel can be trapped inside the pores of the material, directly affecting the spread of combustion [2].

Although many studies investigate small scale smoldering combustion using experiments and numerical models, most of them are limited to specific fixed geometries and simplify assumptions. In addition, the transient characteristics of smoldering, where heat and mass transfer interact with heterogeneous reactions and porous contraction, are frequently simplified, reducing the accuracy of the simulations. For this reason, it is necessary to have a generalized and dimensionless transient modeling that can represent the fundamentals of smoldering combustion and be applied to different reactor configurations and operational conditions. Developing new studies in this area and proposing a new standard of modeling is crucial to simulate with more accuracy smoldering combustion phenomena.

1.2 General objective

Develop a general dimensionless transient model for axisymmetric smoldering combustion reactors.

1.2.1 Specific objectives

- Create a new dimensionless analysis of smoldering combustion in an LTNE domain, based on the important physical existence in this phenomenon;
- Test and validate three case studies using real experimental parameters from the literature;
- Show that the model is capable of simulating both inert and reactive porous beds;
- Demonstrate that the model can simulate different axisymmetric geometries;
- Visualize that the model can operate with different air-supply configurations for smoldering combustion.

1.3 Dissertation structure

The dissertation structure is divided into chapters responsible for addressing the following subjects: the introduction presents the theme, providing context for the subjects and the objectives of the research; the state of the art section reviews what the main authors in the literature state about the smoldering combustion area and the most relevant improvements observed in recent years; the methodology describes the main dimensionless equations considered in the model and details each simulated case study; the results section discusses the main parameters and dimensionless terms obtained

from the nondimensionalization process, as well as the behaviors and results obtained for each numerical simulation; finally, the Appendix includes two papers developed and published in important international congresses, along with the description of a technical visit at the England conducted during the master's degree.

References

1. Santoso, M. A., Christensen, E. G., Yang, J. & Rein, G. Review of the transition from smouldering to flaming combustion in wildfires. *Frontiers in Mechanical Engineering* **5,** 49 (2019).
2. Torero, J. L. *et al.* Processes defining smouldering combustion: Integrated review and synthesis. *Progress in Energy and Combustion Science* **81,** 100869 (2020).
3. Bittencourt, F. L. F. *TOWARD A SAFE AND CIRCULAR THERMOCHEMICAL PROCESS TO SANITIZE HUMAN FECES IN RESOURCE-POOR ENVIRONMENTS* PhD thesis (Universidade Federal do Espírito Santo, 2023).
4. Castanier, L. & Brigham, W. Upgrading of crude oil via in situ combustion. *Journal of Petroleum Science and Engineering* **39,** 125–136. ISSN: 0920-4105. https://www.sciencedirect.com/science/article/pii/S0920410503000445 (2003).
5. Gan, Z. *et al.* Method of smoldering combustion for the treatment of oil sludge-contaminated soil. *Waste Management* **175,** 73–82. ISSN: 0956-053X. https://www.sciencedirect.com/science/article/pii/S0956053X23007845 (2024).
6. Zhao, C., Li, Y., Gan, Z. & Nie, M. Method of smoldering combustion for refinery oil sludge treatment. *Journal of Hazardous Materials* **409,** 124995. ISSN: 0304-3894. https://www.sciencedirect.com/science/article/pii/S0304389420329861 (2021).
7. Gan, Z. *et al.* Experimental investigation on smoldering combustion for oil sludge treatment: Influence of key parameters and product analysis. *Fuel* **316,** 123354. ISSN: 0016-2361. https://www.sciencedirect.com/science/article/pii/S001623612200223X (2022).

8. He, F. & Behrendt, F. A new method for simulating the combustion of a large biomass particle—A combination of a volume reaction model and front reaction approximation. *Combustion and flame* **158,** 2500–2511 (2011).

9. Annamalai, K. & Ryan, W. Interactive processes in gasification and combustion—II. Isolated carbon, coal and porous char particles. *Progress in energy and combustion science* **19,** 383–446 (1993).

10. Anca-Couce, A., Zobel, N., Berger, A. & Behrendt, F. Smouldering of pine wood: Kinetics and reaction heats. *Combustion and flame* **159,** 1708–1719 (2012).

Chapter 2

State of Art

2.1 Numerical simulations challenges

Elaborating numerical simulations allows for a better interpretation of phenomena and enables comparisons with experimental results, as well as the exploration of different conditions and scenarios. Some studies attempt to reproduce smoldering combustion experimentally on a small scale through devices named smoldering reactors. In general, smoldering combustion reactors can vary in geometry, ignition source, burning direction, and propagation modes [1]. Consequently, even a slight change in the way air is supplied to the system can have a significant impact on the entire combustion process [2]. Within this context of small-scale experiments in the scientific field of smoldering simulations, several studies focus on forward smoldering, where air is injected in the same direction as the propagating reaction, while other authors investigate feeding the reaction with airflow in the opposite direction to the propagation. In numerical studies that address these aspects is visualized also porous contraction, which occurs when the process is simulated by accounting

for a permeable fluid–porous interface that decreases in size over time. As expected in this situation, several distinct behaviors are observed: the solid phase undergoes mass and volume loss, chemical reactions release heat and mass into the fluid flow, resulting in gas transport, heat transfer through the porous domain, and the generation of new chemical species in the gas phase [3].

In a smoldering combustion process, it is acknowledged that modeling results depend on assumptions about heat transfer processes and chemical reactions. When used in simulations, the physics of these two subareas require careful interpretation [4]. For example, the work proposed by Huang et al (2015) presented a computational 1D model to investigate smoldering combustion of natural fuels with emphasis on the roles of moisture and inert contents, and simulated the driving phenomenon of wildfires in peatlands. This approach made it possible to understand the influences of kinetic parameters, physical properties, and ignition protocol on this type of phenomenon [5]. To achieve this, several mathematical equations were applied, including mass, energy, and momentum conservation, as well as chemical balance equations related to char oxidation, heterogeneous chemical processes, and the Arrhenius equation. This demonstrates the complexity involved in simulating this type of phenomenon.

Yet in the mathematical context of the smoldering phenomena, several authors have contributed to the development of computational approaches that advance the understanding of smoldering processes. For example, Bittencourt and Martins (2022) conceptualized a cylindrical smoldering reactor

filled with a reactive porous material. In this configuration, airflow is induced to enter the reactor due to a pressure gradient as the combustion front propagates downward [6]. The temperature difference between the combustion front and the stream also initiates buoyancy forces that oppose downward airflow. These physical characteristics were modeled in a 2D numerical analysis with steady-state equations in a dimensionless structure, highlighting the complexity of capturing such coupled mechanisms. To better illustrate this information, Fig. 2.1 presents a vacuum-induced reactor proposed by the author, which typically uses smoldering to perform pyrolysis on specific materials with a forward burning direction [7]. In this device, a pump located at the bottom draws air to sustain combustion. The reactor was also open at the top, which increases natural convection and causes recirculation. While the effects of recirculation are minor with small contractions, as the combustion front begins to widen and the porous bed contraction increases, natural convection also increases and starts to compress the airflow boundary layer against the combustion chamber walls, this last behavior also proves in the work proposed by Riguetti et al (2024) [8]. This process reduces the progress of the combustion front and gradually extinguishes it. When this condition occurs, the front of the propagation and contraction of the porous bed stop. This type of behavior was also identified by [9].

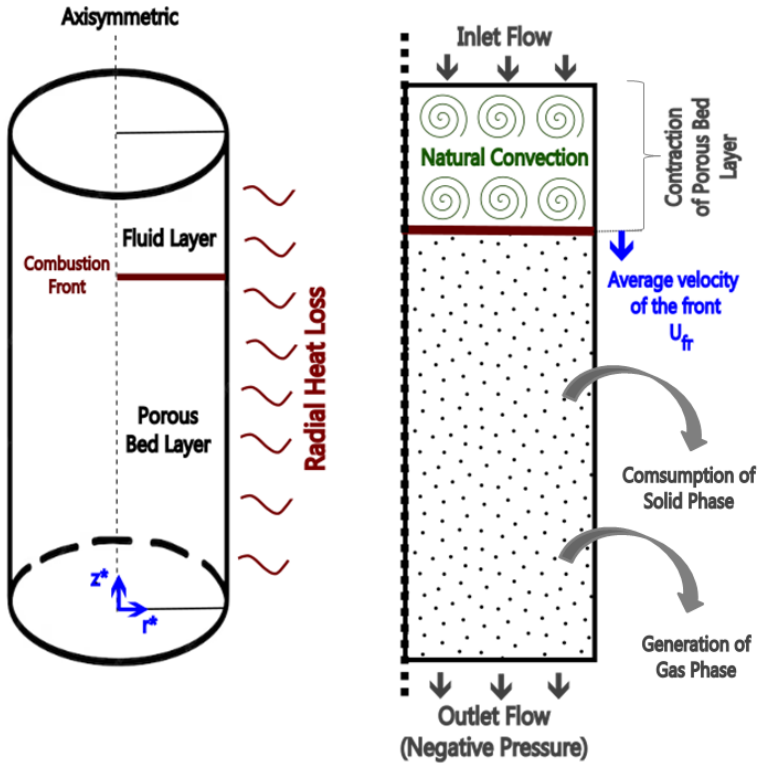

Figure 2.1: General physical behavior of porous interface in smoldering combustion. Developed by the authors.

To simulate this type of vacuum-induced smoldering reactor, several mathematical equations must be modeled. Beyond the equations of mass, energy, and momentum conservation, it is also necessary to capture the phenomenon of recirculation, which can be achieved through adaptations in the momentum conservation equations. Due to the high temperatures, the boundary conditions of heat loss in the upper, lateral, and lower regions should also be considered. Furthermore, the inclusion of transient conditions can provide more detailed insights, since the simulation proposed by this author revealed the recirculation phenomenon at a specific time and at a certain level of porous

bed contraction. Capturing this type of behavior in a time-dependent simulation makes it possible to visualize new processes that depend on the physical interactions represented in the model, promoting greater realism in the results.

Following this line of reasoning, the author Zanoni et al (2020) conducted smoldering column experiments under self-sustaining conditions, with the aim of gradually extinguishing combustion by reducing air flux and fuel concentration [10]. To simulate the experiments, a previously developed 1D numerical model validated for robust smoldering was used. The simulations showed that the model was adequate for robust conditions but failed in scenarios with weak self-sustaining combustion, revealing the limitations of simplified approaches in marginal cases. This numerical model incorporated a general set of physical parameters, which can provide greater flexibility to test specific conditions, but also can introduce challenges. Because smoldering combustion depends on multiple parameters such as kinetics, heat, flow, and mass, this big quantitative of parameters can lead to convergence problems and make it difficult to identify which factor is responsible for errors. Therefore, it is necessary to be careful in this type of system modeling, because the use of many dependent parameters requires attention to ensure correct detail in the implementation inside of numerical software, and the numerical simulations need to present correct results so that the modeling is reliable.

Another relevant aspect in numerical simulations of smoldering to ensure correct results is the consideration of heat transfer mechanisms in porous domains, which can be approached through LTE (Local Thermal Equilibrium) or LTNE (Local Thermal Non-Equilibrium) formulations [11]. While the

first assumes a unique temperature for the solid and gas phases, the latter considers them at different temperatures. When LTNE is implemented, the model becomes more reliable and better represents reality. In this sense, [12] presented a comparison between the LTE and LTNE approaches, showing that in some time steps the difference between the two could reach 100°C. This result clearly demonstrates the importance of the assumptions chosen in numerical simulations and how they can significantly affect the results.

This highlights that accurately capturing the complex behavior of smoldering requires careful consideration of both physical phenomena and numerical assumptions. Continuing comments about considerations in the numerical smoldering area, for instance, the author Zanoni et al (2022) observed that temperatures close to the reactor center followed the advancement of the combustion front, a key physical characteristic in smoldering reactors. The study also showed that oxygen consumption was higher in the center, corresponding to more intense chemical reactions [13]. The authors proposed a permeability heterogeneity analysis, concluding that regions with higher permeability exhibited faster combustion fronts and higher peak temperatures. Based on this numerical model, a new correlation for the interstitial heat transfer coefficient was implemented [12, 14], and, to better simulate reality, a heating process until ignition conditions was included. As a result, it was concluded that increasing airflow strengthens self-sustained combustion by enhancing the oxidation rate. All of these implementations proposed by the authors can help new researchers as a starting point for mathematical equations and additional processes necessary to simulate this type of combustion.

More recently, multidimensional simulations have been explored. Yuan (2023) presented a 2D case study to simulate the lateral and vertical smoldering spread [15]. The model predicted the effects of peat conditions on smoldering propagation and shows how the mechanisms controlling these two propagation modes are validated using a shallow-reactor experiment previously reported in the literature. Similarly, Hansan (2015) detailed the development and validation of a computational model that simulates the spread of a smoldering front through a porous medium. Two-dimensional smoldering propagation experiments were conducted in a steel box, and after calibration to a baseline experiment, the model accurately predicted the outcomes of subsequent tests [16]. These works show that, although such models introduce more complexity and require greater computational power, the possibility of simulating multiple physical directions facilitates the visualization of behaviors occurring inside the porous bed, which could only be captured experimentally with extensive setups, raising the cost of such experimental processes.

Finally, Cheung (2023) [17], who investigated the transport and hazards of CO from smoldering fires in the context of building design, emphasized the importance of accurate input data and model calibration. This work reproduced two full-scale smoldering fire experiments from the late 1970s to calibrate the model settings, shows that the reliability of numerical simulations depends not only on the equations implemented but also on the quality of experimental understanding and precision data collection. This emphasizes

that the choice of initial conditions, boundary conditions, and values of physical parameters can be crucial for the numerical convergence and reliability of the results obtained. Perceptual errors and discrepancies observed between numerical simulations and experimental results in reality may often be caused by wrongly chosen parameters.

Taken together, the works cited previously demonstrate how numerical simulations of smoldering combustion have progressively evolved from simplified one-dimensional approaches to multidimensional, time-dependent, and more physically detailed models. They also reveal how modeling choices such as LTE versus LTNE assumptions, permeability distribution, heat transfer correlations and boundary conditions play a decisive role in capturing the dynamics of smoldering.

2.2 Classical dimensionless scales

As previously mentioned in Section 1, several distinct physical behaviors are observed in smoldering combustion. To optimize numerical analyzes, dimensionless equations can be applied to these problems, enabling the reduction of complex interactions into representative dimensionless groups. Several studies have explored the role of classical scales in interpreting the governing mechanisms of smoldering. The dimensionless numbers most significant for smoldering combustion are presented in Figure 2.2.

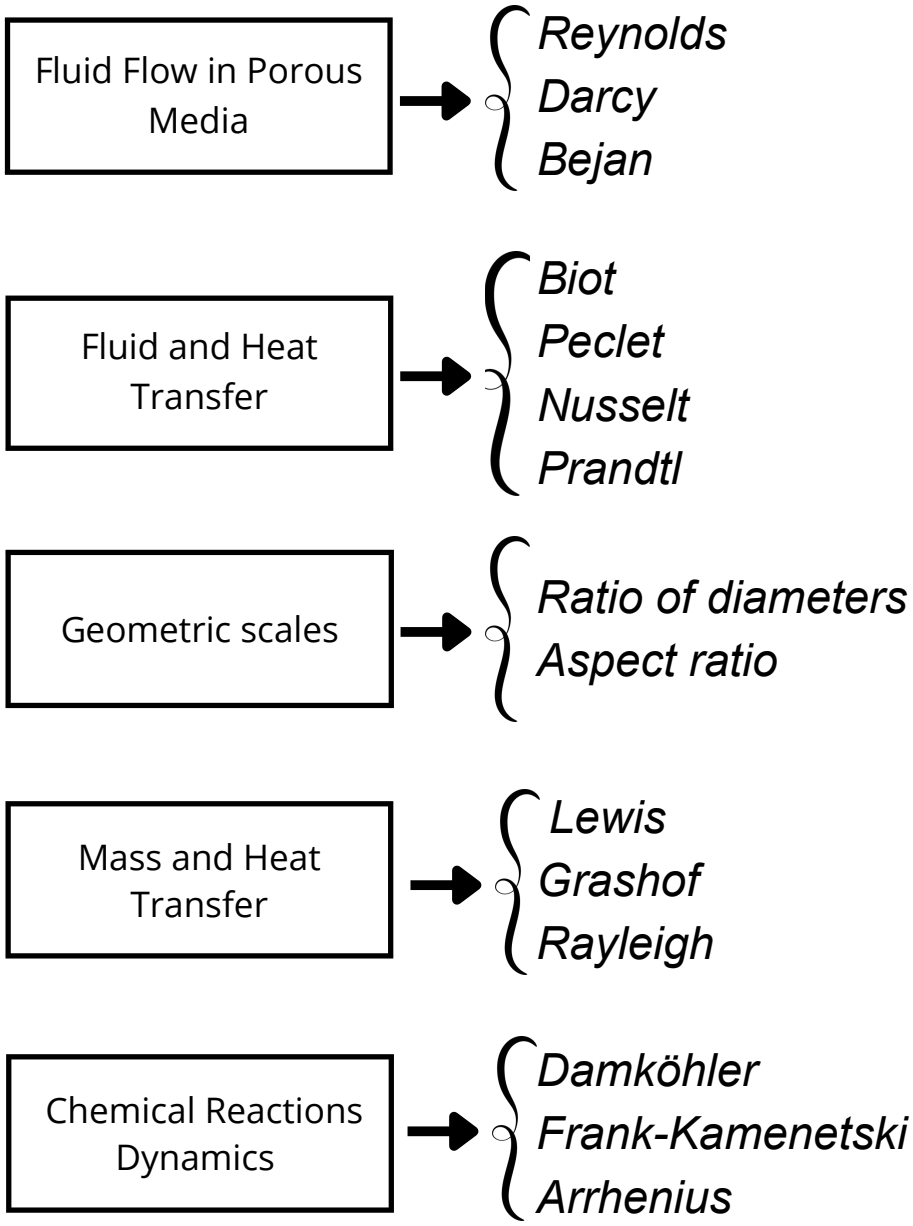

Figure 2.2: Classical dimensionless numbers in smoldering combustion, divided into five important subgroups. Developed by the authors.

The first group of relevant numbers is associated with fluid flow in porous media. The most common is the Reynolds number, which accounts for both

fluid and porous bed material characteristics. Parameters such as the average flow velocity through the cross-sectional area and porosity directly influence its value [18]. Flow resistance within the porous matrix is quantified by the Darcy number, which expresses the relation between viscous and inertial effects. This number is directly linked to air supply, one of the main drivers of smoldering propagation. Jang (19992) and Tong (1986) showed that the Nusselt number is sensitive to permeability and reaches a minimum value at specific porous layer thicknesses according to the varying Darcy number [19] [20]. More recently, Shruti (2023) assessed the combined impact of Darcy and Rayleigh numbers on natural convection [21], showing that with the increase of cylinder reactor size, both Darcy, Rayleigh numbers and heat transfer rates increase, where doubling the diameter of the cylinder enhances heat transport by 41.5 percent. In forced flow conditions, specific scales may be more suitable, such as the Reynolds number when the flux velocity is imposed in the experiment [22], or the Bejan number when pressure differences are the driving force of fluid flow [23–25].

When flow and heat transfer are considered together, the Nusselt number becomes very important. This dimensionless number reveals how thermal energy is transferred from a surface to the surrounding fluid, bridging flow dynamics and your thermal properties [2, 26]. It is related to the convective heat transfer coefficient and depends on correlations involving Reynolds and Prandtl numbers. For smoldering systems, Wakao (1982) proposed a valid correlation for Reynolds between 15 and 8000 [27], while Pallares (2010) [28] modified the correlation of Fujio (2001) [29] to better fit the experimental

results. This shows the evolution of research in convective heat transfer applied to smoldering systems. In these correlations, the Prandtl number also plays a key role, as fluids with large values behave very differently from those with small values [30]. Other scales help describe the balance of conduction and convection. The Biot number indicates whether internal conduction or surface convection dominates, influencing the temperature profiles in solids and fluids [31, 32]. The Peclet number evaluates the relative importance of advection and diffusion and can be combined with other dimensionless groups to describe complex transport behaviors in multiphase porous systems, as mentioned by [33].

Dimensionless geometric scale relations are also widely used. One of them is the ratio of diameters, which influences permeability and flow resistance, where larger pores relative to particles favor higher permeability and lower resistance [2, 26]. This ratio also affects regime transitions, where higher values often result in non-Darcian flows described by the Forchheimer equation [18]. Another example is the aspect ratio of the reactor, given by the relation between height and diameter. In smoldering reactors, this parameter determines important dynamic characteristics, since low aspect ratios modify the distribution of experimental duration time and high aspect ratios enhance vertical mixing, favoring internal convective movements that better distribute mass and energy between different regions of the reactor. Time itself can also be expressed as dimensionless, and studies have applied Dimensionless Time to scale behaviors under different experimental conditions, supporting predictions and making them independent of bed size or absolute duration of

the experiment [12, 34].

Mass and heat transfer coupling is often expressed through the Lewis and Schmidt numbers. The Lewis number measures the balance between heat and mass transfer, while the Schmidt number expresses the ratio between diffusion and viscosity. Since Lewis can be written as Schmidt over Prandtl [35], their combined interpretation becomes important and is frequently applied in dimensionless analyzes of smoldering systems. Experimental studies confirm the importance of these numbers in porous combustion [36, 37]. Buoyancy-driven processes are usually represented by the Grashof number, which quantifies the ratio of buoyancy to viscous forces. Together with the Prandtl number, it can be applied to estimate heat transfer coefficients even under vacuum conditions [38]. The Rayleigh number, defined as the product of Grashof and Prandtl, has long been used in smoldering analyzes. Poulikakos (1986) studied its role in natural convection in coupled fluid-porous systems for Rayleigh values ranging from 10^2 to 10^6 [39], which are values usually above the critical value needed for the onset of convection. The study shows how the domain affects the behavior of recirculations through simple alterations of the porous–fluid interface model to a unic fluid.

Finally, the dynamics of chemical reactions can also be described by dimensionless groups. The Damköhler number compares characteristic times of chemical kinetics with those of mass transport, showing under which conditions reactions dominate or are limited by diffusion [2, 31]. Leach (1998) demonstrated its effect on extinguishing reactions in porous media [40]. The Frank-Kamenetskii number is associated with ignition and thermal stability,

as it indicates when heat release exceeds conduction, potentially leading to instabilities in numerical simulations [2, 31]. Applications of this number include the burning of coal dust layers [40] and is often combined with Darcy and Arrhenius numbers to provide a better interpretation [41]. The Arrhenius number itself captures the exponential dependence of reaction rates on temperature [2, 42] and can be extended to free convection problems [43].

Understanding the classical behaviors expected in smoldering combustion systems is crucial to the development of more reliable numerical simulations that capture the main quantitative phenomena and physical behaviors observed in this type of combustion. Due to the complexity, new comparative frameworks that connect different reactor scales, operating conditions, and physical assumptions are necessary to better understanding the smoldering. These new knowledge scales help clarify how chemical, mass, momentum, and heat behaviors interact in this complex phenomenon. Eventually, the relative importance of each term in a dimensionless equation is indicated by the magnitude of the related dimensionless group [44], which allows researchers to control and evaluate physical aspects indirectly by varying these parameters.

References

1. Duque, J. F. *A novel pathway to recover hydrocarbons from polyethylene residues through the combustion-driven pyrolysis process* PhD thesis (Universidade Federal do Espírito Santo (Vitória, Brasil), 2021).
2. Torero José L., e. a. Processes defining smouldering combustion: Integrated review and synthesis. *Progress in Energy and Combustion Science* **81,** 100869 (2020).
3. Ferreira Martins, M. *Structure d'un front de combustion propagé en co-courant dans un lit fixe de schiste bitumineux broyé* PhD thesis (Diss. Toulouse, 2008).
4. Zanoni, M. A., Torero, J. L. & Gerhard, J. I. Delineating and explaining the limits of self-sustained smouldering combustion. *Combustion and Flame* **201,** 78–92. ISSN: 0010-2180. https://www.sciencedirect.com/science/article/pii/S0010218018305212 (2019).
5. Huang, X., Rein, G. & Chen, H. Computational smoldering combustion: Predicting the roles of moisture and inert contents in peat wildfires. *Proceedings of the Combustion Institute* **35,** 2673–2681. ISSN: 1540-7489. https://www.sciencedirect.com/science/article/pii/S1540748914000510 (2015).
6. Bittencourt Flávio Lopes Francisco, G. D. & Martins., M. F. Free convection development caused by bed shrinkage in a vacuum-induced smoldering reactor. *Chemical Engineering Journal* **430,** 132847 (2022).
7. Bittencourt, F. L. F. *TOWARD A SAFE AND CIRCULAR THERMOCHEMICAL PROCESS TO SANITIZE HUMAN FECES IN RESOURCE-POOR ENVIRONMENTS* PhD thesis (Universidade Federal do Espírito Santo, 2023).

8. Riguetti, R. S., Almeida, G. G., Xavier, A. V., Martins, M. F. & Bittencourt, F. L. F. A Two-Dimensional Modeling of a Permeable Fluid-Porous Interface in COMSOL Multiphysics. *Proceedings of the 20th Brazilian Congress of Thermal Sciences and Engineering (ENCIT 2024)* (2024).
9. Torero, J. & Fernandez-Pello, A. Forward smolder of polyurethane foam in a forced air flow. *Combustion and Flame* **106,** 89–109. ISSN: 0010-2180 (1996).
10. Zanoni, M. A., Torero, J. L. & Gerhard, J. I. Experimental and numerical investigation of weak, self-sustained conditions in engineered smouldering combustion. *Combustion and Flame* **222,** 27–35. ISSN: 0010-2180. https://www.sciencedirect.com/science/article/pii/S0010218020303357 (2020).
11. Nield, D. A., Bejan, A., *et al. Convection in porous media* (Springer, 2006).
12. Zanoni, M. A., Torero, J. L. & Gerhard, J. I. The role of local thermal non-equilibrium in modelling smouldering combustion of organic liquids. *Proceedings of the Combustion Institute* **37,** 3109–3117. ISSN: 1540-7489. https://www.sciencedirect.com/science/article/pii/S1540748918301834 (2019).
13. Miry, S. Z., Zanoni, M. A., Rashwan, T. L., Torero, J. L. & Gerhard, J. I. Investigation of multi-dimensional transfer effects in applied smouldering systems: A 2D numerical modelling approach. *Combustion and Flame* **246,** 112385. ISSN: 0010-2180. https://www.sciencedirect.com/science/article/pii/S001021802200400X (2022).
14. Zanoni, M. A., Torero, J. L. & Gerhard, J. I. Determination of the interfacial heat transfer coefficient between forced air and sand at Reynold's numbers relevant to smouldering combustion. *International Journal of Heat and Mass Transfer* **114,** 90–104. ISSN: 0017-9310. https://www.sciencedirect.com/science/article/pii/S0017931017311985 (2017).
15. Yuan, H., Purnomo, D. M., Sun, P., Huang, X. & Rein, G. Computational study of the multidimensional spread of smouldering combustion at different peat conditions. *Fuel* **345,** 128064. ISSN: 0016-2361. https://www.sciencedirect.com/science/article/pii/S0016236123006774 (2023).
16. Hasan, T., Gerhard, J. I., Hadden, R. & Rein, G. Self-sustaining smouldering combustion of coal tar for the remediation of contaminated sand: Two-dimensional experiments and computational simulations. *Fuel* **150,**

288–297. ISSN: 0016-2361. https://www.sciencedirect.com/science/article/pii/S0016236115001556 (2015).

17. Cheung, W. K., Zeng, Y., Lin, S. & Huang, X. Modelling carbon monoxide transport and hazard from smouldering for building fire safety design analysis. *Fire Safety Journal* **140,** 103895. ISSN: 0379-7112. https://www.sciencedirect.com/science/article/pii/S0379711223001637 (2023).
18. Nield, D. A., Bejan, A., *et al. Convection in porous media* (Springer, 2006).
19. Jang, J. & Chen, J. Forced convection in a parallel plate channel partially filled with a high porosity medium. *International Communications in Heat and Mass Transfer* **19,** 263–273. ISSN: 0735-1933. https://www.sciencedirect.com/science/article/pii/073519339290037I (1992).
20. Tong, T. & Subramanian, E. Natural convection in rectangular enclosures partially filled with a porous medium. *International Journal of Heat and Fluid Flow* **7,** 3–10. ISSN: 0142-727X. https://www.sciencedirect.com/science/article/pii/0142727X86900330 (1986).
21. Shruti, B., Alam, M. M., Parkash, A. & Dhinakaran, S. Darcy number influence on natural convection around porous cylinders in an enclosure using Darcy- Brinkman-Forchheimer model: LBM study. *Case Studies in Thermal Engineering* **45,** 102907. ISSN: 2214-157X. https://www.sciencedirect.com/science/article/pii/S2214157X23002137 (2023).
22. Chakkingal, M. *et al.* Assisting and opposing mixed convection with conjugate heat transfer in a differentially heated cavity filled with coarse-grained porous media. *International Communications in Heat and Mass Transfer* **111,** 104457. ISSN: 0735-1933. https://www.sciencedirect.com/science/article/pii/S0735193319303239 (2020).
23. Zimparov, V. D., Angelov, M. S. & Hristov, J. Y. Critical review of the definitions of the Bejan number - first law of thermodynamics. *International Communications in Heat and Mass Transfer* **124,** 105113. ISSN: 0735-1933. https://www.sciencedirect.com/science/article/pii/S0735193321000075 (2021).
24. Bejan, A. *Convection Heat Transfer* ISBN: 9781118330081. https://books.google.com.br/books?id=9yC91-gpU8sC (Wiley, 2013).
25. Zimparov, V. D., Angelov, M. S. & Hristov, J. Y. New insight into the definitions of the Bejan number. *International Communications in Heat and Mass Transfer* **116,** 104637. ISSN: 0735-1933. https://www.sciencedirect.com/science/article/pii/S0735193320301652 (2020).

26. Kaviany, M. *Principles of convective heat transfer* (Springer Science, 2001).

27. Wakao S. Kaguei, N. Heat and Mass Transfer in Packed Beds. *Gordon and Breach Science Publishers*, 292–294. ISSN: 0017-9310. https://aiche.onlinelibrary.wiley.com/doi/abs/10.1002/aic.690010211 (1982).

28. Pallares, J. & Grau, F. A modification of a Nusselt number correlation for forced convection in porous media. *International Communications in Heat and Mass Transfer* **37,** 1187–1190. ISSN: 0735-1933. https://www.sciencedirect.com/science/article/pii/S0735193310001788 (2010).

29. Kuwahara, F., Shirota, M. & Nakayama, A. A numerical study of interfacial convective heat transfer coefficient in two-energy equation model for convection in porous media. *International Journal of Heat and Mass Transfer* **44,** 1153–1159. ISSN: 0017-9310. https://www.sciencedirect.com/science/article/pii/S0017931000001666 (2001).

30. Chen, S., Li, W. & Mohammed, H. I. Heat transfer of large Prandtl number fluids in porous media by a new lattice Boltzmann model. *International Communications in Heat and Mass Transfer* **122,** 105129. ISSN: 0735-1933. https://www.sciencedirect.com/science/article/pii/S0735193321000233 (2021).

31. Pyle, D. & Zaror, C. Heat transfer and kinetics in the low temperature pyrolysis of solids. *Chemical Engineering Science* **39,** 147–158. ISSN: 0009-2509. https://www.sciencedirect.com/science/article/pii/0009250984801402 (1984).

32. Parhizi, M., Torabi, M. & Jain, A. Local thermal non-equilibrium (LTNE) model for developed flow in porous media with spatially-varying Biot number. *International Journal of Heat and Mass Transfer* **164,** 120538. ISSN: 0017-9310. https://www.sciencedirect.com/science/article/pii/S0017931020334748 (2021).

33. GK, B. *An Introduction to Fluid Dynamics* (Cambridge University Press, England, 2000).

34. Zanoni, M. A., Torero, J. L. & Gerhard, J. I. Determining the conditions that lead to self-sustained smouldering combustion by means of numerical modelling. *Proceedings of the Combustion Institute* **37,** 4043–4051. ISSN: 1540-7489. https://www.sciencedirect.com/science/article/pii/S1540748918305261 (2019).

35. Rapp, B. E. in *Microfluidics: Modelling, Mechanics and Mathematics* (ed Rapp, B. E.) 243–263 (Elsevier, Oxford, 2017). ISBN: 978-1-4557-3141-1. https://www.sciencedirect.com/science/article/pii/B9781455731411500095.

36. Uchida, Y., Kuwana, K. & Kushida, G. Experimental validation of Lewis number and convection effects on the smoldering combustion of a thin solid in a narrow space. *Combustion and Flame* **162,** 1957–1963. ISSN: 0010-2180. https://www.sciencedirect.com/science/article/pii/S0010218014004179 (2015).

37. Kuwana, K., Suzuki, K., Tada, Y. & Kushida, G. Effective Lewis number of smoldering spread over a thin solid in a narrow channel. *Proceedings of the Combustion Institute* **36,** 3203–3210. ISSN: 1540-7489. https://www.sciencedirect.com/science/article/pii/S1540748916302176 (2017).

38. Yamazaki, T., Matsuoka, T. & Nakamura, Y. Near-extinction behavior of smoldering combustion under highly vacuumed environment. *Proceedings of the Combustion Institute* **37,** 4083–4090. ISSN: 1540-7489. https://www.sciencedirect.com/science/article/pii/S1540748918303869 (2019).

39. Poulikakos, D., Bejan, A., Selimos, B. & Blake, K. High Rayleigh number convection in a fluid overlaying a porous bed. *International Journal of Heat and Fluid Flow* **7,** 109–116. ISSN: 0142-727X. https://www.sciencedirect.com/science/article/pii/0142727X86900561 (1986).

40. Leach, S., Ellzey, J. & Ezekoye, O. Convection, pyrolysis, and Damköhler number effects on extinction of reverse smoldering combustion. *Symposium (International) on Combustion* **27,** 2873–2880. ISSN: 0082-0784. https://www.sciencedirect.com/science/article/pii/S008207849880146X (1998).

41. Frank-Kamenetskii, D. A. *Diffusion and heat exchange in chemical kinetics* (Princeton University Press, 2015).

42. Paola Russo Armando De Rosa, M. M. Silo explosion from smoldering combustion: A case study. *The Canadian Journal of Chemical Engineering* **95,** 1721–1729. https://onlinelibrary.wiley.com/doi/10.1002/9781119975465.ch8 (2017).

43. Huang, C.-J. Arrhenius activation energy effect on free convection about a permeable horizontal cylinder in porous media. *Transport in porous media* **128,** 723–740 (2019).

44. Ohlemiller, T. Modeling of smoldering combustion propagation. *Progress in Energy and Combustion Science* **11,** 277–310. ISSN: 0360-1285. https://www.sciencedirect.com/science/article/pii/0360128585900048 (1985).

Chapter 3

Methodology

3.1 Modeling

A 2D axisymmetric numerical model was developed using COMSOL Multiphysics (version 5.4) to simulate a cylindrical reactor with a length L and a radius r. The geometry of the reactor is represented in dimensionless coordinates (r^*, z^*) as illustrated in Fig. 3.1. It is important to note that other axisymmetric geometries can also be simulated, such as conical and spherical shapes. The model incorporates different ways of regulating the airflow inside the reactor. Airflow can be driven by a pressure gradient, with zero pressure at the top (inlet) and negative pressure at the bottom (outlet), simulating a vacuum-induced smoldering reactor. Alternatively, airflow can be worked by forcing air at the inlet, maintaining zero pressure at the bottom. The model developed can simulate either a reactive porous bed or an inert porous bed.

For a reactive porous bed, the ignition can be started at the top, because that is, the combustion front propagates downward, causing the height of the porous layer to decrease over time and creating a fluid domain in the upper

zone of the reactor. The temperature difference between the combustion front and the incoming cold airflow generates buoyancy forces that oppose the downward flow of air entering the reactor. Fig. 3.1 shows the boundary conditions for the two possible domains that can be created due to porous contraction (fluid and porous domains), as well as the constant boundary conditions with the external environment. In addition, most of the dimensional and dimensionless parameters are presented for each domain, which are responsible for governing the main physical behaviors within them.

The displacement of the smoldering front causes the consumption of solid mass and gas generating. All equations related to the phenomena considered and used in the model are presented in a dimensionless form in Section 3.3. In this case, a two-dimensional axisymmetric approach was employed, along with dimensionless parameters for the spatial coordinates (r^*, z^*), time (t^*), velocity field (u_r^*, u_z^*), pressure (p^*), temperature (T_s^*, T_f^*), specific mass (ρ_f^*) and mass fractions for each phase (Y_s^*, Y_f^*). Other assumptions can be considered: a two-temperature model for the porous bed, one for the gas phase and one for the solid phase (LTNE); the chemical reactions considered represent an oxidation process; a homogeneous porous bed with porosity and permeability constant in time and space.

3.2 Dimensionless group

In light of the significant relevance of smoldering combustion within the scientific community, a general mathematical model utilizing dimensionless parameters has been developed primarily for this phenomenon. Although

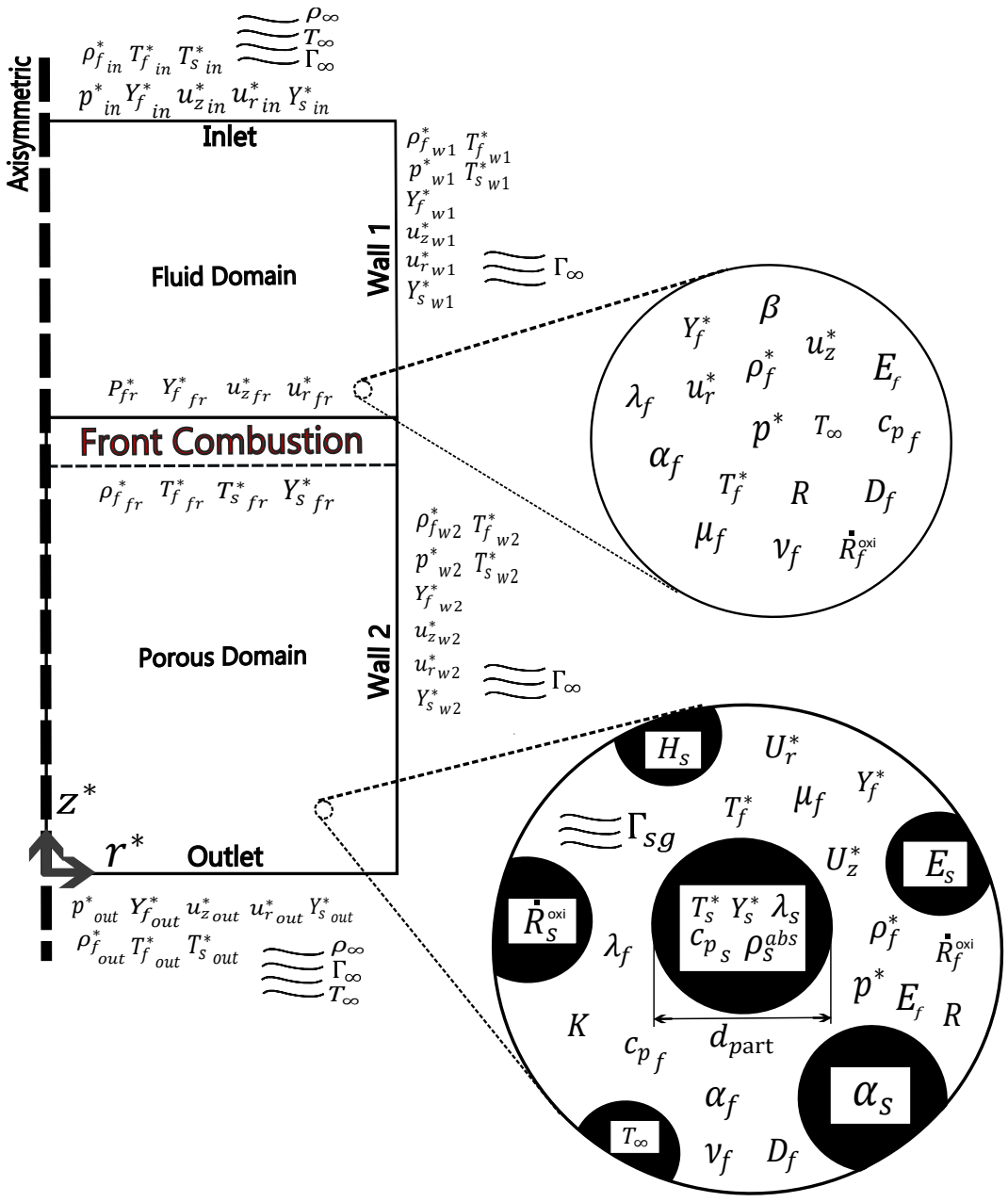

Figure 3.1: Boundary conditions and crucial parameters involved in the general modeling. Developed by the authors.

other simplified processes can be simulate, such as the cooling of the porous bed in the axisymmetric reactor, this will be presented in Section 3.4.2. In what follows, the dimensionless groups proposed in this study are presented, along with the considerations made according to the characteristic scales of smoldering reactors. Figure 3.1 provides a visual representation of the physical phenomena that can influence the system, highlighting the large number of variables involved in this type of analysis. Therefore, adopting a dimensionless approach offers advantages in managing the complexity of the problem and allows to explore important physical parameters.

To address the effects of porous bed contraction, a dimensionless time (Eq. 3.3) based on the total mass change over time (Δm) was proposed. This parameter is associated with the reduction in bed height over time. Moreover, even in cases without combustion or significant temperature gradients, processes involving only heat transfer may still show mass variations due to evaporation, condensation, and diffusion. This supports the idea discussed earlier because the chosen dimensionless time parameter can also be applied to simplified processes in axisymmetric reactors. The longitudinal flow velocity (u_z) is also related to this phenomenon and was incorporated into the dimensionless time parameter, as the flow velocity within the porous bed plays a key role in oxygen supply, solid mass consumption, and directly influences the reaction rate and experiment duration. Airflow is also important in processes without combustion, as it affects convective heat transfer, promotes mass transport, and contributes to phase changes. These aspects reinforce the relevance of including flow velocity in the dimensionless-time formulation, making the

framework applicable to a wider range of thermal and physical processes beyond smoldering combustion.

$$r^* = \frac{r}{d_{part}} \tag{3.1}$$

$$z^* = \frac{z}{d_{part}} \tag{3.2}$$

$$t^* = \frac{t\rho_s^{abs} u_z d_{part}^2}{\Delta m} \tag{3.3}$$

Radial and longitudinal velocities within the reactor are expressed by Eqs. 3.4 – 3.5. The lowercase parameter u refers to the Darcy velocity (average flow velocity), while the uppercase variable U represents the interstitial velocity (Eqs. 3.6 – 3.7). The latter was determined using the Dupuit–Forchheimer relation [1], given by: $u = U\varphi$.

$$u_r^* = \frac{u_r d_{part}}{\nu_f} \tag{3.4}$$

$$u_z^* = \frac{u_z d_{part}}{\nu_f} \tag{3.5}$$

$$U_r^* = \frac{u_r d_{part}}{\varphi \nu_f} \tag{3.6}$$

$$U_z^* = \frac{u_z d_{part}}{\varphi \nu_f} \tag{3.7}$$

A local thermal non-equilibrium (LTNE) can be considered in the model. As the porous bed burns over time, the solid and fluid phase temperatures depend on parameters associated with the chemical reactions. Consequently, the activation energy of the solid material (E_s) and fluid phase (E_f), and the ideal gas constant (R) were combined to define the dimensionless temperature employed in the model (Eqs. 3.8 - 3.9). This correlation aims to capture the influence of the combustion heat release on the modeled temperature field. When combustion is not involved, the dimensionless temperature can be simplified by disregarding the parameters related to chemical reactions (Eqs. 3.10 - 3.11). Then, without smoldering combustion involved in the case, the dimensionless equations presented in Section 3.3 will appear without the Arrhenius number, the source terms related to chemical reactions, and the source terms for the production or consumption of gases and solid materials.

$$T_f^* = \frac{\left(T_f - T_\infty\right) E_f}{R T_\infty^2} \tag{3.8}$$

$$T_s^* = \frac{\left(T_s - T_\infty\right) E_s}{R T_\infty^2} \tag{3.9}$$

$$T_f^* = \frac{\left(T_f - T_\infty\right)}{T_\infty} \tag{3.10}$$

$$T_s^* = \frac{\left(T_s - T_\infty\right)}{T_\infty} \tag{3.11}$$

The dimensionless pressure was defined based on the Bejan number, which quantifies frictional pressure losses in flows through porous media [2]. In this study, the pressure drop was evaluated over a characteristic length taken as the particle diameter of the porous bed (d_{part}), as shown in Eq. 3.12. The fluid phase density was normalized by the ambient density, as described in Eq. 3.13.

$$p^* = \frac{p d_{part}^2}{\mu_f \nu_f} \tag{3.12}$$

$$\rho_f^* = \frac{\rho_f}{\rho_\infty} \tag{3.13}$$

3.3 Dimensionless equations

Detailed considerations that following concepts showed chapter 1, chapter 2 and the initial sections of methodology regarding the mathematical modeling are presented below. Within an interstitial zone characterized by a reactive porous bed layer, oxidation of the solid phase leads to the generation of combustion gases depending on the reaction rate ($\dot{R}_f^{oxi}$). Similarly, the mass fraction of the solid phase reduces over time in accordance with the reaction rates of the associated chemical processes.

It is evident that in almost all the equations of the proposed model, the dimensionless longitudinal velocity (u_z^*) appears in transient terms. This reflects its direct role in the supply of oxygen necessary for smoldering combustion. The Particle Mass Fraction (m_{part}^*) also appears frequently, as it governs how

mass, momentum, and energy evolve over time, depending on the quantitative consumption of solid particles. The last parameter illustrates how the remaining solid mass influences, for example, the specific mass over time. The mass conservation for the fluid phase is expressed as in Eq. 3.14, following Miry et al [3].

$$\varphi m^*_{part} u^*_z \frac{\partial \rho^*_f}{\partial t^*} + \left(\rho^*_f . \nabla\right) \mathbf{u}^* = \dot{v}_f \dot{R}^{oxi}_f \tag{3.14}$$

The solid material remains almost stationary throughout the entire combustion process. Therefore, in the species transport equation for the solid domain (Eq. 3.15), the advective term is not considered. The source term associated with the Damköhler number (Da_s) appears in the equation and represents the intensity of the solid to fluid conversion through a chemical reaction relative to the gas flow velocity through the bed.

$$\frac{\partial Y^*_s}{\partial t^*} = -Da_s \tag{3.15}$$

The porous medium is assumed to be homogeneous, and the effective diffusivity of the gas mixture is assumed to be constant in both time and space. Since the gas phase percolates through the interstices of the porous medium, the species transport equation for the fluid phase structurally includes transient, advective, and diffusive terms (Eq.: 3.16). The Schmidt number appears in the diffusive term, following its classical meaning as defined in the literature.

$$m^*_{part} u^*_z \frac{\partial \left[\rho^*_f Y^*_f\right]}{\partial t^*} + \left[\left(\rho^*_f Y^*_f\right).\nabla\right]\mathbf{u}^* = Sc\left[\nabla^2\left(\rho^*_f Y^*_f\right)\right] + \dot{v}_f \dot{R}^{oxi}_f \tag{3.16}$$

To ensure the 'dynamic coupling' between pressures and velocities of the airflow, a mathematical model consisting of two momentum equations was developed: one for the fluid domain (Eq. 3.17) and the other for the porous domain (Eq. 3.18), (Brinkman equation, an extension of Darcy's law). Since the proposed model addresses a reactor that is geometrically open at the top, natural convection effects occur and are accounted for as a source term in Eq. 3.17. Natural convection effects are expressed through the Grashof number, and the influence of chemical reactions on natural convection is captured via the Arrhenius number, which appears together with it in the source term in Eq. 3.17. This represents the influence of the fluid phase temperature on the buoyancy forces, since the Arrhenius number is related to the dimensionless temperature of the fluid phase, according to Eq. 3.8.

$$m^*_{part} u^*_z \frac{\partial \mathbf{u}^*}{\partial t^*} + \left(\mathbf{u}^*.\nabla\right)\mathbf{u}^* = -\nabla \mathbf{p}^* + \nabla^2 \mathbf{u}^* + \frac{Gr}{Arr}\left(T^*_f\right) \tag{3.17}$$

$$m^*_{part} u^*_z \frac{\partial \mathbf{U}^*}{\partial t^*} + \left[\left(\mathbf{U}^*.\nabla\right)\mathbf{U}^*\right] = -\nabla \mathbf{p}^* + \nabla^2 \mathbf{U}^* - \frac{1}{Da_f}\mathbf{u}^* \tag{3.18}$$

The specific mass and mass fraction of the fluid phase exhibit temporal and spatial variations. The behavior of the specific mass can be represented by the expression based on Equation 3.19, following the properties for the atmosphere air presented by [4, 5].

$$\rho_f^* = -3 \cdot 10^{-7} \cdot {T_f^*}^3 + 0.0001 \cdot {T_f^*}^2 - 0.0152 \cdot T_f^* + 1 \tag{3.19}$$

The energy equation for the fluid domain, in the upper zone of the reactor, is expressed as: Eq. 3.20. The Prandtl number appears in the diffusive term, following its classical meaning as defined in the literature.

$$m_{part}^* u_z^* \frac{\partial T_f^*}{\partial t^*} + \left[\left(\mathbf{u}^* . \nabla \right) T_f^* \right] = \frac{1}{Pr} \left(\nabla^2 T_f^* \right) \tag{3.20}$$

Inside the porous bed layer the Local Thermal Non-Equilibrium (LTNE) model is applied, with separate equations governing the fluid (Eq.: 3.21) and solid (Eq.: 3.22) phases. Chemical reactions occurring at the interstitial scale are primarily responsible for heating both the solid and fluid phases. Regardless of temperature, all physical bodies emit radiation. However, in close proximity to the combustion zone, radiation heat transfer predominantly occurs from the solid phase to the gas phase. Below the combustion zone, where the fluid flow is hotter than the solid phase, radiation heat transfer is primarily directed in the opposite direction. Due to fluid percolation through the porous medium, convective heat transfer also occurs. The direction of this convective heat transfer mirrors the behavior of radiation heat transfer. In Equation 3.22, different of the other equations before, the Thermal Peclet number (Pe) appears in the transient term because the airflow velocity influences the heat extraction from the solid phase. The intensity of this effect is directly related to the amount of heat accumulated in the solid phase over time.

$$\varphi m^*_{part} u^*_z \frac{\partial T^*_f}{\partial t^*} + \left[\left(\mathbf{U}^* . \nabla \right) T^*_f \right] = \varphi \frac{1}{Pr} \left(\nabla^2 T^*_f \right) + \tau_f \frac{Arr_f}{Q^{stg}_f} \dot{R}^{oxi}_f H_f$$
$$+ \frac{Nu_{int}}{Pr} GF \left(T^*_s - T^*_f \right) + \tau_f Arr_f \frac{P^{rad}_s}{Q^{stg}_f} \left[\left(\frac{T^*_s}{Arr_f} + 1 \right)^4 - \left(\frac{T^*_f}{Arr_f} + 1 \right)^4 \right] \tag{3.21}$$

$$\left(1 - \varphi \right) m^*_{part} Pe \frac{\partial T^*_s}{\partial t^*} = \left(1 - \varphi \right) \left(\nabla^2 T^*_s \right) + \tau_s \frac{Arr_s}{Q^{stg}_f} \dot{R}^{oxi}_s H_s$$
$$- Bi_{int} GF \left(T^*_s - T^*_f \right) - \tau_s Arr_s \frac{P^{rad}_s}{Q^{stg}_f} \left[\left(\frac{T^*_s}{Arr_s} + 1 \right)^4 - \left(\frac{T^*_f}{Arr_s} + 1 \right)^4 \right] \tag{3.22}$$

The interstitial heat transfer coefficient (Γ_{sg}) between phases is based on an empirical Nusselt correlation (Nu_{int}) as a function of Reynolds (Re) and Prandtl (Pr) numbers (Eq. 3.23) [6], and can be calculated using Eq. 3.24. The Reynolds number can be related to a dimensionless number proposed in this work, referred to as the dimensionless longitudinal velocity of the fluid phase (u^*_z) (Eq. 3.5).

$$Nu_{int} = 2 \left(1 + \frac{4 \left(1 - \varphi \right)}{\varphi} \right) + \left(1 - \varphi \right)^{0.5} \left(u^*_z \right)^{0.6} \left(Pr \right)^{\frac{1}{3}} \tag{3.23}$$

$$\Gamma_{sg} = \frac{Nu_{int} \lambda_f}{d_{part}} \tag{3.24}$$

The general reaction rate ($\dot{R}_s$) governs the consumption of the solid phase and the corresponding generation of the fluid phase, following the approach described by [3, 7].

$$\dot{R}_s = A_s \cdot exp\left[\frac{-E_s Arr_s}{RT_\infty T_s^* + E_s}\right] \cdot Y_s^* \cdot Y_f^* \tag{3.25}$$

The reaction rate of fluid generation used in equations 3.14, 3.16 and 3.21, denoted as $\dot{R}_f^{oxi}$, and the term of solid mass consumption term used in Equation 3.22, denoted as $\dot{R}_s^{oxi}$, represent the mass generated or consumed per unit volume per unit time in the respective phases. These terms are defined in Equations 3.26 and 3.27 [3], respectively. The parameter b_{O_2} corresponds to the stoichiometric coefficient of oxygen, obtained from the chemical balance of the reaction between carbon and oxygen.

$$\dot{R}_f^{oxi} = b_{o2}\varphi\dot{R}_s\rho_s^{abs} \tag{3.26}$$

$$\dot{R}_s^{oxi} = (1-\varphi)\dot{R}_s\rho_s^{abs} \tag{3.27}$$

3.4 Case studies

To validate the entire methodology described in Sections 3.1, 3.2, and 3.3, it was proposed to perform a series of numerical simulations and compare the results with both experimental data from real conditions and numerical results reported by the literature on smoldering combustion. The following sections of the methodology present three case studies adapted for implementation in the proposed model. The level of complexity increases progressively from the first to the third case, aiming to demonstrate the robustness and versatility of the developed model.

- Case Study 1 – Combustion at the Fluid–Porous Interface: This is the simplest case, which involves a model under local thermal equilibrium (LTE) assumptions and steady-state flow equations. Its main purpose is to verify the model's ability to capture flow recirculation caused by natural convection and to assess how such recirculations affect porous bed contraction and other physical phenomena. This analysis is aligned with the findings of Bittencourt (2023) [8].

- Case Study 2 – Cooling of a Porous Bed: The goal here is to calibrate the convective heat transfer between different phases. This case extends the model to transient conditions and adopts a local thermal non-equilibrium (LTNE) approach for temperature fields. The experimental and numerical results of Martins (2008) [9] serve as a reference for this case.

- Case Study 3 – Combustion in a Porous Bed: This final case aims to extend the model to simulate smoldering combustion as observed in reality. It is based on an experimental setup described by Martins (2008) [9], involving a cylindrical reactor entirely filled with a reactive porous bed.

3.4.1 Combustion at a fluid-porous interface

As previously mentioned above, the software used to implement all the mathematical modeling proposed in Section 3.3 was COMSOL Multiphysics (Version 5.4). This first case study aims to analyze the behavior near the porous interface between distinct domains (fluid and porous). Bittencourt (2023) proposed

a steady-state numerical simulation of a smoldering combustion process using the same software, with the goal of capturing secondary flow recirculations observed in their experimental data and visualized during tests Bittencourt [8]. To better understand the case study, a vacuum-induced smoldering reactor with an internal diameter of 83 mm and a height of 300 mm was equipped with six inline thermocouples, strategically placed at different heights along the reactor axis. This arrangement enabled temperature measurements at multiple points within the chamber and allowed for monitoring of the combustion front's path. A vacuum pump connected at the bottom of the reactor was responsible for creating a suction pressure to induce air flow through the reactor bed. More details of the physics simulated in this first case study are presented in Fig. 3.2. The author identified that the reactor geometry (open at the top) and the height of the porous layer (h_p) influence the natural convection process above the porous interface during smoldering. Therefore, analyzing the dimensionless contraction of the porous bed was important, and this parameter was defined as $h^* = h_p / L$.

Their methodology also employed a dimensionless approach using COMSOL, similar to the one proposed in this work, but based on the classical equations provided by the software, such as Porous Media and Subsurface Flow (Brinkman Equations), Heat Transfer in Fluids, and Heat Transfer in Solids. Based on the dimensional analysis presented by Bittencourt (2023) [8], five dimensionless equations were considered to describe the problem. These equations correspond to mass conservation (Eq. 3.28); momentum conservation in the fluid (Eq. 3.29) and porous (Eq. 3.30) layers; and energy

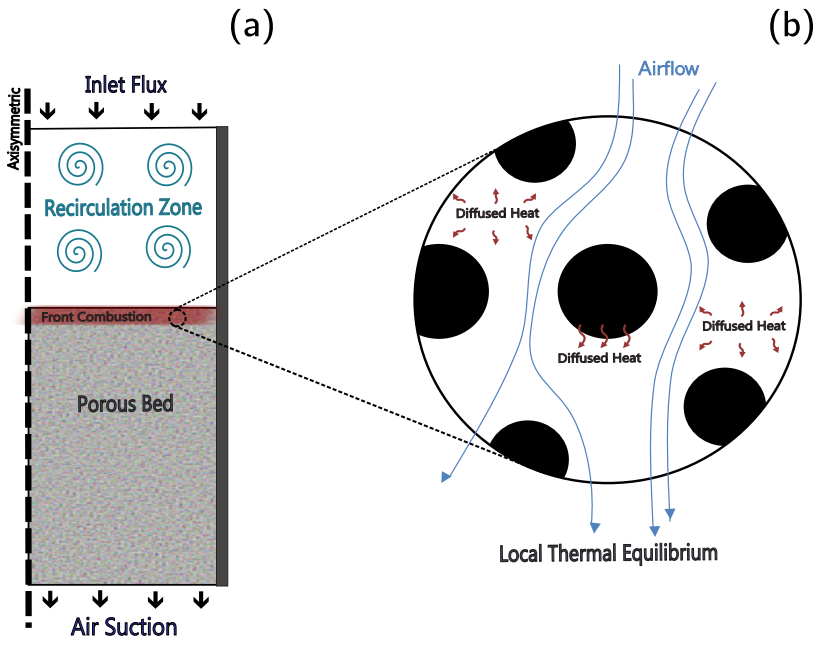

Figure 3.2: (a) Physical behavior of a vertical cylindrical - case 01. (b) Interstitial behavior of heat and flux - case 01. Developed by the authors.

conservation in the fluid (Eq. 3.31) and porous (Eq. 3.32) layers. The dimensionless terms identified through this process are presented below, including classical dimensionless numbers commonly used in smoldering studies, such as the Prandtl, Grashof, and Darcy numbers. It is important to note that the author adopts a single-temperature model for the porous bed, which implies local thermal equilibrium (LTE). As shown in Eq. 3.32, this is evident from the fact that the temperature variable appears without any subscript that indicates the fluid or solid phase, being represented simply as T^*.

$$\nabla . \mathbf{u}^* = 0 \tag{3.28}$$

$$\left(\mathbf{u}^*.\nabla\right)\mathbf{u}^* = -\nabla p^* + \nabla^2\mathbf{u}^* + Gr\left(T^*\right) \tag{3.29}$$

$$\left(\mathbf{U}^*.\nabla\right)\mathbf{U}^* = -\nabla p^* + \nabla^2\mathbf{U}^* - \frac{1}{Da_f}\mathbf{u}^* \tag{3.30}$$

$$\left(\mathbf{u}^*.\nabla\right)T^* = \frac{1}{Pr}\left(\nabla^2 T^*\right) \tag{3.31}$$

$$\left(\mathbf{U}^*.\nabla\right)T^* = \frac{1}{Pr_p}\left(\nabla^2 T^*\right) + q^*_{rad} \tag{3.32}$$

In this work, the modeling of the permeable fluid-porous interface of the smoldering combustion reactor was proposed using a generic PDEs provided by COMSOL Multiphysics. This approach allows for greater flexibility in modeling equations in a dimensionless format. One of the mathematical interfaces used to model the problem was the Coefficient Form PDE. This equation template provides a powerful general interface for specifying linear and nonlinear equations, including the classical Poisson's and Laplace structure. In the COMSOL interface, this PDE appears as the structure below Eq. 3.33:

$$e_a\frac{\partial^2\mathbf{u}}{\partial t^2} + d_a\frac{\partial\mathbf{u}}{\partial t} + \nabla.\left(-c\nabla\mathbf{u} - \alpha\mathbf{u} + \gamma\right) + \beta.\mathbf{u} + a\mathbf{u} = f \tag{3.33}$$

This equation contains terms that can be transformed into advection and conduction components, and it is also possible to include source terms. The parameter **u** is not a velocity vector in this case, but a generic vector that can be used to specify all independent variables. The coefficients e_a, d_a, c, α, γ, β, a and f can be scalar parameters, vectors or tensors of different orders, depending on the number of independent variables chosen for modeling the problem and whether the phenomenon is isotropic or not. Another generic mathematical interface available in COMSOL is the Stabilized Convection-Diffusion Equation, which has the structure described below (Eq. 3.34). In this equation, fewer components are visible, and the parameter u is not a generic vector, but a unique independent variable.

$$d_a \frac{\partial u}{\partial t} + \nabla.\big(-c\nabla u + \alpha u\big) + \beta.u + au = f \tag{3.34}$$

The boundary conditions used can include the Dirichlet Boundary Condition, which allows for the definition of a constant value for a specific parameter at the edge of the domain, as well as the Flux/Source conditions, which reference the Neumann Boundary Condition. The latter specifies the values that the derivative of a solution should take at the boundary of the domain. By applying tensorial calculations, it was possible to transform the PDE Eq. (3.33) in Eq. (3.28), Eq. (3.29), and Eq. (3.30), and through the same process, it was possible to transform the PDE Eq. (3.34) in Eq. (3.31) and Eq. (3.32). Therefore, the Coefficient Form PDE was designed to encompass the same structure as the Brinkman equation, meaning that through this PDE, it is possible to model governing equations related to the conservation of mass

and momentum. Furthermore, the Stabilized Convection-Diffusion Equation was designed to encompass the same structure as the Heat Transfer in Fluids and Solids, meaning that through this PDE, it is possible to model governing equations related to energy conservation in the fluid and porous bed domain.

Because it is a circumferential geometry, one of the boundary conditions used to one edge of the reactor is axisymmetric (Fig. 3.3). Other boundary conditions used by the author of reference are those of a dimensionless constant temperature on the reactor walls, as well as at the fluid inlet and outlet. Furthermore, a constant dimensionless temperature is considered between the fluid and porous domains, which is called the dimensionless combustion front temperature T_h^*, and because it is always the highest temperature existing within the system, it receives a dimensionless value always equal to 1. Other boundary conditions related are: zero velocity on the wall, a prescript value of $p_{in}^* = 0$ to the top of the reactor and $p_{out}^* = -Be$ to the bottom. In this case, the Bejan number is responsible for characterizing the induced airflow, which competes with free convection due to the shrinkage of the bed [2]. These boundary conditions, along with others, were implemented in the PDEs using Dirichlet Boundary Conditions. The locations of these conditions are shown in Fig. 3.3. All dimensionless parameters considered and their respective values are presented in Table 3.1, together with the initial conditions (Table 3.2) and the boundary conditions (Table 3.3). The tables present the dimensionless parameters, initial conditions, and boundary conditions for the four simulations performed, considering porous bed contractions of 10%, 20%, 30%, and 40%, which correspond, respectively, to h^* values of 0.9, 0.8, 0.7, and 0.6.

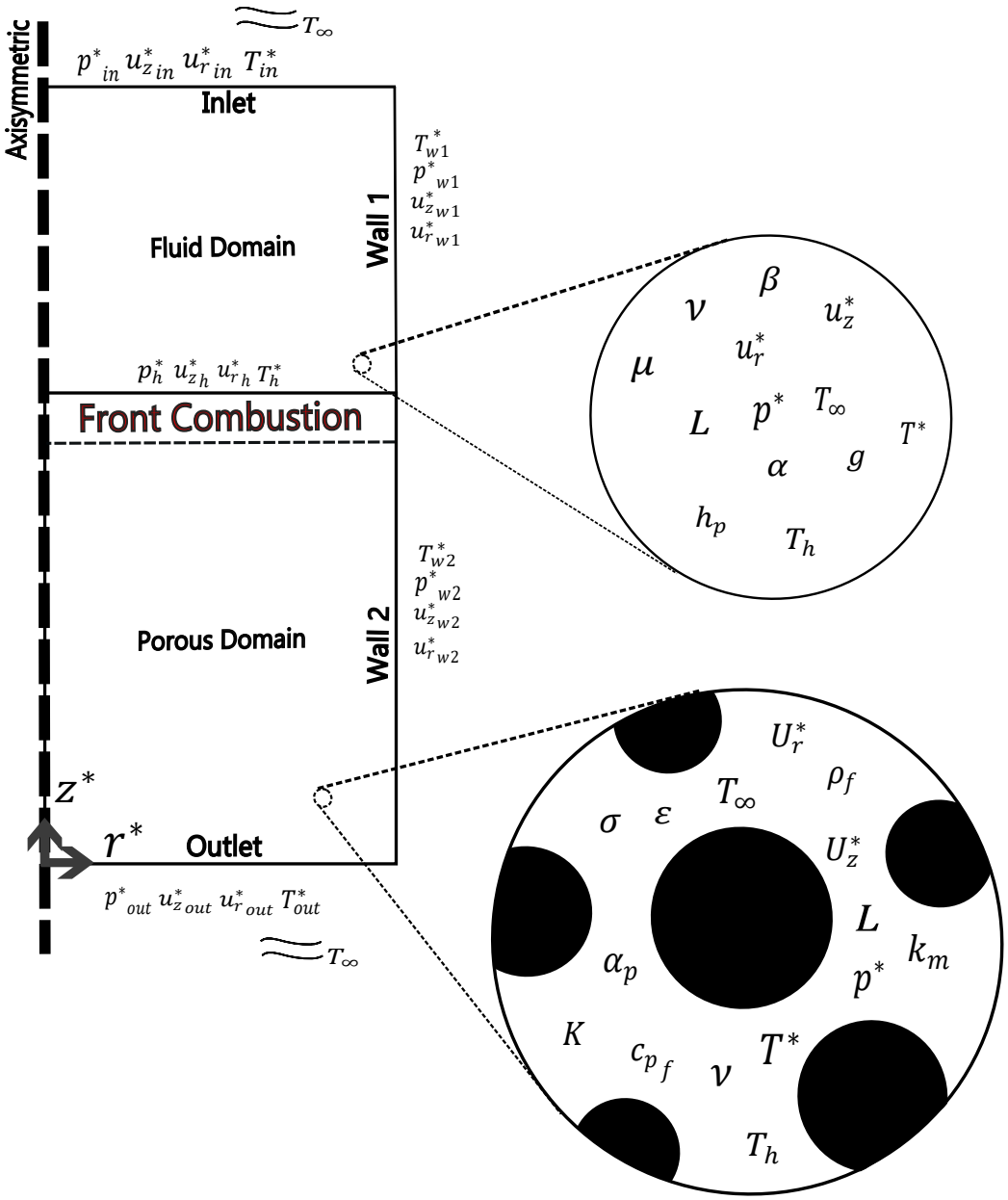

Figure 3.3: Representation of boundary conditions and crucial parameters involved in case 01. Developed by the authors.

Table 3.1: Value of dimensionless numbers. Results obtained to Bittencourt (2023) in a real experimental measure. Developed by the authors.

h^*	Gr x $[10^{-7}]$	Pr	Pr_p	Be x $[10^{-10}]$	Da_f x $[10^{9}]$
0.9	0.5	0.69	2.5	16.3	1.0
0.8	2.7	0.69	2.9	13.4	1.0
0.7	7.3	0.69	3.3	10.9	1.0
0.6	18.1	0.69	3.8	7.4	1.0

Table 3.2: Initial condition in numerical simulation - case 01.

Nomenclature	Describe	Value
u_z^*	Longitudinal dimensionless velocity of fluid	0
u_r^*	Radial dimensionless velocity of fluid	0
p^*	Dimensionless pressure of fluid	0
T^*	Dimensionless temperature of fluid	0

Table 3.3: Value of boundary conditions to numerical analyses. Results obtained to Bittencourt (2023) in a real experimental measure. Developed by the authors.

h^*	T_{in}^*	T_{w1}^*	T_{w2}^*	T_{out}^*
0.9	0.29	0.29	0.33	0.04
0.8	0.25	0.25	0.38	0.06
0.7	0.12	0.12	0.61	0.02
0.6	0.13	0.13	0.77	0.07

3.4.2 Cooling of a porous bed

The mathematical model based on dimensionless parameters was developed primarily to simulate smoldering combustion. However, it can also be applied to other simplified processes, such as the cooling of a porous bed in a axisymmetric reactor, as conducted by Martins (2008) [9], provided that small

adaptations are considered in the model. The experimental setup conducted by the author of reference features a vertical cylindrical with an internal diameter of 91 mm and a height of 300 mm. The reactor is equipped with high-precision instrumentation. Six in-line thermocouples (T1, T2, T3, T10, T11, T12), each with a diameter of 0.96 mm, are strategically placed at different heights along the reactor axis: z = 0, 45, 90, 180, 225, and 270 mm (measured from top to bottom). This arrangement enables temperature measurements at multiple points within the device. A total of 2340 g of a 3.6/96.4 wt charcoal/sand mixture were introduced into the cylindrical. The sand particles used in the mixture varied in size, ranging from 315–500 m, 500–1000 m, and 1–2 mm. The charcoal particles were ground to a size between 500–1000 m.

To ensure a homogeneous mixture of charcoal and sand, a mortar preparation method was used. The mixture was initially wetted and thoroughly mixed before being placed in the device. It was then left to dry overnight to remove any residual moisture within the porous bed. Initially, the dry mixture of charcoal and sand was heated to 68.2 °C in an oven. However, for this numerical simulation, the porous bed is assumed to be entirely composed of sand. This assumption is justified by the fact that sand constitutes more than 95% of the mixture in the experimental setup. Subsequently, the top of the cell was exposed to forced cold air, as illustrated in Fig. 3.4. As cold air percolated through the porous bed, it was cooled to ambient temperature (approximately 19°C). The equations used to model this case include Eqs. 3.14, 3.18 – 3.19, 3.21 - 3.24. It is important to note that the specific source terms in some equations were disregarded. For example, terms related to chemical

reactions and radiative heat transfer were omitted from the energy equations (Eqs. 3.21 and 3.22), as the objective of case 02 is to calibrate the model's cooling process based on experimental data. Consequently, source terms for convective heat transfer between the solid and gas phases are considered to ensure the model accurately reflects experimental conditions. Radial heat loss was also considered. Equations 3.15 and 3.16 were not applied, as the objective does not involve the evaluating of chemical species transport. The specific mass of the fluid phase was modeled according to Equation 3.19. In line with the proposed simplifications, Equations 3.17 and 3.20 were excluded, as the reactor is entirely filled with a porous bed. Arrhenius numbers (Arr_s and Arr_f) were not included in the dimensionless temperature group because the experiment was conducted at low temperatures, where activation energy is not significant. With this assumption, Eqs. 3.8 and 3.9 take a simplified form, excluding both the activation energy and the ideal gas constant, as expressed in the Eqs. 3.10 and 3.11. The other dimensionless parameters described in Section 3.2 follow their standard formulations.

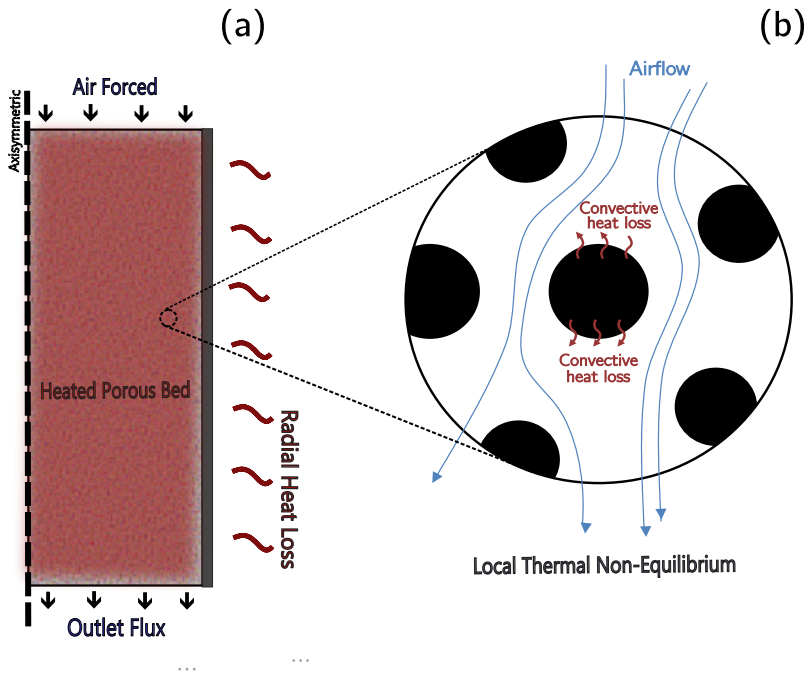

Figure 3.4: (a) Physical behavior of a vertical cylindrical - case 02. (b) Interstitial behavior of heat and flux - case 02. Developed by the authors.

One parameter that is difficult to estimate is the permeability of the sand. However, Fan et al (2021) evaluated the permeability of calcareous sand using a three-dimensional method and reported values on the order of 10^{-10} m² for particle sizes ranging from 0.075 mm to 2 mm [10]. This value was adopted in this case. Considering that the particle size used by Martins (2008) ranged from 0.315 mm to 2 mm, an average particle size of 0.75 mm was assumed. All physical parameters considered and their respective values are presented in Table 3.4, along with the initial conditions (Table 3.5) and boundary conditions (Tables 3.6 and 3.7). It is noticeable that the number of variables is small compared to the general visual model shown in Figure 3.1, and there is only one domain composed of a porous bed.

Table 3.4: Numerical model input parameters - case 02

Nomenclature	Value	Unity	Ref
φ	0.47	[1]	[9]
u_z	0.035	$[m/s]$	[9]
ρ_s^{abs}	2200	$[kg/m^3]$	[9]
d_{part}	0.75	[mm]	[9]
λ_s	0.3	$[W/m.K]$	[9]
c_{p_s}	900	$[J/kg.K]$	[11]
ρ_∞	1.2754	$[kg/m^3]$	[11]
K	1×10^{-10}	$[m^2]$	[10]
Δm	25	$[g]$	[9]
ν_f	38.6×10^{-6}	$[m/s]$	[4]
μ_f	184.6×10^{-7}	$[Pa.s]$	[4]
c_{p_f}	1007	$[J/kg.K]$	[4]
λ_f	26.3×10^{-3}	$[W/m.K]$	[4]
T_∞	291.15	$[K]$	[9]

Table 3.5: Initial condition in numerical simulation - case 02.

Nomenclature	Describe	Value
u_z^*	Longitudinal dimensionless velocity of fluid	-1.0402
u_r^*	Radial dimensionless velocity of fluid	0
ρ_f^*	Dimensionless specific mass of fluid	1
p^*	Dimensionless pressure of fluid	0
T_f^*	Dimensionless temperature of fluid	0
T_s^*	Dimensionless temperature of solid	0.1684
t^*	Dimensionless time	10^{-6}

Table 3.6: Boundary condition in numerical simulation - case 02.

Nomenclature	Value
p^*_{in}	non prescribed
$u^*_{z\,in}$	-1.0402
$u^*_{r\,in}$	0
$\rho^*_{f\,in}$	1
$T^*_{f\,in}$	0
$T^*_{s\,in}$	non prescribed
p^*_{out}	0
$u^*_{z\,out}$	non prescribed
$u^*_{r\,out}$	non prescribed
$T^*_{f\,out}$	0
$T^*_{s\,out}$	non prescribed
$\rho^*_{f\,out}$	non prescribed
p^*_{w2}	non prescribed
$\rho^*_{f\,w2}$	non prescribed
$u^*_{z\,w2}$	0
$u^*_{r\,w2}$	0
$T^*_{f\,w2}$	non prescribed
$T^*_{s\,w2}$	non prescribed

Table 3.7: Flux/source boundary conditions - case 02.

Coordinates	Boundary Condition
$r = 0.0455$ and $0 < z < 0.3$	$\begin{cases} -\frac{\partial T^*_f}{\partial r^*} = Nu_{ext} T^*_f \\ -\frac{\partial T^*_s}{\partial r^*} = Bi_{ext} T^*_s \end{cases}$
$z = 0$ and $0 < r < 0.0455$	$\begin{cases} -\frac{\partial T^*_s}{\partial z^*} = Bi_{ext} T^*_s \end{cases}$
$z = 0.3$ and $0 < r < 0.0455$	$\begin{cases} -\frac{\partial T^*_s}{\partial z^*} = Bi_{ext} T^*_s \end{cases}$

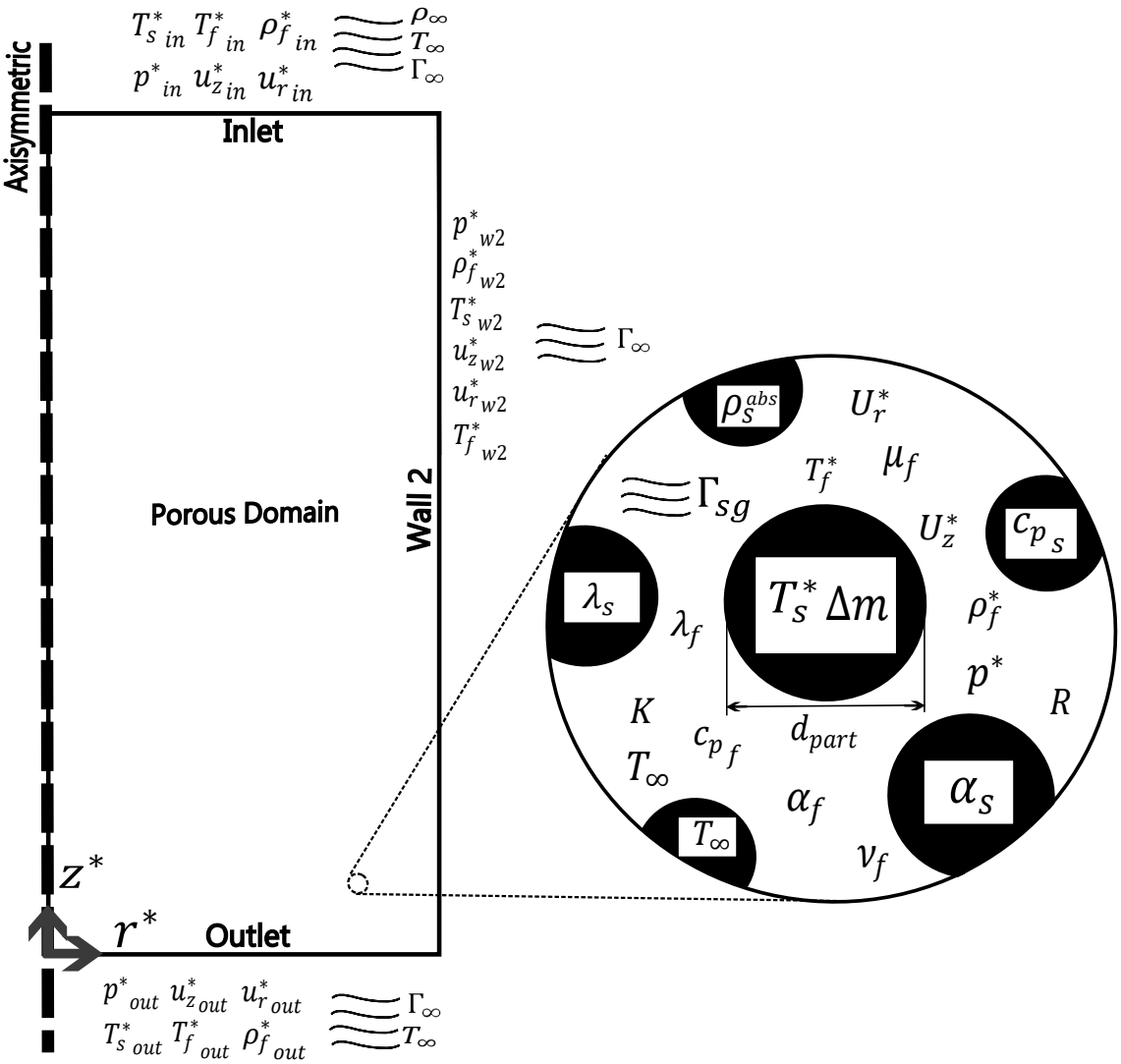

Figure 3.5: Representation of boundary conditions and crucial parameters involved in case 02. Developed by the authors.

The visual representation of the boundary conditions is shown in Figure 3.5, and it is important to mention that the dimensionless time t^* considered in this numerical simulation is 0.0026. To highlight the differences between the experimental data and the simulation results, the maximum error observed at each thermocouple can be estimated. This approach helps identify regions where the behavior significantly deviates from the experimental data, indicating necessary adjustments in the proposed model. The maximum error is calculated according to Equation 3.35.

$$error_{max} = \frac{MAX\left(\triangle T_{(t)}\right)}{MED\left(T_{(t)}\right)} \tag{3.35}$$

3.4.3 Combustion in porous bed

A cold porous bed composed of 3.6% charcoal and 96.4% sand is simulated in a smoldering process, with heating applied at the top to initiate the ignition process. Forced air is also introduced from the top of the reactor, generating a fluid flow through the reactor bed. This air flow drives the downward propagation of the combustion front, where chemical reactions sustain smoldering combustion. A local thermal non-equilibrium (LTNE) is considered and heat transfer between the different phases occurs through convection. The experimental setup follows the geometric parameters and considerations adopted by Martins (2008) [9]. The smoldering reactor has an internal diameter of 91 mm and a height of 300 mm, and is equipped with six inline thermocouples strategically positioned at different heights along the reactor axis. This configuration allows temperature measurements at multiple points within

the chamber, enabling the tracking of the combustion front progression. The charcoal and sand particles have a medium size of 0.75 mm. Convection heat losses on the wall are also considered. These physical behaviors are shown in Figure 3.6.

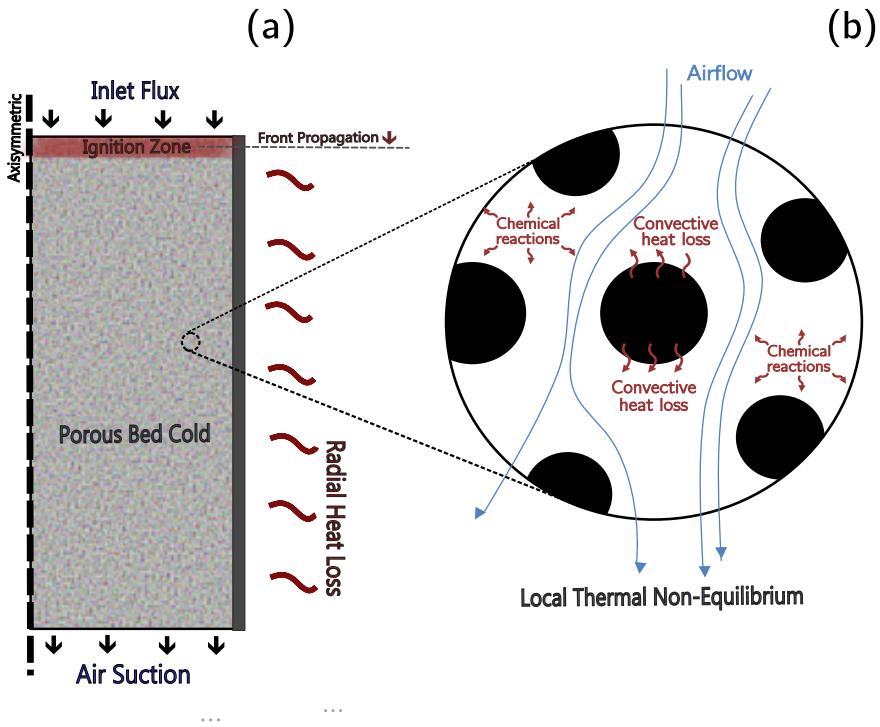

Figure 3.6: (a) Physical behavior of a vertical cylindrical - case 03. (b) Interstitial behavior of heat and flux - case 03. Developed by the authors.

In the experiments conducted by the author of reference, since the reactor was open on top, the heater was positioned on the inlet surface and switched on to initiate the ignition process of the porous medium. To simulate this ignition process in the present model, a heat flux/source of 40,000 $[W/m^2]$ was applied at the upper boundary. This value corresponds to the lowest radiation heat transfer measured during their ignition process and, in dimensionless

form (q^*_{ig}), for this model it is equal to 204.54. To maintain the connection between the experimental runs and the dimensionless smoldering combustion model proposed in Section 3.1, the experimental input parameters are summarized in Table 3.8.

Table 3.8: Numerical model input parameters - case 03.

Nomenclature	Value	Unity	Ref
φ	0.4	[1]	[9]
ν_f	0.000038	$[m^2/s]$	[4]
μ_f	10^{-5}	$[Pa.s]$	[4]
ρ_s^{abs}	1284.9	$[kg/m^3]$	[9]
d_{part}	0.75	[mm]	[9]
λ_s	0.3	$[W/m.K]$	[4]
λ_f	0.0043	$[W/m.K]$	[4]
c_{p_s}	1100	$[J/kg.K]$	[11]
c_{p_f}	1007	$[J/kg.K]$	[11]
ρ_∞	1.2754	$[kg/m^3]$	[11]
K	10^{-10}	$[m^2]$	[8]
E	23,250	$[J/mol]$	[-]
A_s	0.327	$[1/s]$	[-]
R	8.314	$[J/mol.K]$	[4]
Δm	0.0832	$[kg]$	[9]
H_s	32	$[MJ/kg]$	[-]
D_f	0.000043	$[m^2/s]$	[4]
T_∞	288.15	$[K]$	[9]
q^*_{ig}	204.54	[1]	[9]

The configuration of the boundary and initial conditions for this case study is illustrated in Fig. 3.7, and the corresponding values are provided in Tables 3.9, 3.10 and 3.11. It is worth noting that the number of boundary conditions and parameters in this case is greater than in the others. This is because the source term associated with chemical reactions is included in the porous-solid

energy equation, as previously shown in Equation 3.22. The porous-fluid energy equation 3.21, however, in this case study, does not have this chemical contribution. As a result, since chemical reactions generate gas and consume solid material, the mass fractions of both phases are modeled using Equations 3.15 and 3.16, as discussed earlier in Section 3.3. Radiation-related source terms were not included in this simulation. The fluid phase starts with a mass fraction of ($Y_{f,0} = 0.23$), since only oxygen is considered in the fluid phase, which approximately matches its concentration in air. To represent the airflow imposed at the top, a dimensionless negative longitudinal velocity is applied because the longitudinal coordinates raise your values from the bottom to the top, following the same approach used by Martins (2008), therefore, ($u^*_{z\,in}$) assumes the value of -0.4641, as specified in Table 3.10. The mesh configuration consists of a free triangular structure with a maximum element size of 0.001 m. The solver setup adopts PARDISO, with all equations fully coupled and a nonlinear constant (Newton) method, using a damping factor of 0.7 and a maximum of 25 iterations. The initial time step is set to 10^{-6}, and the dimensionless time used during the simulation is 0.0002. In their numerical simulation, the author of reference had to apply an ignition time of 380 seconds to correctly reproduce the ignition behavior and to overcome the thermal inertia of the porous bed. In the simulations of this work, the ignition process lasted 228 seconds, which corresponds to a dimensionless time of 0.04558. This value was obtained through continuous test executions.

Table 3.9: Initial condition in numerical simulation - case 03.

Nomenclature	Describe	Value
u_z^*	Longitudinal dimensionless velocity	0
u_r^*	Radial dimensionless velocity	0
p^*	Dimensionless pressure	0
T_f^*	Dimensionless temperature of fluid	0
T_s^*	Dimensionless temperature of solid	0
ρ_f^*	Dimensionless specific mass	1
Y_s^*	Mass fraction of solid	1
Y_f^*	Mass fraction of fluid	0.23
t^*	Dimensionless time	10^{-6}

Table 3.10: Boundary condition in numerical simulation - case 03.

Nomenclature	Value
$u^*_{z\,in}$	-0.4641
$u^*_{r\,in}$	0
$p^*_{\ in}$	0
$\rho^*_{f_{in}}$	1
$Y^*_{f_{in}}$	0.23
$Y^*_{s\,in}$	non prescribed
$u^*_{z\,out}$	non prescribed
$u^*_{r\,out}$	non prescribed
$p^*_{\ out}$	0
$\rho^*_{f_{out}}$	non prescribed
$Y^*_{f_{out}}$	non prescribed
$Y^*_{s\,out}$	non prescribed
$u^*_{z\,w2}$	0
$u^*_{r\,w2}$	0
$p^*_{\ w2}$	non prescribed
$\rho^*_{f_{w2}}$	non prescribed
$Y^*_{f_{w2}}$	non prescribed
$Y^*_{s\,w2}$	non prescribed

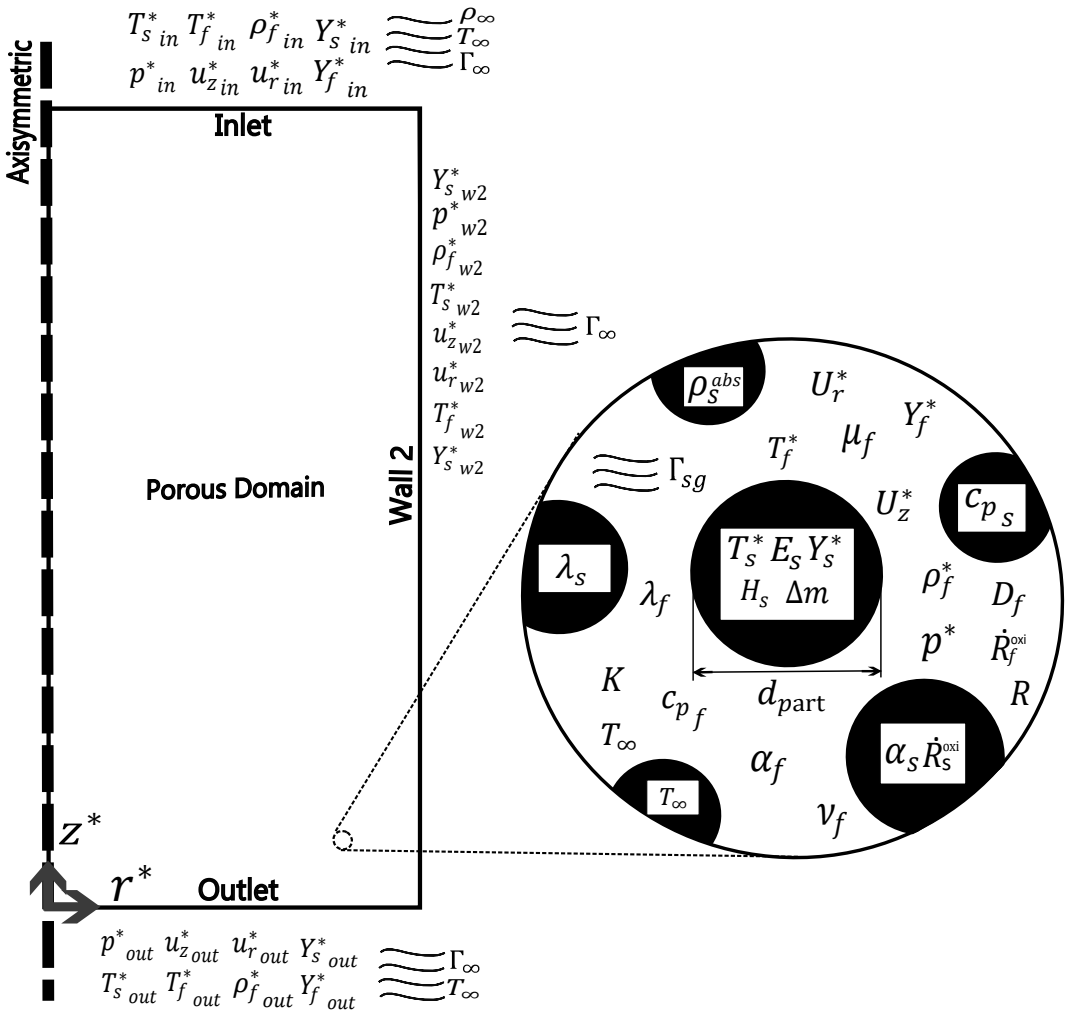

Figure 3.7: Representation of boundary conditions and crucial parameters involved in case 03. Developed by the authors.

Table 3.11: Flux/source boundary conditions - case 03.

Coordinates	Value
$z = 0.3$ & $0 < r < 0.0415$	$\Rightarrow \begin{cases} t < 0.04558 \rightarrow -\dfrac{\partial T_s^*}{\partial z^*} = -q_{ig}^*, \\ t > 0.04558 \rightarrow -\dfrac{\partial T_s^*}{\partial z^*} = Bi_{ext} T_s^*, \\ -\dfrac{\partial Y_s^*}{\partial z^*} = 0, \end{cases}$
$z = 0$ & $0 < r < 0.0415$	$\Rightarrow \begin{cases} -\dfrac{\partial Y_s^*}{\partial z^*} = 0 \\ -\dfrac{\partial T_f^*}{\partial z^*} = 0, \\ -\dfrac{\partial Y_f^*}{\partial z^*} = \dfrac{u_z^* \nu_f}{d_p D_f}\left[Y_f^* - Y_{f,0}\right] + \left[\dfrac{\partial \rho_f^*}{\partial z^*}\dfrac{Y_f^*}{\rho_f^*}\right], \end{cases}$
$r = 0.0415$ & $0 < z < 0.3$	$\Rightarrow \begin{cases} -\dfrac{\partial Y_s^*}{\partial r^*} = 0 \\ -\dfrac{\partial Y_f^*}{\partial r^*} = 0 \\ -\dfrac{\partial T_f^*}{\partial r^*} = Nu_{ext} T_f^* \\ -\dfrac{\partial T_s}{\partial r^*} = Bi_{ext} T_s^* \end{cases}$

References

1. Nield, D. A., Bejan, A., *et al. Convection in porous media* (Springer, 2006).
2. Zimparov, V. D., Angelov, M. S. & Hristov, J. Y. New insight into the definitions of the Bejan number. *International Communications in Heat and Mass Transfer* **116,** 104637. ISSN: 0735-1933. https://www.sciencedirect.com/science/article/pii/S0735193320301652 (2020).
3. Miry, S. Z., Zanoni, M. A., Rashwan, T. L., Torero, J. L. & Gerhard, J. I. Investigation of multi-dimensional transfer effects in applied smouldering systems: A 2D numerical modelling approach. *Combustion and Flame* **246,** 112385. ISSN: 0010-2180. https://www.sciencedirect.com/science/article/pii/S001021802200400X (2022).
4. Çengel Y.A. e Cimbala, J. *Mecânica dos Fluidos - Fundamentos e Aplicações* (McGraw-Hill Interamericana do Brasil Ltda, Brazil, 2007).
5. Incropera, F. P. & De Witt, D. P. Fundamentals of heat and mass transfer (1985).
6. Pallares, J. & Grau, F. A modification of a Nusselt number correlation for forced convection in porous media. *International Communications in Heat and Mass Transfer* **37,** 1187–1190. ISSN: 0735-1933. https://www.sciencedirect.com/science/article/pii/S0735193310001788 (2010).
7. MAIOLI, A. G. Cfd openfoam: Implementaçao da combustao smouldering e sua avaliaçao paramétrica. *Universidade Federal do Espírito Santo* (2016).
8. Bittencourt, F. L. F. *TOWARD A SAFE AND CIRCULAR THERMOCHEMICAL PROCESS TO SANITIZE HUMAN FECES IN RESOURCE-POOR ENVIRONMENTS* PhD thesis (Universidade Federal do Espírito Santo, 2023).
9. Ferreira Martins, M. *Structure d'un front de combustion propagé en co-courant dans un lit fixe de schiste bitumineux broyé* PhD thesis (Diss. Toulouse, 2008).

10. Fan, Z. *et al.* Three-dimensional pore characteristics and permeability properties of calcareous sand with different particle sizes (2021).

11. Callister Jr, W. D. & Rethwisch, D. G. *Materials science and engineering: an introduction* (John wiley & sons, 2020).

Chapter 4

Results and Discursion

4.1 Resulting scales

According to the considerations presented in Section 3, the dimensionless analysis results in the dimensionless terms listed in Table 4.1. This table illustrates the physical meaning of these terms and their relevance for the phenomena simulated in this work. Some of the identified dimensionless numbers retain their classical significance for the smoldering phenomena and are commonly found in similar studies in the literature. Other terms, however, emerged specifically during the nondimensionalization process applied in this work, and their interpretation is inferred based on their structure and the physical parameters that define them.

Table 4.1: Significance of dimensionless terms obtained in the dimensional analysis. Developed by the author.

PARAMETER	PHYSICAL REPRESENTATION
$Bi_{ext} = \frac{d_{part}\Gamma_\infty}{k_s}$	For the solid phase, this term is associated with heat loss to the environment, relating the internal heat conduction of the solid phase to the external wall convection resistance of the reactor.
$Bi_{int} = \frac{d_{part}\Gamma_{sg}}{k_s}$	For the solid phase, this term is associated with interstitial heat exchange, linking the internal heat conduction of the solid matrix to the convective resistance of the flux percolating through the porous bed.
$Nu_{ext} = \frac{d_{part}\Gamma_\infty}{k_f}$	For the fluid phase, this term is associated with heat loss to the environment, relating the internal heat conduction of the fluid phase to the external wall convection resistance of the reactor.
$Nu_{int} = \frac{d_{part}\Gamma_{sg}}{k_f}$	For the fluid phase, this term is associated with interstitial heat exchange, linking the internal heat conduction of the fluid phase to the convective resistance of the flux percolating through the porous bed.
$Pr = \frac{\mu_f c_{p_f}}{k_f}$	The Prandtl number represents the ratio of momentum diffusivity to thermal diffusivity in a fluid.
$Da_f = \frac{K}{d_{part}^2}$	The Darcy number represents the effect of permeability relative to the cross-sectional area of the porous medium.
$Gr = \frac{g\beta T_\infty d_{part}^3}{\nu_f^2}$	It represents the relative effect of buoyancy and viscous forces in natural convection.
$Sc = \frac{D_f}{\nu_f}$	The Schmidt number represents the ratio between momentum diffusivity and mass diffusivity in the fluid.
$Arr_s = \frac{E_s}{RT_\infty}$	It represents the influence of solid phase activation energy on chemical reactions and quantifies the temperature dependence of the reaction rate.
$Arr_f = \frac{E_f}{RT_\infty}$	It represents the influence of fluid phase activation energy on chemical reactions and quantifies the temperature dependence of the reaction rate.
$Pe = \frac{u_z d_{part}}{\alpha_s}$	The Peclet number represents the propagation of heat diffusion in the solid phase relative to heat advection in the gas phase.
$m^*_{part} = \frac{\rho_s^{abs} d_{part}^3}{\Delta m}$	It relates to how the quantity of mass evolves as the solid undergoes combustion. It relates how the remaining solid mass influences the mass, momentum, and energy evolve over time.
$u_z^* = \frac{u_z d_{part}}{\nu_f}$	It represents the inertia forces relative to viscous forces in the fluid phase. It relates how flow velocity within the porous bed plays a key role in oxygen supply, solid mass consumption, and directly influences the reaction rate and experiment duration.
$Da_s = \frac{\dot{R}_s \Delta m}{\rho_s^{abs} u_z d_{part}^2}$	It represents the rate of solid-to-gas conversion relative to fluid advection.

The dimensional analysis of the governing equations for smoldering combustion revealed several characteristic scales that help to explain the physics of the process. One of them is:

$$\tau_s = \frac{d_{part}^2}{\alpha_s}$$

which defines the characteristic time for heat to diffuse through the solid matrix, and another is

$$\tau_f = \frac{d_{part}^2}{\nu_f}$$

which represents the characteristic time for fluid mixing effects to become relevant. These characteristic time scales appear in the source terms related to the heat released by chemical reactions in the Eqs. 3.21 and 3.22. When both are large, a greater amount of heat released from chemical reactions is transferred to the solid and fluid phases. The scale related to the variation rate specific volume of the fluid phase is represented by:

$$\dot{v}_f = \frac{d_{part}^2}{\rho_\infty \nu_f}$$

indicating the intensity with which gaseous species are produced as a result of flow effects. Higher values lead to a more intense gas release, which can affect the pressure distribution inside the porous medium. In contrast, lower values correspond to slower and more stable gas release, which can help maintain combustion under controlled conditions. Energy storage in the fluid phase is given by:

$$Q_f^{stg} = \rho_\infty c_{p_f} T_\infty$$

and it quantifies the accumulation of heat in the gas phase as a result of

chemical reactions, convective and radiative heat transfer. This parameter appears in some parts of the equations associated with these mechanisms. When this term increases, the gas is able to retain more heat, which contributes to sustaining combustion and helps the process to remain self-sustained. If this parameter is low, the gas stores little energy, making the system more dependent on heating from the solid phase. The power of heat transfer by radiation is described by:

$$P_s^{rad} = \epsilon\sigma\delta T_\infty^4$$

The energy value becomes significant at high temperatures, providing an additional mechanism for energy exchange. Large values of P_s^{rad} indicate strong radiative transfer within the pores of the medium, which can substantially influence the overall heat balance. An dimensionless geometric factor defined as:

$$GF = d_p\delta$$

can be related to the intensity of heat transfer between phases. This factor measures how much surface area is available for heat exchange for each characteristic particle. An increase in particle size does not cause a significant increase in the specific surface area; however, a reduction in particle size leads to a larger surface area available for heat transfer. Therefore, high values of the geometric factor are associated with small particles and high specific surface area, leading to a tendency toward local thermal equilibrium between the solid and fluid phases and to the formation of a thinner thermal front in porous media. In contrast, low values of the dimensionless geometric factor are associated with large particles and low specific surface area, which can

lead to lower heat generation per unit volume, lower peak temperatures, and weak thermal coupling between the solid and fluid phases.

Together, all these characteristic scales and dimensionless numbers, describe the balance between heat transfer, flow dynamics, and chemical conversion in smoldering combustion.

4.2 Results - Combustion in a fluid-porous interface

The first numerical simulation was validated through the modeling performed in COMSOL using generic PDEs, as streamlines similar to those presented by Bittencourt (2023) in their work were obtained. All numerical simulations and boundary conditions shown in Tables 3.1 and 3.3 were tested, and a similar fluid flow behavior was observed [1]. Figure 4.1 presents a comparison with the results obtained by the author. As expected and mentioned in Section 1.2, due to buoyancy forces, a secondary recirculating flow appears in the upper zone of the reactor as the porous bed contracts.

In addition, an important mathematical framework was tested and validated, although some differences were observed in the flow fields. These differences can be attributed to numerical uncertainties. Although the governing physical equations were formulated in the same way in both analyzes, in the study by Bittencourt (2023) and in the present work, COMSOL does not handle classical physics interfaces such as the Brinkman equations, heat transfer in fluids, and heat transfer in solids in the same manner as a model implemented through generic PDE interfaces. The built-in physics modules

apply their own discretization strategies and stabilization methods, which are not automatically reproduced when the equations are manually defined using the Coefficient Form PDE or the Stabilized Convection–Diffusion interfaces. As a result, even when the same mathematical equations are imposed, the two models rely on numerically different formulations, leading to variations in the flow fields, especially in regions where recirculation, sharp gradients, or viscous effects depend strongly on the numerical treatment.

As mentioned in Section 3.4.1, the use of the generic PDEs provided by COMSOL offers more flexibility to adapt the equations and physical phenomena involved, especially in smoldering combustion, which requires complex equations with several independent variables and associated physical and chemical parameters. This mathematical complexity becomes even greater when using an axisymmetric configuration together with transient simulations.

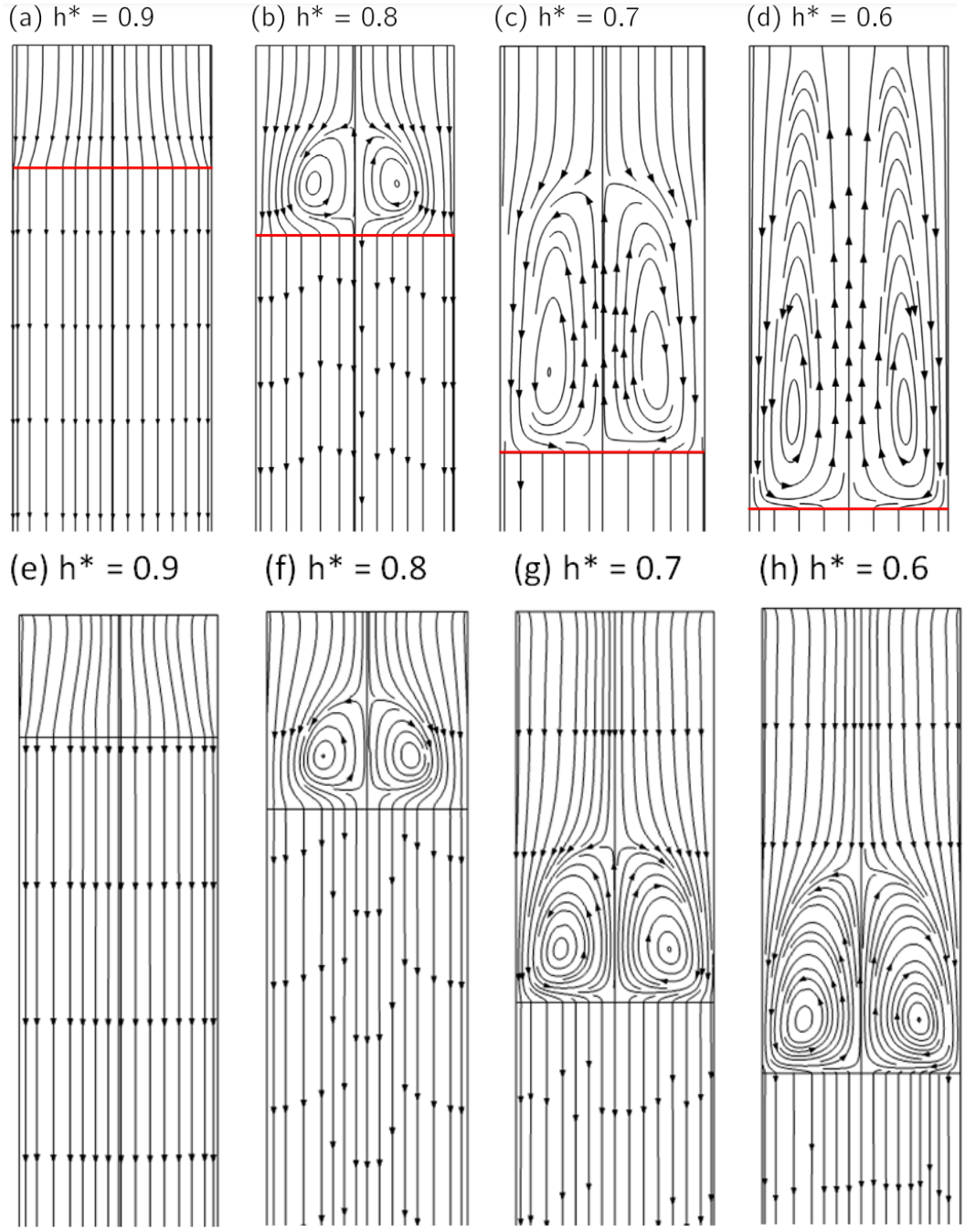

Figure 4.1: Comparison with Bittencourt (2023): Streamlines at various stages of pore bed contraction. Subfigures (a), (b), (c), and (d) are derived from the work of Bittencourt, while subfigures (e), (f), (g), and (h) correspond to the same stages of pore bed contraction for this work, respectively. Developed by the authors.

An important result of the author referenced in this case study was that the intensity of the recirculation reduces the supply of oxygen necessary for the combustion chemical process to occur. This can be better visualized in Figure 4.2, where, for a contraction of about 40% ($h^* = 0.6$), it is possible to observe that the streamlines are squeezed toward the wall near the porous interface, implying a variation in the thickness of the boundary layer (green line in the graphic) that feeds the thermochemical phenomena occurring inside the porous layer. It is also possible to see how the flow velocity profile (blue line in the graphic) is distorted by the recirculation caused by buoyancy forces in the fluid domain. This supports the conjecture of Fernandez (1996) [2], which described the behavior of forced flow in a conduit under the influence of buoyancy forces. In addition, the temperature gradient increases near the wall as a result of the temperature difference between the fluid and the wall. Additionally, it can be observed that near the axisymmetric contour, the flow is hotter than near the wall (red line in the graph). This behavior is expected because of the recirculation, which moves the flow upward and transports heat from the upper part of the porous bed, where the combustion front is located.

Additional results are discussed in the research of Bittencourt (2023) [1]. However, these discussions are not addressed here, as the main objective was to reproduce the same case study using the generic COMSOL PDE interface. This generic approach allows for the development of more advanced simulations in the future that involve increased physical and geometrical complexity.

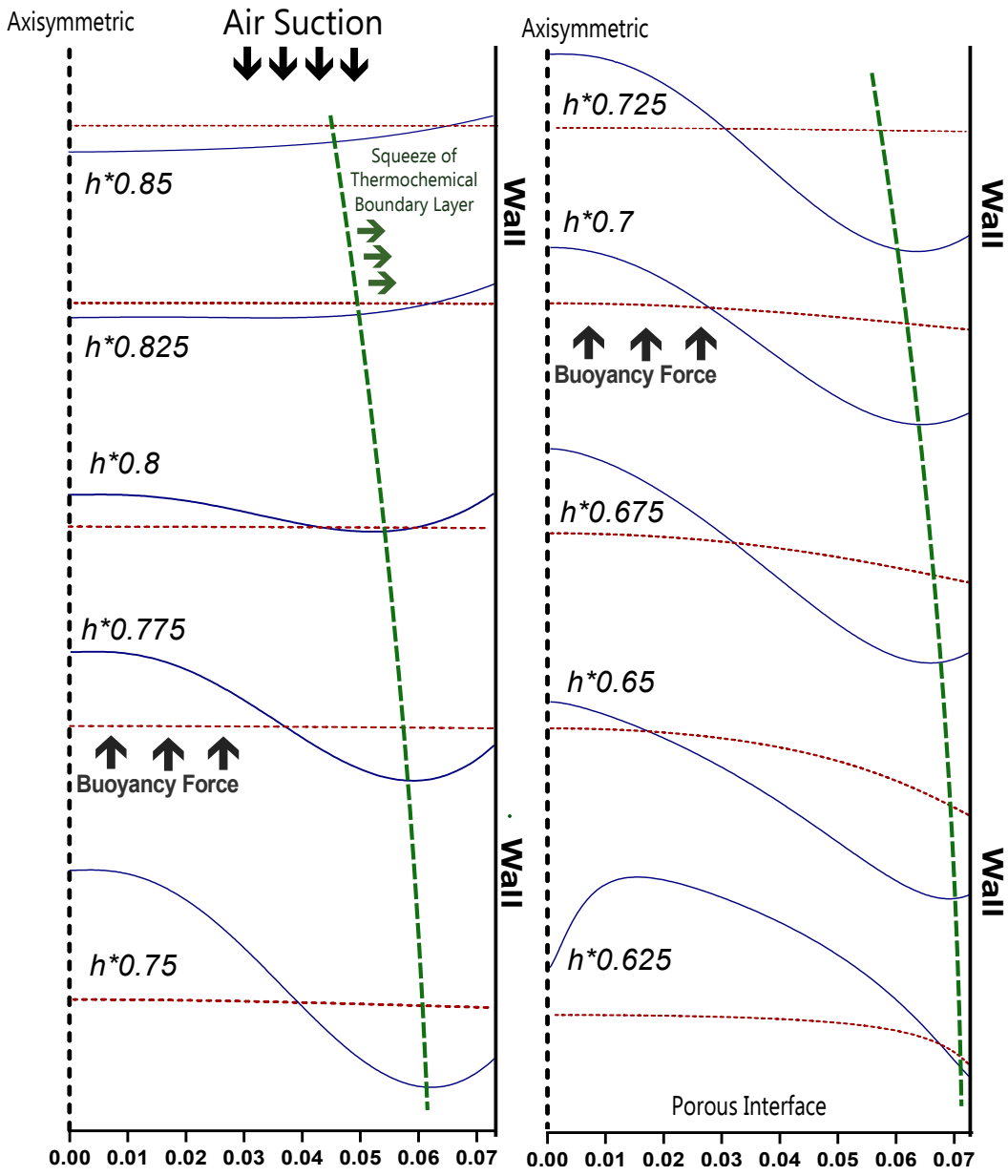

Figure 4.2: Deformation of the longitudinal velocity profile, fluid temperature variation and compression of the boundary layer that feeding thermochemical phenomena, considering ($h^* = 0.6$). Blue line: Velocity profile. Red line: Temperature profile. Green line: Compression of fluid boundary layer that feeds the thermochemical phenomena. Developed by the authors.

4.3 Results - Cooling of a porous bed

The temperatures measured by the thermocouples in the experimental study by Martins (2008) [3] closely approximate the solid-phase temperature in this numerical simulation of this work. Figure 4.3 illustrates the comparison and highlights the approximate maximum error observed at a specific time step for each thermocouple evaluated. The reason for these error values can be due to the manner in which the mixture was prepared following the method described by the author of reference, using water to form a conglomerate of charcoal and sand; some residual moisture may have remained in the interstitial spaces of the porous bed after drying overnight. Evaporation by mass transport probably occurred in reality and was not considered in the simulation, which explains part of this discrepancy. This evaporation likely intensified the cooling process, and as a result, some model parameters needed to be adjusted to achieve better agreement with the experimental observations. This effect is likely to occur with greater intensity near the middle and lower of the reactor, where the airflow that percolates the porous bed during the overnight drying is less intense. This hypothesis is supported by the fact that the thermocouples T3 and T12 exhibited a temperature difference of approximately 25% and 15%, respectively. Thus, the model performs better near the upper regions of the reactor, where the errors are smaller compared to the central and lower zones of the porous bed.

It is worth highlighting that the temperatures of both phases remained very close throughout the entire simulation, even though an LTNE approach was adopted. This behavior indicates that heat transfer between the solid

and fluid phases is highly efficient under the thermal conditions analyzed. Because the temperature differences are small, the cooling process evolves slowly across most regions of the porous domain, which is consistent with the thermal inertia observed experimentally. This result also allows us to conclude that an LTE assumption would be adequate for this specific case, since the system operates at relatively low temperatures and both phases exhibit nearly identical temperature evolution over time. LTNE becomes more relevant in high temperature applications such as smoldering combustion, where strong thermal gradients and reaction-induced heating can generate significant solid–fluid thermal disequilibrium with peak temperatures approaching 1000 °C. Yet is important to mention that Martins (2008) imposed a velocity flux of 0.0538 [m/s] at the top of the cylinder during the test [3]. However, the numerical simulation showed a velocity range of 0.035 - 0 [m/s] inside the porous medium, with values equal to zero near the wall and a little small when compared with the flux imposed at the top. The values founded are coherent and expected because the packed particles create resistance to the flow that depends on the permeability of the bed. In general, the results obtained for case 02 show that the model, although designed for smoldering combustion, can also be applied to other types of process, such as the cooling of a porous bed described in this section. This reinforces that the model is capable of simulating inert porous-bed conditions as well.

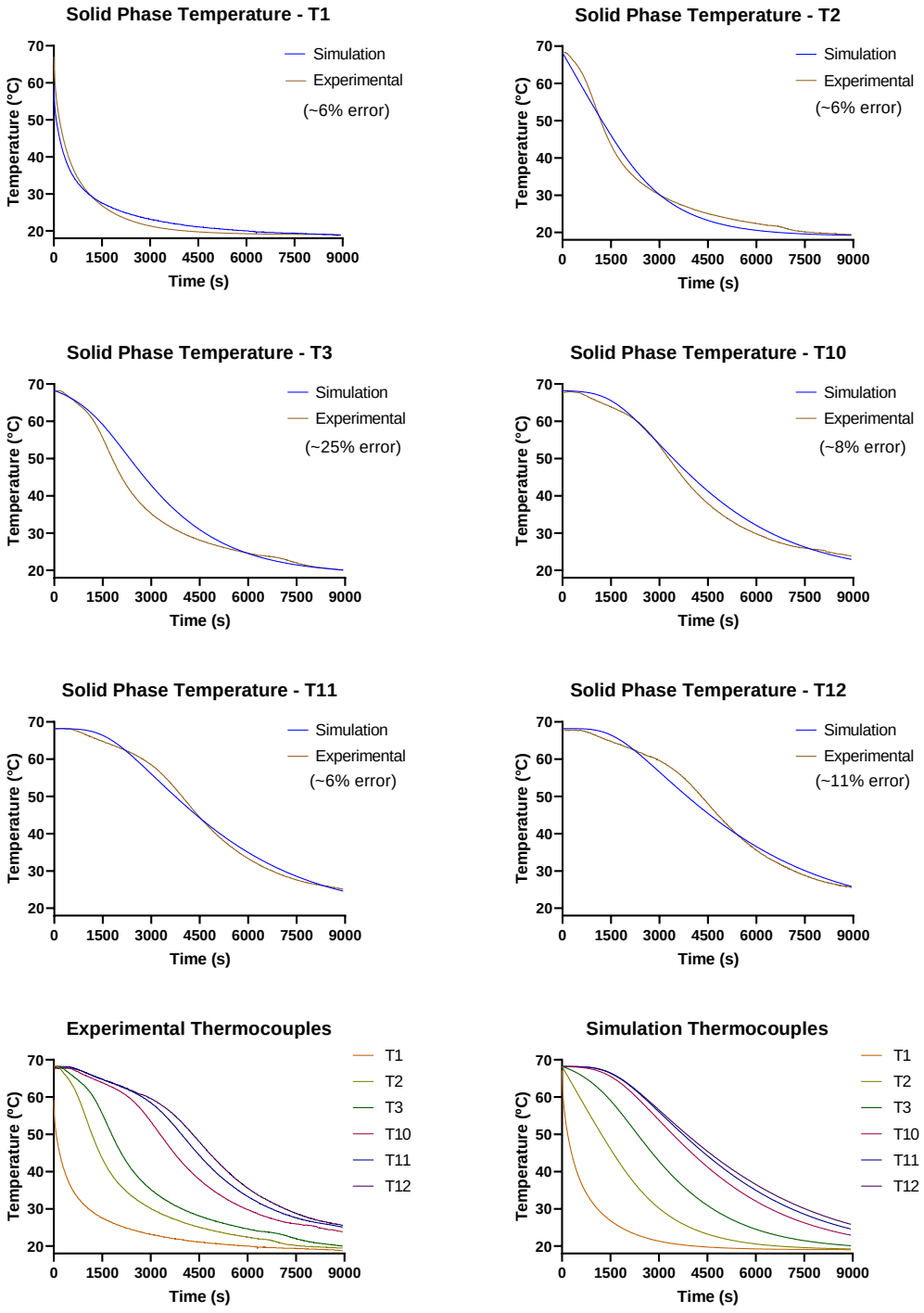

Figure 4.3: Comparison between a experimental test and simulation propose in the Section 3.4.2. Developed by the authors.

4.4 Results - Combustion in porous bed

The temperatures measured by the thermocouples in the experimental study by [3] also closely approximate the solid-phase temperature obtained in this numerical simulation. Figure 4.4 presents the comparison for each thermocouple. The discrepancies observed in the graph can be attributed to the complexity of smoldering combustion, as well as to certain assumptions and simplifications in the model, such as: no bed contraction was considered ([3] reported an axial bed contraction of 16%); a simplified chemical structure, considering only oxidation as the dominant chemical phenomenon occurring in the interstitial zone; among other effects.

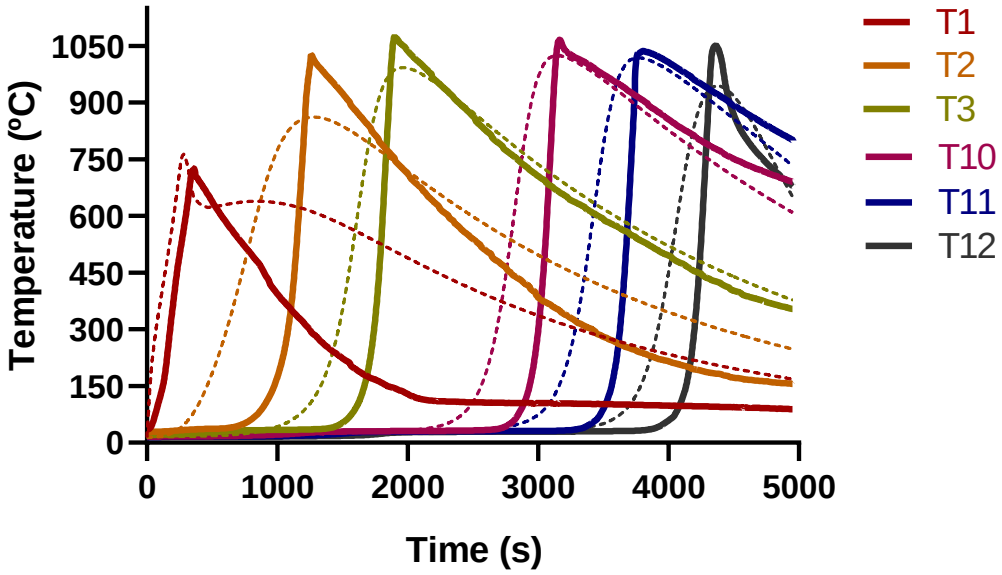

Figure 4.4: Comparison between the experimental test and the simulation proposed in Section 3.4.3. The continuous line corresponds to the temperature measured by thermocouples, while the dashed line represents the result obtained through the numerical simulation. Developed by the authors.

In general, the model performs better in the middle and lower regions of the reactor, where the differences between the curves are smaller compared to the top region of the porous bed. This can be seen in more detail in Figure 4.5. The peaks and slopes of the curves for thermocouples T3, T10, T11, and T12 are quite similar, while thermocouples T1 and T2 do not show such satisfactory behavior. For example, in T1, the temperature remains high after ignition of the combustion. This probably happens because the convective heat loss in the boundary conditions in the top region of the reactor need more refinement during the model to reach the correct behavior with the reality, which caused the solid phase to cool more slowly. The second thermocouple did not reach the peak temperature measured in the experiment, probably because the equation of the chemical structure model was not complete because it considers only oxidation as a single chemical phenomenon. Mainly in the top region, evaporation and devolatilization can be very important to consider for the temperature behavior in the bed. Overall, all thermocouples recorded peak temperatures close to those measured experimentally. The thermocouple near the surface (T1) registered a peak temperature of about 750 °C, while others along the axis (T3, T10, T11, and T12) showed peaks around 1050 °C, except for T2, whose peak was less similar. Some parts of the dimensionless solid-phase energy equations and some boundary conditions were slightly adjusted on the bases of the trends observed in the numerical simulation. After these adjustments, the calibrated parameters resulted in interstitial and external heat transfer coefficients of about 66 – 68 $W/m^2 \cdot K$ and 0.172 – 20 $W/m^2 \cdot K$, respectively.

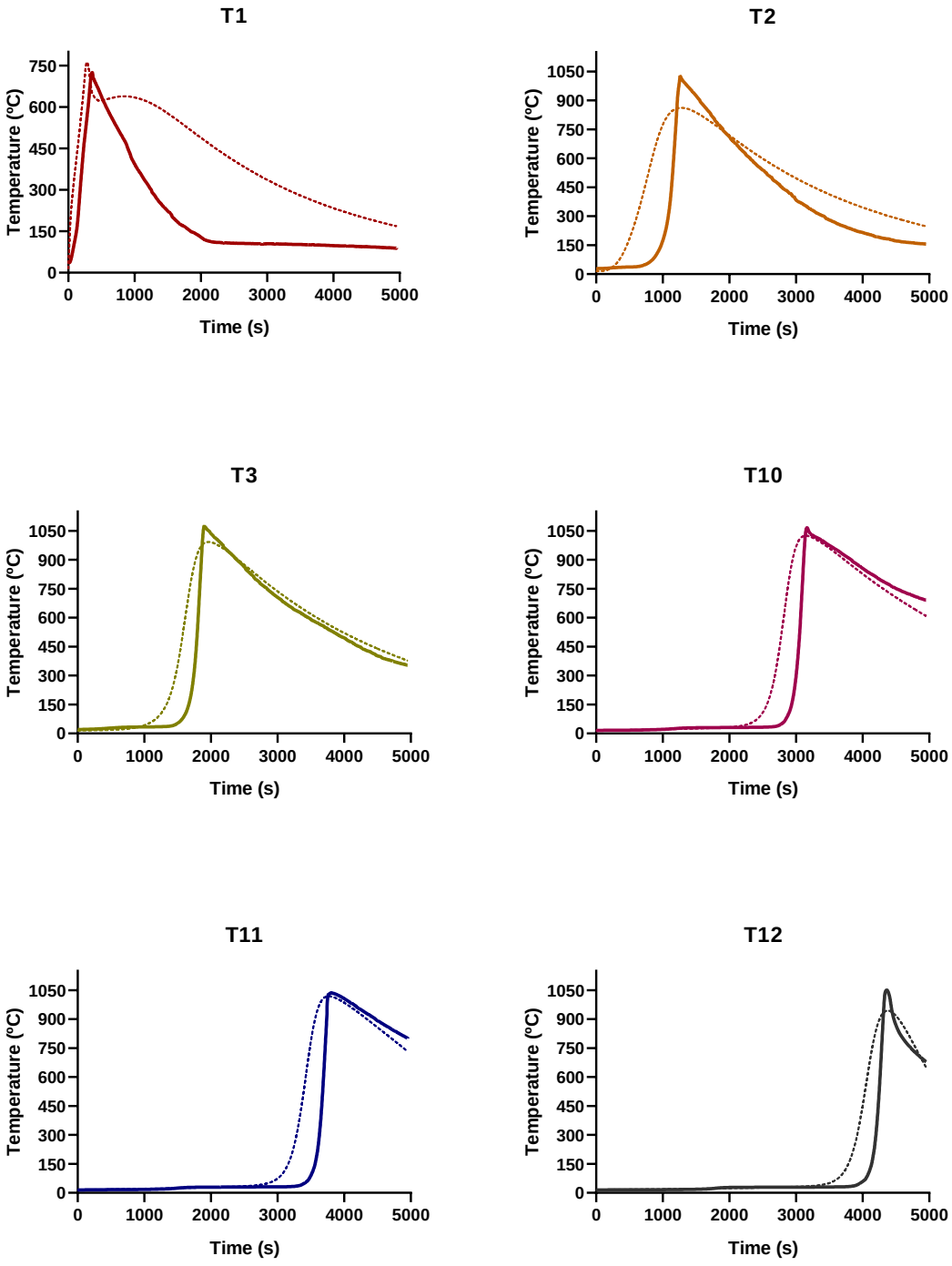

Figure 4.5: Comparison between each experimental and simulation thermocouple. Developed by the authors.

Although adjustments were made to the dimensionless solid energy equation, the expected physical behavior occurred well, and the combustion front propagated downward through the porous bed, as shown in Figure 4.6. In the figure cited before, a kind of "red heat zone" can be observed moving across the porous bed, with its size and diameter changing as time progresses and the temperature intensity varies. As the front moved downward, the temperature behind it decreased as a result of heat loss through the walls and the entry of cold air into the smoldering reactor. This behavior aligns well with the experimental observations reported by different authors in the literature.

Although the overall thermal behavior of the combustion front was satisfactory, the shape and size of the combustion front, characterized as a red heat zone, were not as expected (Figure 4.6). A thinner combustion front leaving a smaller amount of residual heat behind was expected, since this behavior would result in a temperature–time curve for each thermocouple with a slope closer to 90°, as observed in the experiments. The discrepancy in the shape and size of the combustion front may be due to the use of a Nusselt correlation (Eq. 3.23) that is not such appropriate for low Reynolds numbers, as typically found in smoldering combustion applications like that. In addition, the excessively large combustion front can be associated with an overestimated solid-phase reaction rate, suggesting that the parameter values used in this equation 3.27) were not accurately used and require revision.

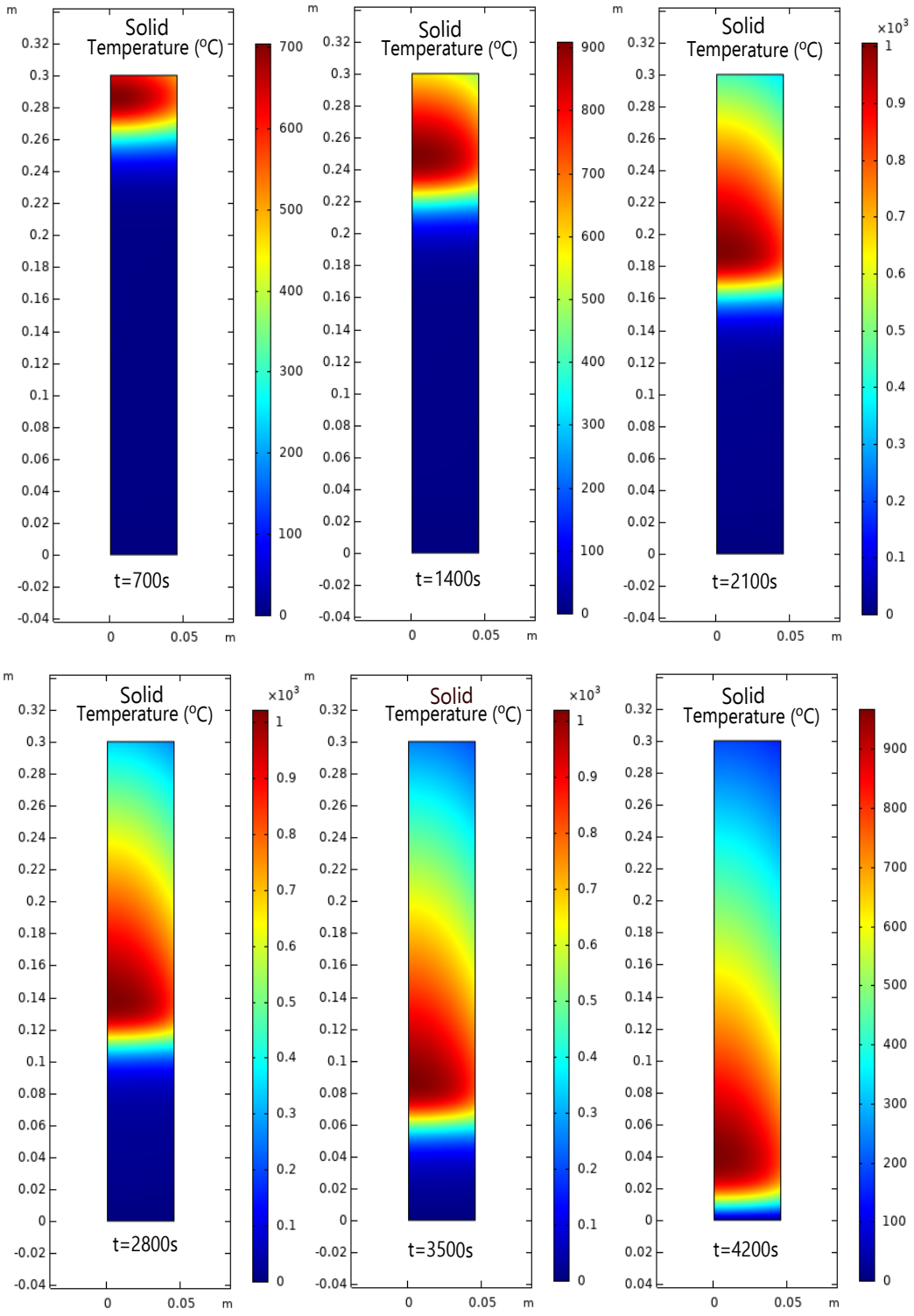

Figure 4.6: Front combustion evolution downward across the porous bed. Developed by the authors.

Martins (2008) imposed a Darcy velocity of 0.024 m/s at the top of the reactor during the test. In the simulation, the velocity inside the porous medium ranged from 0.025 m/s to zero, with values near zero close to the wall and slightly lower than the imposed flux at the top. However, the flow accelerates in some regions of the porous domain, mainly near the combustion front. These results make sense because, although the particles create resistance to the flow, higher velocities are expected in areas of elevated temperature. In these regions, the air becomes highly heated, less viscous, and flows more easily through the pores.

During smoldering experiments with imposed airflow, the pressure inside the reactor does not remain constant over time. This occurs because of bed contraction, temperature variations, and the movement of the combustion front. In this case study, however, the airflow imposed at the top was assumed to be constant, and the pressure was observed to decrease gradually throughout the reactor, this can be another specific factor that disturbs the model to reach more accurate results. Figure 4.7 illustrates the variation of pressure in the domain; the reduction of the solid phase mass fraction to zero behind the smoldering combustion front, due to the consumption provided by the chemical reactions; and the influence of elevated temperatures near the combustion front on the specific mass of the fluid, all during the intermediate time of the experiment.

The pre-exponential value, activation energy and solid phase enthalpy were defined through numerical tests until achieve results consistent with the experimental data. Initially, tried to use the same kinetic reaction parameters

reported by [3], but the behavior was not satisfactory. Using 54.2 [kJ/mol] for activation energy and 9.1 [1/s] for the pre-exponential factor resulted in an intense and uncontrollable reaction rate. A review of the literature indicated that for coal combustion, typical values are close to 20 [kJ/mol] for activation energy, close to 1 [1/s] for the pre-exponential factor and 30 [MJ/kg] for the enthalpy, which is approximately the values adopted in this study: 23.25 [kJ/mol] for activation energy, 0.327 [1/s] for the pre-exponential value and 32 [MJ/kg] for the solid phase enthalpy, both within the same order of magnitude as those reported in the literature [4–6]. It is also important to note that [3] modified his pre-exponential value to 0.50925 [1/s] for use in his numerical simulations. The different activation energy, pre-exponential value and enthalpy used in this study are justified because they allowed the simulation to successfully reproduce the experimental results. Such parameter adjustments are a common and accepted practice in modeling complex systems such as smoldering combustion.

As mentioned before, certain portions of the solid energy equation were adjusted for validation purposes. The final magnitudes of these terms are presented in Table 4.2. The main adjustments include: an increase in the transient term in the energy equation of the solid phase, which is responsible for maintaining thermal inertia during the heating and cooling of the material; a reduction in the conduction term in the same equation to control the smoldering front propagation rate and minimize heat loss through the walls; and an increase in the boundary condition terms related to heat loss at the reactor wall and at the reactor top, due to the interaction of cold air

with the heated wall and with the hot solid phase in the top region; the terms related to the interstitial heat transfer between different phases and the source term provided by the chemical reaction do not need to be altered but are shown in Table 4.2. However, in conclusion, the numerical model successfully reproduced the experimental behavior observed by Martins (2008) [3].

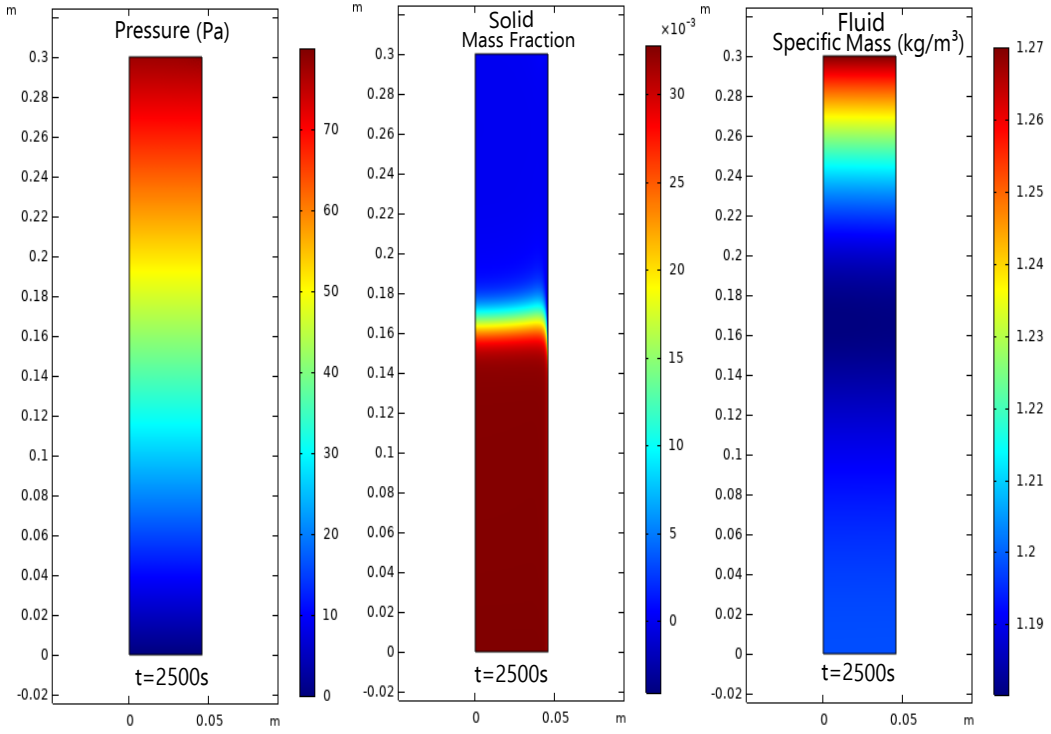

Figure 4.7: Pressure, solid mass fraction and fluid specific mass behavior across the reactor for 2500 seconds. Developed by the authors.

Table 4.2: Term's magnitudes of the different portions of the equations - case 03.

Describe	Structure	Order of magnitude
Transient portion of solid phase energy equation	$(1-\varphi)m^{*}_{part}Pe$	10^{2}
Diffusivity portion of solid phase energy equation	$(1-\varphi)$	10^{0}
Heat exchange in the interstitial zone of the porous bed	Bi_{int}	10^{2}
Chemical heat source in the interstitial zone of the porous bed	$\tau_s \frac{A_{rr}}{Q_f^{stg}} H_s \dot{R}_s^{dev}$	10^{5}
Heat loss of the solid phase in the reactor wall	Bi_{ext}	10^{-2}
Heat loss of the solid phase through in the reactor top	Bi_{ext}	10^{-2}

References

1. Bittencourt, F. L. F. *TOWARD A SAFE AND CIRCULAR THERMOCHEMICAL PROCESS TO SANITIZE HUMAN FECES IN RESOURCE-POOR ENVIRONMENTS* PhD thesis (Universidade Federal do Espírito Santo, 2023).
2. Torero, J. & Fernandez-Pello, A. Forward smolder of polyurethane foam in a forced air flow. *Combustion and Flame* **106,** 89–109. ISSN: 0010-2180 (1996).
3. Ferreira Martins, M. *Structure d'un front de combustion propagé en co-courant dans un lit fixe de schiste bitumineux broyé* PhD thesis (Diss. Toulouse, 2008).
4. Zanoni, M. A., Torero, J. L. & Gerhard, J. I. Delineating and explaining the limits of self-sustained smouldering combustion. *Combustion and Flame* **201,** 78–92. ISSN: 0010-2180. https://www.sciencedirect.com/science/article/pii/S0010218018305212 (2019).
5. Nunes, K. G. P. & Marcilio, N. R. Determination of the kinetic parameters of Oxy-fuel combustion of coal with a high ash content. *Brazilian Journal of Chemical Engineering* **32,** 211–223 (2015).
6. Bews, I., Hayhurst, A., Richardson, S. & Taylor, S. The order, Arrhenius parameters, and mechanism of the reaction between gaseous oxygen and solid carbon. *Combustion and Flame* **124,** 231–245 (2001).

Chapter 5

Conclusions and further work

The research on smoldering combustion, its applications, the challenges of numerical simulations in this field, and the classical physical representation of some dimensionless numbers contributed to a deeper understanding of the mathematical modeling of the phenomenon simulated in this work. It also clarified the considerations and simplifications adopted by different authors in this field and the complications that these choices can introduce into the results of numerical simulations.

This knowledge made it possible to decide on a new approach to the dimensionless groups that can characterize smoldering combustion. The use of dimensionless temperature based on chemical kinetic parameters and dimensionless time as a parameter related to the porous bed contraction represents a new way of studying smoldering combustion simulations. By this analysis it was possible to obtain a governing equation structure composed of both classical and new dimensionless numbers, as well as new characteristic scales of smoldering phenomena, each contributing to the understanding of the process. Future studies should further investigate the real influence of each

new parameter on the dynamics of smoldering, with the aim of quantifying their impact on the processes of advection, accumulation, and diffusion of heat and mass during this phenomenon.

In general, conducting three different case studies, each based on different contexts and physical mechanisms, was valuable for testing and evaluating the performance of the computational model developed in this work. The behavior observed in the final case study demonstrates that the model can simulate smoldering combustion using a new dimensionless analysis, which was one of the main objectives of this work, although some adjustments and new tests are still necessary. Furthermore, in case study 1, which occurred at the fluid–porous interface, the numerical simulation successfully reproduced the behavior observed by Bittencourt (2023), including the formation of secondary recirculating flows in the upper zone of the reactor due to buoyancy forces. The results highlight how flow recirculation affects oxygen supply, boundary layer thickness, and temperature distribution within the porous bed. The use of COMSOL's generic PDE interface proved effective in capturing these complex phenomena and provided a reliable foundation for more advanced future simulations with increased physical and geometrical complexity, allowing the formulation of mathematical equations with additional terms and components. In case study 2, known as the cooling of a porous bed, the numerical model accurately reproduced the experimental temperature trends reported by Martins (2008), especially in the upper regions of the reactor. These results demonstrate that the model can simulate an inert process in a porous bed, without chemical reactions, providing predictions of temperature profiles and

thermal behavior throughout the reactor.

In case study 3, named combustion in a porous bed, the temperature profiles and the propagation of the combustion front in the reactor showed good agreement with the experimental data. It was possible to observe solid consumption along the length of the reactor as the combustion front propagated downward through the porous bed. Adjustments to the solid energy equation, boundary conditions, and kinetic parameters were necessary to allow the model to capture the key physical phenomena. For this last case, new tests using a more appropriate Nusselt correlation, revision of some variables, and a more detailed chemical modeling are necessary. It is believed that this also contributed to the need to adjust portions of the governing equations discussed previously. For future work, it is proposed to simulate smoldering phenomena in which the porous domain is reduced in size during the simulation, following the contraction velocity measured experimentally. It has already been observed that COMSOL Multiphysics provides a physical feature known as the Deformed Geometry functionality, which allows this type of domain contraction to be implemented during the simulation time steps. Therefore, in general, many research efforts can still be carried out in this field, as the model proposed here leaves research gaps for further numerical and experimental investigations.

Appendix A

Appendix

A.1 Presented paper in the ENCIT 2024

This section presents a paper published in the international congress ENCIT (Brazilian Congress of Thermal Sciences and Engineering), which took place at the end of 2024. The paper compares simulations conducted in a smoldering combustion reactor, considering a porous interface and a contraction of the porous medium. In this comparison study, a mathematical model was tested and confirmed using a basic physics tool from COMSOL called Partial Differential Equations (PDE) to set up the main equations needed to solve the smoldering combustion problem. Like in the work of Bittencourt (2023), the model showed the same flow patterns, identifying recirculation areas caused by natural convection. It was also possible to measure the thickness of the boundary layer, showing how the flow gets squeezed near the reactor walls. The paper was presented as an oral presentation and will be included in the conference proceedings.

ENCIT2024
20th Brazilian Congress of Thermal Sciences and Engineering

ABCM Associação Brasileira de Engenharia e Ciências Mecânicas

20th Brazilian Congress of Thermal Sciences and Engineering
November 10th–14th, 2024, Foz do Iguaçu - PR - Brazil

A TWO-DIMENSIONAL MODELING OF A PERMEABLE FLUID-POROUS INTERFACE IN COMSOL MULTIPHYSICS

Ruan Schultz Riguetti
Márcio Ferreira Martins
Gabriel Gusmão Almeida
André Veríssimo Xavier
Multiphysics Modeling Laboratories (MM Labs), Department of Postgraduate Studies in Mechanical Engineering, Federal University of Espírito Santo (UFES), Brazil.
ruan.riguetti@edu.ufes.br
marcio.martins@ufes.br
gabrielgusmaoalmeida@hotmail.com
andre.xavier@edu.ufes.br

Flávio Lopes Francisco Bittencourt
Federal Institute of Science, Technology, and Education of Espírito Santo, Piúma, Brazil
flavio.lopes@ifes.edu.br

Abstract. *The smoldering combustion process has been studied from various perspectives and in different contexts. One device responsible for enjoying this process is the vacuum-induced reactor for pyrolysis. It performs pyrolysis in your central zone through the smouldering combustion that occurs in your annular zone. Furthermore, the reactor is open at the top, this intensifies the natural convection process in the upper zone of the device. Buoyancy forces may compete with the airflow entering the reactor, resulting in recirculation zones and stagnating the smoldering front. From the moment the thermal plume starts to grow, the boundary-layer is squeezed to the reactor wall, gradually quenching the combustion front. The objective is to model the heat transfer problem in a vacuum-induced smouldering reactor using generic Partial Differential Equations (PDEs) provided by COMSOL Multiphysics. Therefore, intend to address the main physical characteristics involved in a permeable fluid-porous interface through a similar case study known in the literature. The momentum and energy transport equations were employed to mathematically describe the problem. The COMSOL physical-mathematical models, namely the Coefficient Form PDE and the Stabilized Convection-Diffusion Equation, were utilized to formulate the governing equations, incorporating tensor analysis. The dimensional groups selected for modeling the problem were defined through dimensional analysis conducted by a researcher. By varying the identified dimensional numbers and terms, it is possible to evaluate how each physical phenomenon influences heat exchange effects in the permeable fluid-porous interface of the reactor. Furthermore, the validity of the PDE modeling was confirmed by comparing current lines with a case study proposed by an author in the same study area. Due to the secondary flow comprising recirculations within the fluid domain, it is observed that the streamlines are squeezed towards the wall, indicating a variation in the boundary layer thickness that feeds the thermochemical phenomena occurring inside the porous layer. For future analysis, the use of COMSOL's mathematical physics module, like those used in this work, allows greater flexibility in modeling equations in dimensionless form and including another important physics present in the system.*

Keywords: *pyrolysis, natural convection process, boundary-layer, dimensional analysis.*

1. INTRODUCTION

1.1 Contributions to the state of art

Smouldering combustion has been studied by many ambiental contexts (Torero, 2020), for example: heating of waste piles for international treatment of contaminated soil and reducing the volume of landfills. It can be differentiated mainly due to the geometry of where combustion occurs, ignition source and burning direction propagation modes. The forward propagation mode is more used in experiments because towards the heat to the fuel (Zanoni *et al.*, 2019a). Forward smouldering has been intentionally applied as a degradation technique for liquid and solid contaminants, are they: oils, tar, biosolids. Experimental work had the idea of using the smoldering combustion mechanism and the pyrolysis process to transform, for example, feces into solid and gaseous products without pathogens, in other words, to sanitize this raw material in a certain way (Bittencourt, 2023). As well as transforming polyethylene into a material with energy potential,

aiming to recover hydrocarbons (Duque, 2021). The pyrolysis process is endothermic and, depending on the way it is carried out, it suffers significant heat losses. Large losses often result in the need for continuous supplement inputs. However, smouldering is highly controllable, since the rate of fuel consumption is generally proportional to the mass flow of air entering the reactor, and this is easily controlled in specific systems (Torero, 2020). Therefore, smouldering combustion technology appears to be an alternative resource to performing pyrolysis and with good viability.

In the smoldering combustion process aiming to perform pyrolysis, several parameters contribute and influence the operating efficiency of the device, or even the chemical composition of the material obtained after the experiment, these are: heating rate, residence time, type of reactor and operating pressure (Duque, 2021). Not to mention the many other variables that exist in the problem, both related to the characteristics and composition of the chosen porous medium, as well as the material on which the pyrolysis will be carried out (Ferreira Martins, 2008). In cases like this, the non-dimensionalization procedure of the equations appears to facilitate the analysis of results in numerical simulations, after all, this procedure increases the researcher's perception of the relationships between the parameters, reduces the number of variables in the problem and allows the extrapolation of untested values (Çengel, 2007). This type of procedure has already been implemented in works focused on this area, such as: (Bittencourt and Martins., 2022).

Smouldering combustion modeling may be of interest: estimating the resistance to ignition by smouldering combustion, the rate of production of toxic chemical species, how heat transfer occurs within a piece of equipment, in addition to visualizing how the movement of oxygen occurs to feed the combustion process. It also appears when experimental tests are financially unfeasible, such as in reduced gravity environments. To model it in detail, it is suggested to include the chemical reactions that occur in the solid fuel and consider the chemical kinetics that govern the global rate of heat and mass release in the process (Rein *et al.*, 2006). Thus, advanced smoldering combustion models require quantitative information about the heterogeneous reactions occurring in the solid. Therefore, the smouldering combustion modelling require appropriate analyse about chemistry and heat transfer. Smouldering kinetic mechanisms are described, typically, terms of Arrhenius equations. Furthermore, there is two approaches for designed the smouldering models treat heat transfer: Local Thermal Equilibrium (LTE) and Local Thermal Non-Equilibrium (LTNE). The first one former assumes that the gas and the solid are in thermal equilibrium while the latter allows for heat exchange between them (Zanoni *et al.*, 2019b).

1.2 Physics involved in fluid-porous interface

One device responsible to enjoy the phenomena is the vacuum-induced smouldering reactor, how can visualize in the Fig. 1.

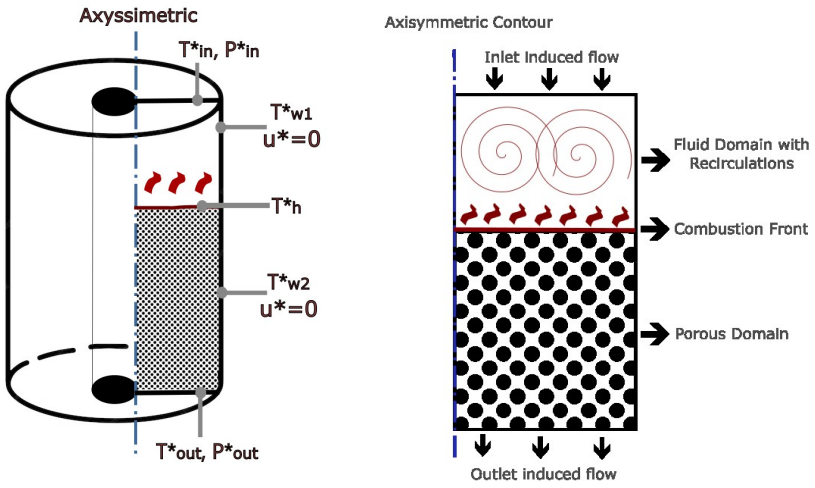

Figure 1. A permeable fluid-porous interface in a vacuum-induced smouldering combustion reactor for pyrolisis. Developed by the authors

This device performs pyrolisis in your central cylindrical zone through that smouldering combustion that occur in your annular cylindrical zone (combustion zone). As the combustion front burns the porous bed from top to bottom, this layer reduces in size during the time, and this is responsible for create a fluid domain in the upper zone of the reactor. The device is open at the top and this intensifies a natural convection process (Bittencourt, 2023). These effects are still insignificant when the contraction is small, however, from the moment the combustion front begins to expand in width, the effects of natural convection begin to "compress" the airflow boundary layer against the walls of the combustion chamber, slowing the progress of the combustion front and gradually extinguishing it. Furthermore, there is air suction through a pump located at the bottom of the device responsible for sucking air and feeding the combustion (Ferreira Martins,

Nomenclature	Describe	Subscripts/Superscript	Describe
$\mathbf{u}$	Flow velocity vector	$*$	Non-dimensional
Da	Darcy Number	rad	Radiation
Pr	Prandtl Number	h	Referring to the combustion front
Gr	Grashof Number	in	Inlet
Be	Bejan number	out	Outlet
∇	Nabla operator	w	Wall
T	Temperature	r	Spacial radial dimension
P	Pressure	z	Spacial longitudinal dimension
q	Heat Transfer	∞	Referring to the environment
		p	Porous medium

2008). When the combustion happens slowly, the combustion reaction is limited by the rate of oxygen that can spread to the surface of the fuel, resulting in low temperatures and slow rates of occurrence compared to burning combustion. Smouldering combustion is characterized as self-sustaining when the occurrence of oxidation generates sufficient energy, in the form of heat, to overcome heat losses and sustain the propagation of the indefinite combustion front (Fabris *et al.*, 2017).

2. METHODOLOGY

2.1 Modelling Governing Equations with PDE's

One software commonly used for simulating diverse physics and engineering applications, especially those involving coupled phenomena and multiphysics is COMSOL Multiphysics. This software uses finite element analysis for resolution and simulation. It provides ready-made physics for computer simulation in heat transfer, fluid flow, chemical species transport problems, and many others. Many real-world applications involve simultaneous couplings in a system of Partial Differential Equations (PDEs) (Pryor, 2009). PDEs appear in numerous process engineering applications, from fluid flow problems to heat transfer. Generally, most problems lead to parabolic equations, which are time-independent and represent unsteady-state processes. In contrast, steady-state problems lead to elliptic PDEs (Wang and Cao, 2013).

In this work, the modeling of the permeable fluid-porous interface of the smoldering combustion reactor for pyrolysis was proposed using a generic PDEs provided by COMSOL Multiphysics. This approach allows for greater flexibility in modeling equations in a dimensionless format. One of the mathematical interfaces used to model the problem was the Coefficient Form PDE. This equation template provides a powerful general interface for specifying linear and nonlinear equations, including the classical Poisson's and Laplace equations. In the COMSOL interface, this PDE appears as the structure below Eq. 1:

$$e_a \frac{\partial^2 \mathbf{u}}{\partial t^2} + d_a \frac{\partial \mathbf{u}}{\partial t} + \nabla.\big(- c\nabla \mathbf{u} - \alpha \mathbf{u} + \gamma\big) + \beta.\mathbf{u} + a\mathbf{u} = f \tag{1}$$

This equation contains terms that can be transformed into advection and conduction components, and it is also possible to include source terms. The parameter $\mathbf{u}$ is a generic vector that can be used to specify all the independent variables. The coefficients e_a, d_a, c, α, γ, β, a and f can be scalar parameters, vectors, or tensors of different orders, depending on the number of independent variables chosen for modeling the problem and whether the phenomenon is isotropic or not.

Another mathematical interface available in COMSOL is the Stabilized Convection-Diffusion Equation, which has the structure below Eq. 2. In this equation, fewer components are visible, and the parameter u is not a generic vector but a unique independent variable.

$$d_a \frac{\partial u}{\partial t} + \nabla.\big(- c\nabla u + \alpha u\big) + \beta.u + au = f \tag{2}$$

COMSOL allows the insertion of domains within each PDE used in the program. In problems related to porous media, this is particularly useful for describing the different physical properties present in the permeating fluid. The boundary conditions used can include the Dirichlet Boundary Condition, which allows for the definition of a constant value for a specific parameter at the edge of the domain, as well Flux/Source conditions, which reference the Neumann Boundary Condition. The latter specifies the values that the derivative of a solution should take at the boundary of the domain.

2.2 Case study

Thought the modelling with generic PDE's, following the methodology of heat transfer and the same dimensionless group proposed by (Bittencourt and Martins., 2022), the objective is to achieve similar flow streamlines through a dimensional analysis conducted by these researchers and to demonstrated that the flux boundary layer is squeezed close to the secondary flow existent in a fluid domain. The previous numerical analysis by these authors utilized COMSOL Multiphysics, employing pre-configured modules made available by COMSOL, such as Porous Media and Subsurface Flow (Brinkman Equations), Heat Transfer in Fluids, and Heat Transfer in Solids.

The dimensional analysis obtained to (Bittencourt and Martins., 2022), five dimensionless equations were found to describe the problem. These equations pertain to mass conservation (Eq. 3), momentum conservation in the fluid (Eq. 4) and porous (Eq. 5) layers, and energy conservation in the fluid (Eq. 6) and porous (Eq. 7) layers. The dimensionless terms identified through this process are shown below. It's important to mention that the researchers adopt a single temperature model for the porous bed, characterizing a local thermal equilibrium (LTE), as show in Eq. 7.

$$\nabla.\mathbf{u}^* = 0 \tag{3}$$

$$\big(\mathbf{u}^*.\nabla\big)\mathbf{u}^* = -P^* + \nabla^2\mathbf{u}^* + G_r\big(T^*\big) \tag{4}$$

$$\big(\mathbf{u}^*.\nabla\big)\mathbf{u}^* = -P^* + \nabla^2\mathbf{u}^* - \frac{1}{D_a}\mathbf{u}^* \tag{5}$$

$$\big(\mathbf{u}^*.\nabla\big)T^* = \frac{1}{Pr}\big(\nabla^2 T^*\big) \tag{6}$$

$$\big(\mathbf{u}^*.\nabla\big)T^* = \frac{1}{Pr_p}\big(\nabla^2 T^*\big) + q^*_{rad} \tag{7}$$

By applying tonsorial calculations it was possible to transform the PDE Eq. (1) into Eq. (3), Eq. (4), and Eq. (5), and through the same process, it was possible to transform the PDE Eq. (2) into equations Eq. (6) and Eq. (7). Therefore, the Coefficient Form PDE was designed to encompass the same structure as the Brinkman Equations, meaning that through this PDE, it is possible to model governing equations related to the conservation of mass and momentum. Furthermore, the Stabilized Convection-Diffusion Equation was designed to encompass the same structure as the Heat Transfer in Fluids and Solids, meaning that through this PDE, it is possible to model governing equations related to energy conservation in the fluid and porous bed domain.

Because it is a circumferential geometry one them boundary conditions used to one edge of the reactor is the axisymmetric (Fig. 1). Other boundary conditions used by the authors (Bittencourt and Martins., 2022) are those of dimensionless constant temperature on the reactor walls, as well as at the fluid inlet and outlet. Furthermore, a dimensionless constant temperature is considered between the fluid and porous domains, which is called combustion front temperature T^*_h, and because it is always the highest temperature existing within the system, it receives the dimensionless value equal to 1. The boundary conditions related about flux are: zero velocity in the wall, prescript value of $P^*_{in} = 0$ to the top of the reactor and $P^*_{out} = -B_e$ to the bottom. In this case, the Bejan Number is responsible for characterizing the induced airflow, which competes with the free convection due to the bed shrinkage (Zimparov *et al.*, 2020). These boundary conditions, along with others, were implemented in the PDEs using Dirichlet Boundary Conditions. The locations of these conditions are shown in Fig. 1. In Tab. 1, all boundary conditions can be observed, including the dimensionless numbers obtained through dimensional analysis. All these parameter conditions were measured in a real experimental setup as proposed in (Bittencourt and Martins., 2022).

Table 1. Value of dimensionless numbers and boundary conditions to numerical analyse. Results obtained to (Bittencourt and Martins., 2022) in a real experimental measure. Developed by the authors.

Dimensionless Parameter						Temperature Boundary Conditions			
h^*	G_r x [10^-7]	Pr	Pr_p	B_e x [10^-10]	Da x [10^9]	T^*_{in}	T^*_{w1}	T^*_{w2}	T^*_{out}
0.9	0.5	0.69	2.5	16.3	1.0	0.29	0.29	0.33	0.04
0.8	2.7	0.69	2.9	13.4	1.0	0.25	0.25	0.38	0.06
0.7	7.3	0.69	3.3	10.9	1.0	0.12	0.12	0.61	0.02
0.6	18.1	0.69	3.8	7.4	1.0	0.13	0.13	0.77	0.07

3. RESULTS

A way to validate the modeling done in COMSOL through generic PDEs was to achieve the similar streamlines as those obtained for (Bittencourt and Martins., 2022). All numerical simulations proposed in Tab.1 were tested and similar behavior of the fluid flow was observed. For example, in Fig. 2 it can be compared to the results of some simulations carried out by these authors. As expected and cited in the Section 1.2, due the buoyancy forces, a secondary flow with recirculation appears in the upper zone of the reactor as the porous bed contracts.

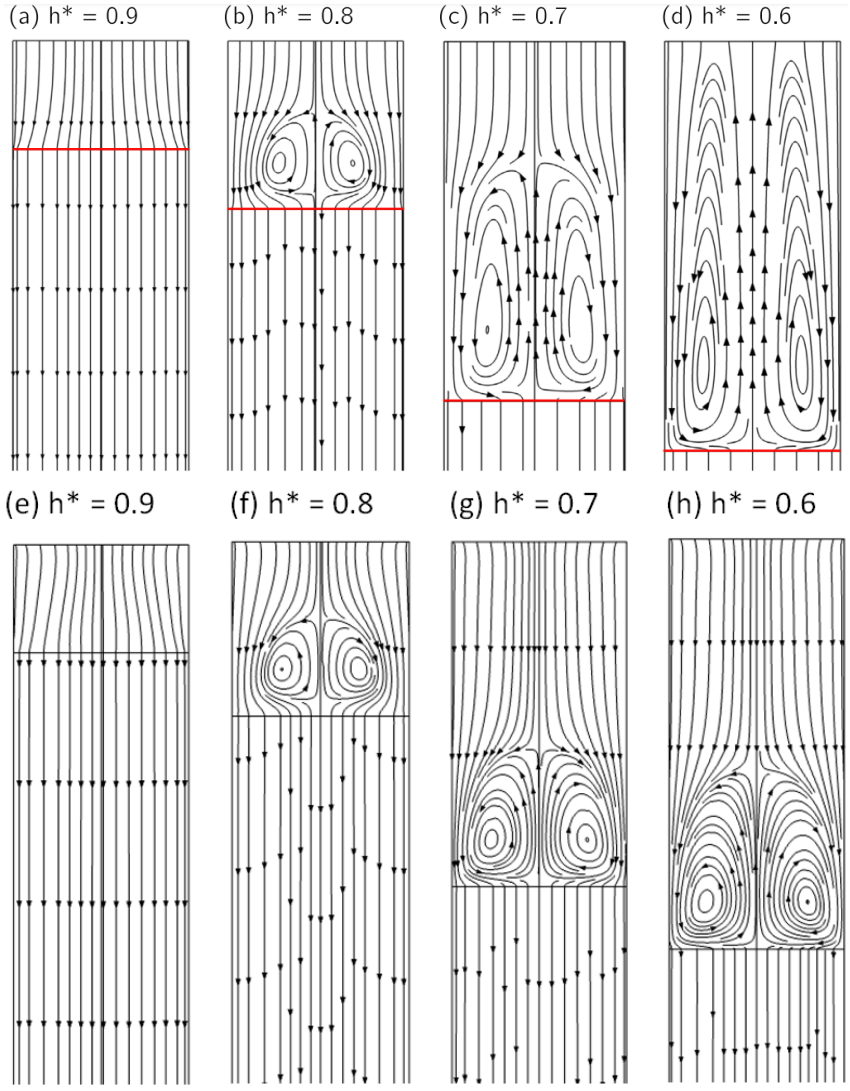

Figure 2. Comparison with (Bittencourt and Martins., 2022): Streamlines at various stages of pore bed contraction. Subfigures (a), (b), (c), and (d) are derived from the work of (Bittencourt and Martins., 2022), while subfigures (e), (f), (g), and (h) correspond to the same stages of pore bed contraction, respectively. Developed by the authors.

Furthermore, it is possible to observe that the streamlines are squeezed towards the wall when proximity of porous interface, this phenomenon can be visualized in Fig. 2, implying a thickness variation in the boundary layer that feeding the thermochemical phenomena that occur inside porous layer, as show in Fig. 3. It's still possible to see how the flow velocity profile is being distorted by this recirculations caused by buoyancy forces in the fluid domain. This proves the conjecture of (Torero and Fernandez-Pello, 1996) that showed how is the behavior of forced flow in a dute with buoyancy forces. It is possible to observe that the temperature gradient increases near the wall due to the temperature difference between the flow and the wall. Additionally, it can be noted that near the axisymmetric contour, the flow is hotter than the wall contour. This observation is expected due to the recirculation that moves the flow upwards and brings heat from the upper part of the porous bed, the region where the combustion front is located.

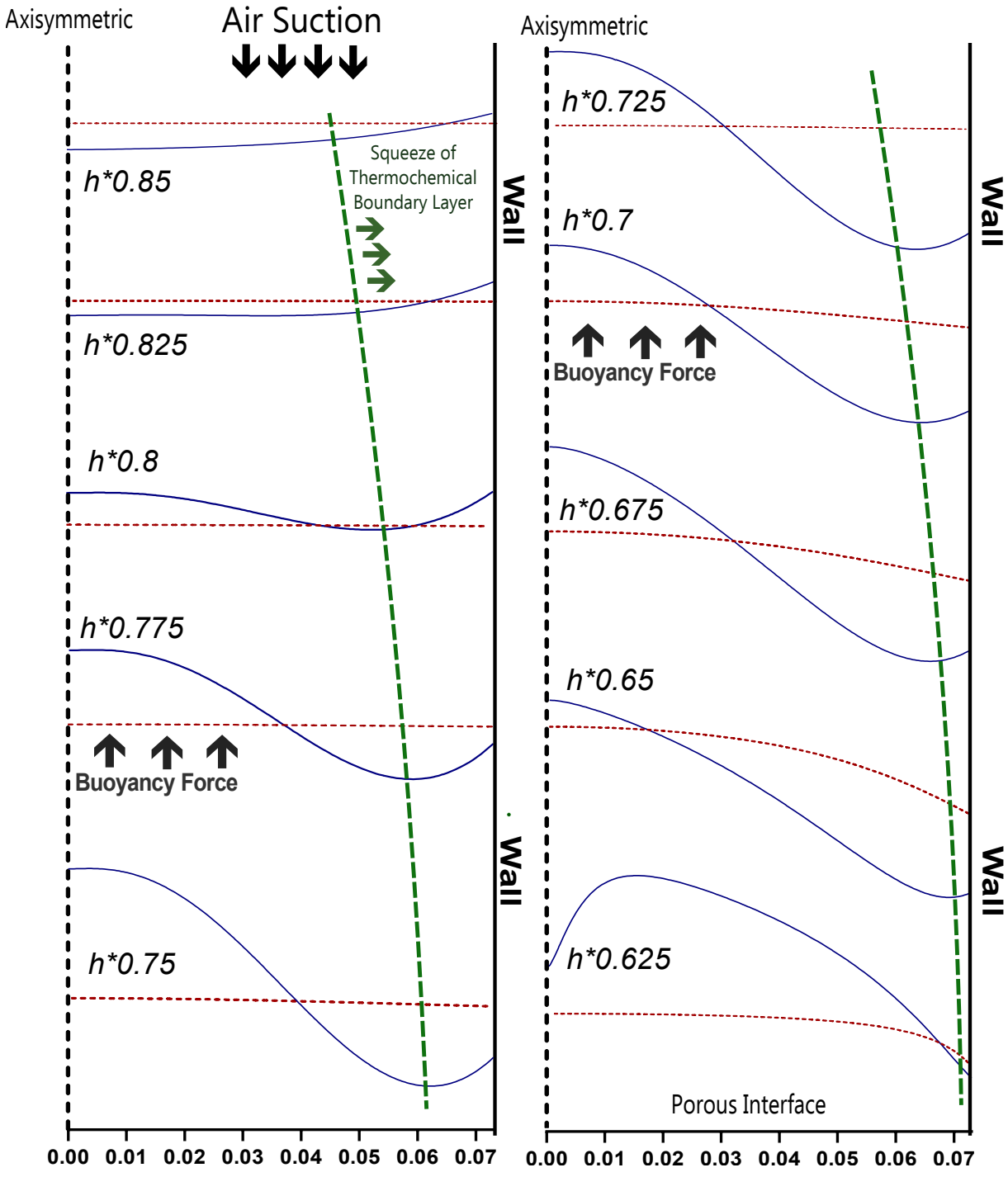

Figure 3. Deformation of the longitudinal velocity profile, fluid temperature variation and compression of the boundary layer that feeding thermochemical phenomena, ($h^* = 0.6$). Blue line: Velocity profile. Red line: Temperature profile. Green line: Compression of fluid boundary layer that feeds the thermochemical phenomena. Developed by the authors.

4. CONCLUSIONS

The heat transfer mechanisms in a porous interface were investigated using COMSOL Multiphysics. The heat transfer problem in the reactor was formulated using Partial Differential Equations (PDEs), with attention given to the effects of

buoyancy forces that causes recirculation zones, which influence the velocity of propagation of the combustion front.

A similar case study about the dimensional analysis made by (Bittencourt and Martins., 2022) was conducted to understand the interactions among the key physical parameters at the permeable fluid-porous interface of the reactor. Mathematical models, such as the Coefficient Form PDE and the Stabilized Convection-Diffusion Equation, were employed through COMSOL to represent the governing equations for mass, momentum, and energy conservation. The modeling was validated, focusing mainly on the particularity that the thickness of the boundary layer is changed proximity the interface fluid-porous. This phenomena impact the thermochemical processes within the porous medium.

Future work can expand the mathematical equations by incorporating additional physical phenomena in a dimensionless format, thus enhancing the flexibility and accuracy of the modeling. Equations about chemical species transport can be implemented and new dimensionless numbers can be evaluated and discussion.

5. REFERENCES

Bittencourt, F.L.F., 2023. *TOWARD A SAFE AND CIRCULAR THERMOCHEMICAL PROCESS TO SANITIZE HUMAN FECES IN RESOURCE-POOR ENVIRONMENTS*. Ph.D. thesis, Universidade Federal do Espírito Santo.

Bittencourt, Flávio Lopes Francisco, G.D. and Martins., M.F., 2022. "Free convection development caused by bed shrinkage in a vacuum-induced smoldering reactor". *Chemical Engineering Journal*, Vol. 430, p. 132847.

Duque, J.F., 2021. *A novel pathway to recover hydrocarbons from polyethylene residues through the combustion-driven pyrolysis process*. Ph.D. thesis, Universidade Federal do Espírito Santo (Vitória, Brasil).

Fabris, I., Cormier, D., Gerhard, J.I., Bartczak, T., Kortschot, M., Torero, J.L. and Cheng, Y.L., 2017. "Continuous, self-sustaining smouldering destruction of simulated faeces". *Fuel*, Vol. 190, pp. 58–66. ISSN 0016-2361. doi: https://doi.org/10.1016/j.fuel.2016.11.014.

Ferreira Martins, M., 2008. *Structure d'un front de combustion propagé en co-courant dans un lit fixe de schiste bitumineux broyé*. Ph.D. thesis, Diss. Toulouse.

Pryor, R.W., 2009. *Multiphysics modeling using COMSOL®: a first principles approach*. Jones & Bartlett Publishers.

Rein, G., Lautenberger, C., Fernandez-Pello, A.C., Torero, J.L. and Urban, D.L., 2006. "Application of genetic algorithms and thermogravimetry to determine the kinetics of polyurethane foam in smoldering combustion". *Combustion and Flame*, Vol. 146, No. 1, pp. 95–108. ISSN 0010-2180. doi:https://doi.org/10.1016/j.combustflame.2006.04.013.

Torero, José L., e.a., 2020. "Processes defining smouldering combustion: Integrated review and synthesis". *Progress in Energy and Combustion Science*, Vol. 81, p. 100869.

Torero, J. and Fernandez-Pello, A., 1996. "Forward smolder of polyurethane foam in a forced air flow". *Combustion and Flame*, Vol. 106, No. 1, pp. 89–109. ISSN 0010-2180. doi:https://doi.org/10.1016/0010-2180(95)00245-6.

Wang, X. and Cao, S., 2013. "Modeling paper drying with comsol multiphysics modeling tool".

Zanoni, M.A., Torero, J.L. and Gerhard, J.I., 2019a. "Determining the conditions that lead to self-sustained smouldering combustion by means of numerical modelling". *Proceedings of the Combustion Institute*, Vol. 37, No. 3, pp. 4043–4051. ISSN 1540-7489. doi:https://doi.org/10.1016/j.proci.2018.07.108.

Zanoni, M.A., Torero, J.L. and Gerhard, J.I., 2019b. "The role of local thermal non-equilibrium in modelling smouldering combustion of organic liquids". *Proceedings of the Combustion Institute*, Vol. 37, No. 3, pp. 3109–3117. ISSN 1540-7489. doi:https://doi.org/10.1016/j.proci.2018.05.177.

Zimparov, V.D., Angelov, M.S. and Hristov, J.Y., 2020. "New insight into the definitions of the bejan number". *International Communications in Heat and Mass Transfer*, Vol. 116, p. 104637. ISSN 0735-1933. doi: https://doi.org/10.1016/j.icheatmasstransfer.2020.104637.

Çengel, Y.A. e Cimbala, J., 2007. *Mecânica dos Fluidos - Fundamentos e Aplicações*. McGraw-Hill Interamericana do Brasil Ltda, Brazil.

6. RESPONSIBILITY NOTICE

This research was supported by various theoretical contributions from all the authors. We extend our gratitude to Ruan Schultz Riguetti, Gabriel Gusmão Almeida, Flávio Lopes Franscisco Bittencourt, and Márcio Ferreira Martins for their contributions to the development of the manuscript and the mathematical modeling within the COMSOL Multiphysics software. We acknowledge and thank Dr. Márcio Ferreira Martins for providing the entire computational infrastructure belonging to the Multiphysics Modeling Laboratories (MM Labs) necessary for conducting the numerical analyses. We also appreciate the valuable comments from André Veríssimo Xavier and other anonymous volunteers who helped improve the manuscript, particularly the figures.

The authors are the only responsible for the printed material included in this paper.

A.2 Presented paper in the COBEM 2025

This section presents a paper published in the International Congress COBEM (International Congress of Mechanical Engineering), which took place at the end of 2025. The paper compares simulations conducted in a cylindrical reactor for cooling a porous bed, focusing on the calibration of the heat transfer coefficient between the different internal phases. In this comparative study, a dimensionless mathematical model was implemented and validated according to the study by Martins (2008). The results show cooling curves similar to those obtained by Martins. The paper was presented as an oral presentation and will be included in the conference proceedings.

COBEM 2025
28TH INTERNATIONAL CONGRESS OF MECHANICAL ENGINEERING

ABCM Brazilian Society of Mechanical Sciences and Engineering
28th ABCM International Congress of Mechanical Engineering
November 09-14, 2025, Curitiba-PR, Brazil

COB-2025-0119
CALIBRATION OF A NUMERICAL MODEL FOR COOLING SIMULATION IN A POROUS BED

Ruan Schultz Riguetti
Márcio Ferreira Martins
Multiphysics Modeling Laboratories (MM Labs), Department of Postgraduate Studies in Mechanical Engineering, Federal University of Espírito Santo (UFES), Brazil.
ruan.riguetti@edu.ufes.br
marcio.martins@ufes.br

Flávio Lopes Francisco Bittencourt
Federal Institute of Science, Technology, and Education of Espírito Santo, Piúma, Brazil
flavio.lopes@ifes.edu.br

Abstract. *This study have the objective validate a numerical model for simulating the cooling process in a porous bed, focousing in the calibration of convective heat transfer between solid and fluid phases. The experiment performed for this calibration was conducted in a vertical cylindrical combustion chamber with an internal diameter of 91 mm and a height of 300 mm, equipped with six thermocouples distributed along the vertical axis to monitor temperature at different heights. The experimental mixture used for the porous bed contained 2340 g of charcoal and sand, with particle sizes ranging from 0.315 to 2 mm. The porous bed was prepared following a process of mixture and homogenizing of sand and charcoal, followed by an overnight drying to eliminate residual moisture. On dimensionless numerical modeling, the bed physical properties considered was entirely of the sand, as it accounted for more than 95% of the mixture used in the experimental study used for comparison. Dimensionless conservation equations for mass, momentum, and energy were applied. The comparison between simulated temperatures and experimental data temperature revealed good model performance in the upper regions of the reactor, while some discrepancies were observed in the central and lower zones. The highest percentage errors, 25% and 15%, occurred at thermocouples T3 and T12, located in the intermediate and lower regions of the cylinder, respectively, possibly due to the presence of residual moisture in the bed that remained after the overnight drying. It is likely that evaporation through mass transport occurs in reality but was not considered in the simulation, which may explain part of this discrepancy. Parts of the energy conservation equations were adjusted to improve the comparison between numerical simulation data and experimental data, along with heat transfer parameters such as the Biot and Nusselt numbers. These adjustment makes it possible to understand the behavior that each part of the equations contributes to in modeling the cooling phenomenon, and in this way, it was possible to obtain the correct magnitude of these terms. Overall, the results indicate that the proposed model is effective in simulating the cooling of the porous bed, although further adjustments are necessary to reduce the observed differences in the data. Therefore, a good numerical dimensionless model was obtained with adjusted convective heat transfer, that will contributed for simulating smoldering combustion in a cylindrical reactor in the future.*
Keywords: *Numerical model, Porous bed, Heat transfer, Cooling process.*

1. INTRODUCTION

Smoldering combustion is a slow and flameless process that occurs in porous media with limited oxygen conditions. It is considered the dominant phenomenon in large-scale natural fires, such as those in peat and coal deposits (Torero, 2020), and is also applicable in industrialized systems for heat generation and waste treatment. This process offers high thermal efficiency and small emissions compared to other combustion modes (Bittencourt, 2023), making it an attractive alternative to sustainable technologies. Its practical applications from improved oil recovery through in situ combustion, to the treatment of oil sludge-contaminated soils (Zhao *et al.*, 2021), and even to sanitation solutions for low-income regions by promoting energy-efficient destruction of human feces (Bittencourt, 2023). In these systems, pyrolysis usually is applied, as it converts organic materials into fuel products and can be sustained by the heat generated by smoldering (Gan *et al.*, 2022). Simulating smoldering combustion involves understanding several complex physical and chemical interactions. Parameters such as porosity, permeability, fluid flow, particle size, convective heat transfer, and moisture affect combustion front behavior and heat transfer within the porous domain. The assumption of local thermal equilibrium (LTE) is a common approach, as it simplifies the system and reduces the number of equations in the model by employing a single energy equation for both the fluid and solid phases. However, smoldering systems demand a more detailed description and often require modeling under local thermal non-equilibrium (LTNE) conditions to accurately

represent the distinct temperature fields of the solid and fluid phases (Zanoni *et al.*, 2019). In this context, the cooling and heating processes that occur between different phases, mainly driven how convective heat transfer takes place within the interstitial zone, are crucial for understanding self-sustaining combustion. To address these challenges, several numerical models have been developed using LTE or LTNE approaches, with increasing use of dimensionless analysis to simplify governing equations and facilitate comparison between different scenarios (Miry *et al.*, 2022)(Bittencourt and Martins., 2022)(Ferreira Martins, 2008). Dimensionless groups such as Nusselt, Biot, Prandtl, Reynolds, Peclet, and Damköhler numbers are used to analyze convective heat transfer, flow characteristics, and the balance between transport and chemical reaction rates (Wakao, 1982) (Nield *et al.*, 2006). In this study, a dimensionless numerical model was developed and calibrated to simulate the cooling of a porous bed composed primarily of sand and referred a real experiment. This will ensure accurate convective heat transfer between the phases within the porous medium in future numerical simulations of smoldering combustion.

Table 1. Describe of some parameters used in the model.

Nomenclature	Describe	Subscripts/Superscript	Describe
$\mathbf{u}$	Flow velocity vector of Darcy	$*$	Non-dimensional
$\mathbf{U}$	Interstitial flow velocity vector	f	Fluid phase
p	Pressure	s	Solid phase
T	Temperature	in	Inlet
t	Time	out	Outlet
ρ	Specific mass	$w1$	Reactor wall
λ	Thermal conductivity	r	Spatial radial dimension
h	Convection heat transfer coefficient	z	Spatial longitudinal dimension
c_p	Specific heat	int	Internal
μ	Dynamic viscosity	ext	External
ν	Kinematic viscosity	∞	Referrer to the ambient
m	Mass	MAX	Referrer to the maximum value
d	Diameter	abs	Absolute
φ	Porosity	$part$	Particle
K	Permeability		
∇	Nabla operator		
Δ	Refers to the variation		

2. METHODOLOGY

2.1 EXPERIMENTAL SETUP

The experimental setup consists in a vertical cylindrical combustion chamber with an internal diameter of 91 mm and a height of 300 mm, as described by (Ferreira Martins, 2008). Six inline thermocouples (T1, T2, T3, T10, T11, T12) are positioned at different heights along the reactor axis at z = 0, 45, 90, 180, 225, and 270 mm (measured from top to bottom). This configuration allows for temperature measurements at multiple points within the cylinder.

A total of 2340 g of a 3.6/96.4 wt% charcoal/sand mixture were put into the combustion cell. The sand particles were classified into three size ranges: 315–500 µm, 500–1000 µm, and 1–2 mm. The charcoal particles were ground to sizes between 500–1000 µm. To ensure a homogeneous mixture, the materials were combined using a mortar mixing method. The mixture was initially wetted, thoroughly mixed and then placed in the reactor. Subsequently, it was allowed to dry overnight to remove any residual moisture from the porous bed.

Initially, the dry mixture was heated to 68.2 ºC in an oven. However, for numerical simulation, it is assumed that the porous bed is composed entirely of sand. This simplification is justified based on the design of (Ferreira Martins, 2008), which indicate that sand represents more than 95% of the mixture by mass in the experimental setup. Before heating, the top of the cell was exposed to forced cold air, as illustrated in Figure 1. After that, the porous bed was cooled to ambient temperature, approximately 18 ºC. The governing equations used to simulate this case are described in Section 2.2. Therefore, source terms related to convective heat transfer between the solid and fluid phases are estimated to ensure that the numerical model accurately replicates the experimental conditions. Radial heat losses are also considered in the model like visualized by (Ferreira Martins, 2008) in your tests.

2.2 MODELING AND MATHEMATICAL EQUATIONS

A dimensionless 2D axisymmetric numerical model was developed using COMSOL Multiphysics to simulate a cylindrical reactor with length L and radius r. The reactor is initially filled with a porous material, represented in dimensionless

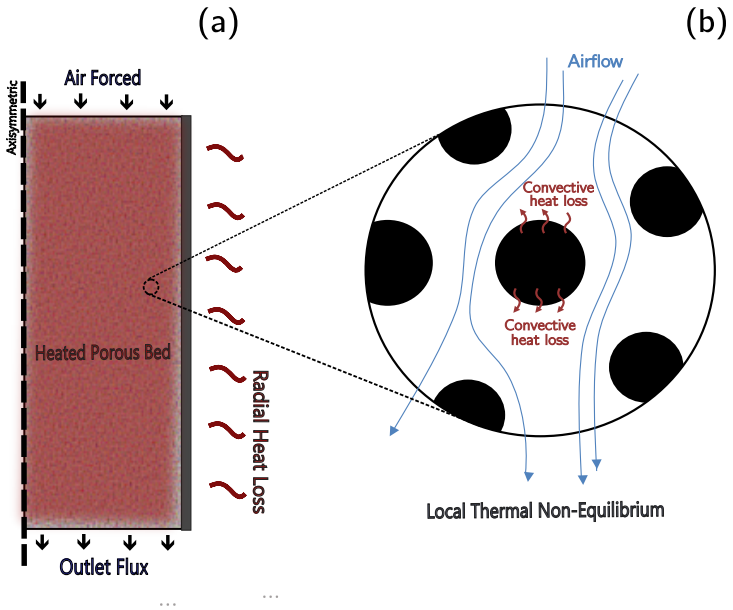

Figure 1. (a) Physical behavior of a vertical cylindrical. (b) Intersticial parameters adopted and heat transfer behavior. Developed by the authors.

cylindrical coordinates (r^*, z^*) as illustrated in Figure 2. Since the model is generic, several parameters can be configured and monitored within the numerical domain, such as the specific mass of the fluid phase, as well as pressure and velocity fields. In this work, the governing equations of mass, momentum, and energy are dimensionless using characteristic scales and dimensionless groups specifically chosen to represent the key physical phenomena of smoldering combustion. As a result, the model can also be applied in a simplified form to simulate the cooling process in a porous bed, since the main physical phenomena involved are more basic but are similar to those found in smoldering combustion. The detailed assumptions and equations that constitute the mathematical model are presented below, while the definitions of the parameters and the subscripts/superscripts can be found in Tab. 1. The porosity is considered constant in both time and space. The conservation of mass for the fluid phase is described by Eq. 1.

$$\varphi m^*_{part} u^*_z \frac{\partial \rho^*_f}{\partial t^*} + \nabla.\left(\rho^*_f \mathbf{u}^*\right) = 0 \tag{1}$$

As discussed in topic 1 of this work, during the smoldering process, air flows through the porous bed. Therefore, it is necessary to apply a mathematical model that accounts for momentum transport in porous media, using the Brinkman equation (Nield *et al.*, 2006), which is an extension of Darcy's law, as expressed in Eq. 2.

$$m^*_{part} u^*_z \frac{\partial \mathbf{U}^*}{\partial t^*} + \left[\left(\mathbf{U}^*.\nabla\right)\mathbf{U}^*\right] = -\nabla p^* + \nabla^2 \mathbf{U}^* - \frac{1}{Da_f}\mathbf{u}^* \tag{2}$$

The specific mass of the fluid phase varies with time and space and is calculated according to the expression presented in its dimensionless form in Eq. 3 (Incropera and De Witt, 1985).

$$\rho^*_f = -3 \cdot 10^{-7} \cdot T^{*3}_f + 0.0001 \cdot T^{*2}_f - 0.0152 \cdot T^*_f + 1 \tag{3}$$

Inside the porous bed layer, the Local Thermal Non-Equilibrium (LTNE) model is applied, with separate energy equations for the fluid phase (Eq. 4) and the solid phase (Eq. 5). As a result, the solid temperature T^*_s differs from the fluid temperature T^*_f. In this case, convective heat transfer predominantly occurs from the solid phase to the fluid phase because the solid is hotter.

$$\varphi m^*_{part} u^*_z \frac{\partial {T_f}^*}{\partial t^*} + \left[\left(\mathbf{u}^*.\nabla\right){T_f}^*\right] = \varphi \frac{1}{Pr}\left(\nabla^2 {T_f}^*\right) + \frac{Nu_{int}}{Pr}\left(T^*_s - T^*_f\right) \tag{4}$$

$$\left(1-\varphi\right) m^*_{part} Pe \frac{\partial {T_s}^*}{\partial t^*} = \left(1-\varphi\right)\left(\nabla^2 {T_s}^*\right) - Bi_{int}\left(T^*_s - T^*_f\right) \tag{5}$$

The interstitial heat transfer coefficient (h_{sg}) between the solid and fluid phases is determined using an empirical Nusselt correlation, where (Nu) appear as a function of Reynolds (Re) and Prandtl (Pr) numbers, as shown in Eq. 6 (Pallares and Grau, 2010). The Reynolds number is associated with a dimensionless parameter proposed in this work, known as the longitudinal dimensionless velocity of the fluid phase (u_z^*).

$$Nu_{int} = 2\left(1 + \frac{4(1-\varphi)}{\varphi}\right) + (1-\varphi)^{0.5}\left(u_z^*\right)^{0.6}\left(Pr\right)^{\frac{1}{3}} = \frac{h_{sg} d_{part}}{\lambda_f} \tag{6}$$

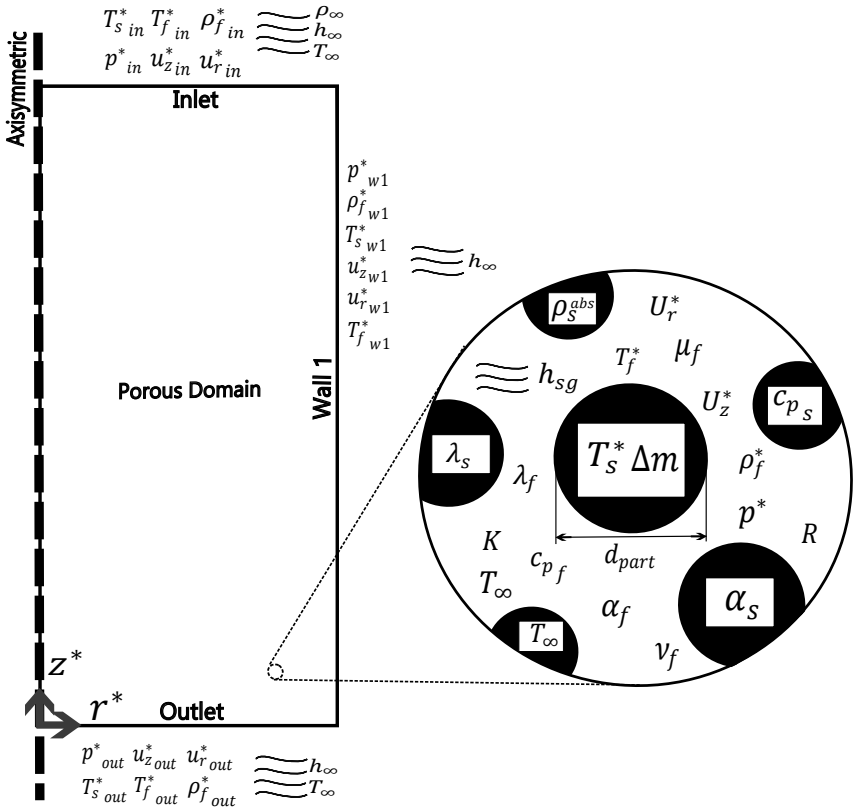

Figure 2. Representation of boundary conditions and crucial parameters involved in the model.
Developed by the authors.

The physical parameters of the model, as shown in the methodology equations, are presented in Figure 2 together with some boundary conditions. The value of numerical input parameters, initial and boundary conditions are summarized in Tab. 2, 3, 4 and 5. In order to highlight the differences between the experimental data and the simulation results, the absolute error observed at each thermocouple was calculated. This approach allows to identify regions where the model behavior significantly deviates from the experimental data and shows that is necessary to provide adjustments to improve the proposed model. The absolute error is calculated using Eq. 7.

$$error_{abs} = \frac{MAX\left(\triangle T_{(t)}\right)}{\left(T_{(t)}\right)} \tag{7}$$

A parameter that is particularly challenging to estimate is the permeability of the sand. However, (Fan *et al.*, 2021) experimentally determined the permeability of calcareous sand using a three-dimensional method and reported values close to 10^{-10} m² for particle sizes ranging between 0.075 and 2 mm. On the basis of this, the same permeability value was adopted for the present simulation. Considering that the particle size distribution used by (Ferreira Martins, 2008) ranges from 0.315 to 2 mm, an average particle size of 0.75 mm was assumed for the numerical model.

Table 2. Numerical model input parameters.

Nomenclature	Describe	Value	Unity	Ref
φ	Porosity of the porous bed	0.47	[1]	Ferreira Martins (2008)
u_z	Longitudinal velocity of fluid	0.0538	$[m/s]$	Ferreira Martins (2008)
ρ_s^{abs}	Specific mass of solid	2200	$[kg/m^3]$	Ferreira Martins (2008)
d_{part}	Particle diameter of solid	0.75	[mm]	Ferreira Martins (2008)
λ_s	Thermal conductivity of solid	0.3	$[W/m.K]$	Ferreira Martins (2008)
c_{p_s}	Specific heat of solid	900	$[J/kg.K]$	Callister Jr and Rethwisch (2020)
ρ_∞	Specific mass of fluid	1.2754	$[kg/m^3]$	Callister Jr and Rethwisch (2020)
K	Permeability of the porous bed	10^{-10}	$[m^2]$	Fan *et al.* (2021)
Δm	Mass variation in the solid	25	$[g]$	Ferreira Martins (2008)
ν_f	Kinematic viscosity of fluid	38.6×10^{-6}	$[m/s]$	Çengel (2007)
μ_f	Dinamic viscosity of fluid	184.6×10^{-7}	$[Pa.s]$	Çengel (2007)
c_{p_f}	Specific heat of fluid	1007	$[J/kg.K]$	Çengel (2007)
λ_f	Thermal conductivity of fluid	26.3×10^{-3}	$[W/m.K]$	Çengel (2007)
T_∞	Ambient temperature	291.15	$[K]$	Ferreira Martins (2008)
α_s	Thermal diffusivity of solid	1.5×10^{-7}	$[m^2/s]$	Callister Jr and Rethwisch (2020)

Table 3. Boundary condition in the numerical simulation.

Nomenclature	Describe	Value
$p^*{}_{in}$	Dimensionless pressure of fluid inlet	non prescribed
u^*_{zin}	Longitudinal dimensionless velocity of fluid inlet	-1.0402
u^*_{rin}	Radial dimensionless velocity of fluid inlet	0
$\rho^*_{f\,in}$	Dimensionless specific mass of fluid inlet	1
$T^*_{f\,in}$	Dimensionless temperature of fluid inlet	0
$T^*_{s\,in}$	Dimensionless temperature of solid inlet	non prescribed
$p^*{}_{out}$	Dimensionless pressure of fluid outlet	0
$u^*_{z\,out}$	Longitudinal dimensionless velocity of fluid outlet	non prescribed
$u^*_{r\,out}$	Radial dimensionless velocity of fluid outlet	non prescribed
$T^*_{f\,out}$	Dimensionless temperature of fluid outlet	0
$T^*_{s\,out}$	Dimensionless temperature of solid outlet	non prescribed
$\rho^*_{f\,out}$	Dimensionless specific mass of fluid outlet	non prescribed
$p^*{}_{w1}$	Dimensionless pressure of fluid wall	non prescribed
$\rho^*_{f\,w1}$	Dimensionless specific mass of fluid Wall	non prescribed
$u^*_{z\,w1}$	Longitudinal dimensionless velocity of fluid wall	0
$u^*_{r\,w1}$	Radial dimensionless velocity of fluid wall	0
$T^*_{f\,w1}$	Dimensionless temperature of fluid wall	non prescribed
$T^*_{s\,w1}$	Dimensionless temperature of solid wall	non prescribed

Table 4. Initial condition in numerical simulation.

Nomenclature	Describe	Value
u^*_z	Longitudinal dimensionless velocity of fluid	-1.0402
u^*_r	Radial dimensionless velocity of fluid	0
ρ^*_f	Dimensionless specific mass of fluid	1
p^*	Dimensionless pressure of fluid	0
T^*_f	Dimensionless temperature of fluid	0
T^*_s	Dimensionless temperature of solid	0.1684
t^*	Dimensionless time	0.0026

Some boundary conditions of heat flux were added to the temperature variable in both phases, based on the study by (Ferreira Martins, 2008), which mentions, for example, heat loss through the walls. In addition, at the inlet and outlet, the solid phase is in contact with cold air and ambient temperature, which increases heat loss in these specific regions. Table 5 presents the locations and mathematical expressions of the heat loss boundaries. Table 6 presents the structure of the dimensionless numbers used in the numerical simulation, along with the specific parameters that compose them. The classical numbers already known from the literature keep their usual meaning. The term m^*_{part} is related to how the flow of mass, momentum and energy changes over time, depending on how much of the solid is burning. It helps show how the mass of a solid particle affects the heating of the different phases as time goes on.

Table 5. Heat flux in the boundary conditions.

Coordinates	Boundary Condition
$r = 0.0455$ and $0 < z < 0.3$	$\begin{cases} -\frac{\partial T_f^*}{\partial r^*} = \frac{Nu_{ext}}{Pr} T_f^* \\ -\frac{\partial T_s^*}{\partial r^*} = Bi_{ext} T_s^* \end{cases}$
$z = 0$ and $0 < r < 0.0455$	$\begin{cases} -\frac{\partial T_s^*}{\partial z^*} = Bi_{ext} T_s^* \end{cases}$
$z = 0.3$ and $0 < r < 0.0455$	$\begin{cases} -\frac{\partial T_s^*}{\partial z^*} = Bi_{ext} T_s^* \end{cases}$

Table 6. Structure of the dimensionless numbers.

Nomenclature	Structure	Describe
t^*	$\frac{t\rho_s^{abs} u_z d_{part}^2}{\Delta m}$	Dimensionless time
m^*_{part}	$\frac{\rho_s^{abs} d_{part}^3}{\Delta m}$	Particle Mass Fraction
Pr	$\frac{\mu_f c_{p_f}}{\lambda_f}$	Prandtl Number
Da_f	$\frac{K}{d_{part}^2}$	Darcy Number
u_z^*	$\frac{u_z d_{part}}{\nu_f}$	Longitudinal dimensionless velocity
Pe	$\frac{u_z d_{part}}{\alpha_s}$	Peclet number
Bi_{ext}	$\frac{h_\infty d_{part}}{\lambda_s}$	External biot number
Bi_{int}	$\frac{h_{sg} d_{part}}{\lambda_s}$	Internal biot number
Nu_{ext}	$\frac{h_\infty d_{part}}{\lambda_f}$	External nusselt number
Nu_{int}	$\frac{h_{sg} d_{part}}{\lambda_f}$	Internal nusselt number

3. RESULTS AND DISCUSS

The temperatures measured by the thermocouples in the experimental study by (Ferreira Martins, 2008) closely approximate the solid-phase temperature in this numerical simulation. Figure 3 illustrates the comparison and highlights the approximate maximum error observed at a specific time step for each thermocouple evaluated. It is believed that since the mixture was prepared following the method described by (Ferreira Martins, 2008) using water to form a conglomerate of charcoal and sand, some residual moisture may have remained in the interstitial spaces of the porous bed after drying overnight.

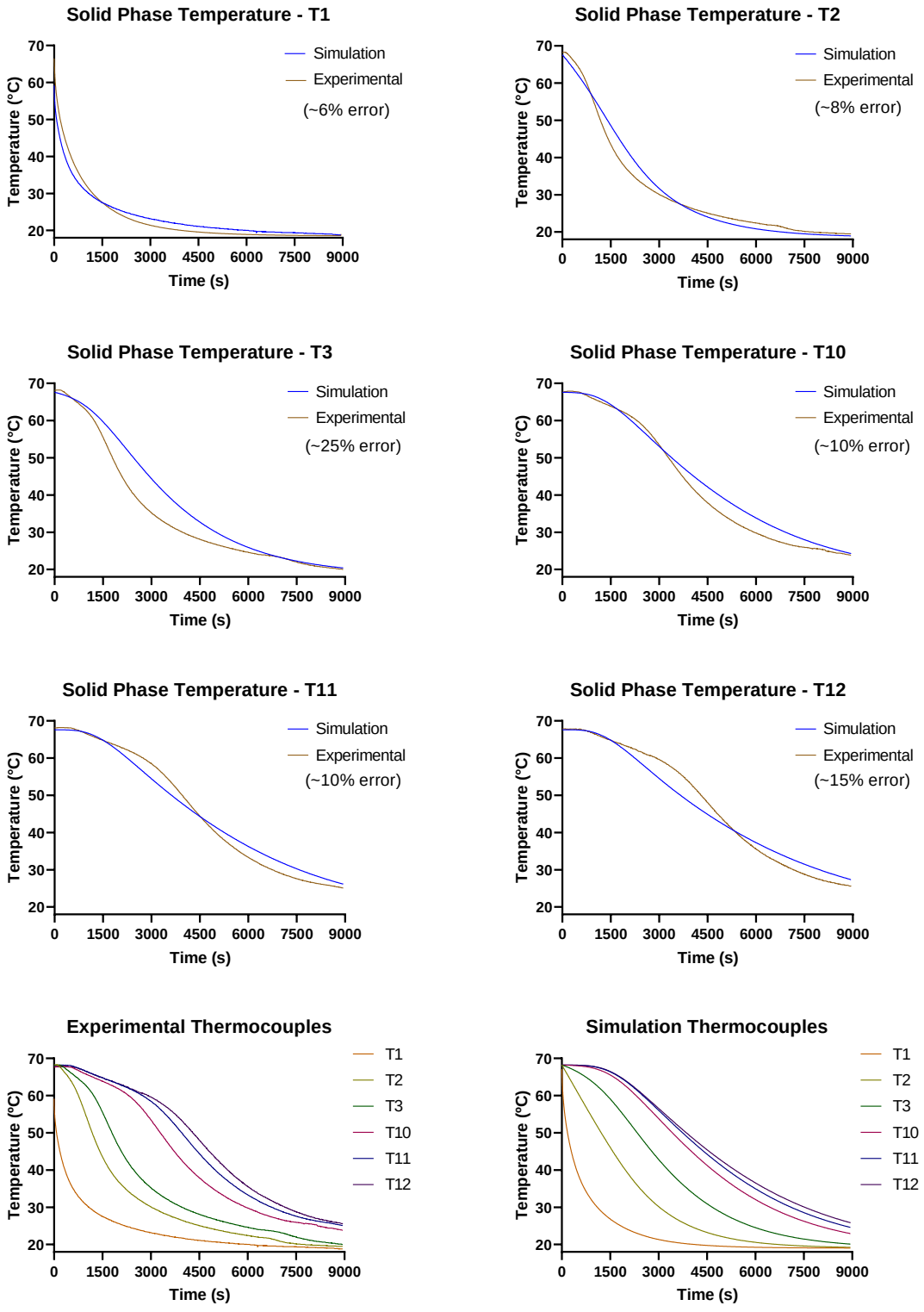

Figure 3. Comparison between a experimental test and simulation propose in the Section 2.2. Developed by the authors.

This effect is likely to occur near the middle and lower of the reactor, where the airflow that percolates the porous bed during overnight drying was less intense. This hypothesis is supported by the fact that the thermocouples T3 and T12 exhibited a temperature difference of approximately 25% and 15%, respectively. Thus, the model is expected to perform

better near the upper regions of the reactor, where errors are smaller compared to the central and lower zones of the porous bed. Evaporation by mass transport probably occurred in reality but was not considered in the simulation, which explains part of this discrepancy. This evaporation likely intensified the cooling process, and as a result, some model parameters needed to be adjusted to achieve better agreement with the experimental observations.

The most portions of the dimensionless equations and some boundary conditions of flux were adjusted up or down based on trends observed in the experimental data. This means that terms like the Nusselt number (Nu) and Biot number (Bi) were changed and calibrated to help validate the numerical simulation. After these adjustments, the calibrated parameters resulted in interstitial and external heat transfer coefficients of about 694 – 2,140 [kW/m².K] and 0.024 – 20 [kW/m².K], respectively. For comparison, the interstitial convective heat transfer coefficient reported by (Ferreira Martins, 2008) in a numerical simulation involving oil shale was around 544 [kW/m².K], which is within the same order of magnitude as the range obtained in this study. The author did not measure the values for the external convective heat transfer coefficient, which prevents a direct comparison. However, the values obtained in the present work are consistent with those typically found in simulations involving porous media. It is noticeable that the heat transfer coefficients are high, but in porous media systems, this is possible because the large interstitial surface area, which enables efficient heat transfer between the fluid and the solid structure. It is also important to mention that the temperatures of both phases remained closed throughout the simulation, even though a LTNE approach was used.

The author (Ferreira Martins, 2008) imposed a velocity flux of 0.0538 [m/s] at the top of the cylinder during the test. However, the numerical simulation showed a velocity range of 0.035 - 0 [m/s] inside the porous medium, with values equal to zero near the wall and a little small when compared with the flux imposed at the top. The values founded are coherent and expected because the packed particles create resistance to the flow that depending on the permeability of bed. As mentioned before, to validate the simulation, certain portions of the equations were adjusted, and ultimately their term magnitudes were defined as shown in Tab. 7. The most sensitive parts adjusted were related to the energy conservation equation for the solid phase and its heat loss to the boundaries. Some alterations implemented and some behaviors visualized can be cited: the transient term in the solid phase energy equation is related to the thermal inertia of the solid during cooling, and its value was raised, if this value is increased, it becomes more difficult for the solid to cool down and reach ambient temperature; the diffusion term affects how close the cooling curves measured by each thermocouple are to each other; the value of the source term is associated with the cooling rate of the solid phase over time, and a higher value leads to faster cooling; the heat loss of the solid phase in the upper and lower zones of the reactor influences the initial slope of the cooling curve for each thermocouple; the heat loss terms through the reactor wall, for both the fluid and solid phases, affect the intermediate slope of the cooling curves. The other portions were modified to a lesser extent, but they still play an important role in calibrating of the thermal cooling.

Table 7. Term's magnitudes present in the different portions of the equations.

Describe	Structure	Order of magnitude
Transient portion of solid phase energy equation	$\big(1-\varphi\big)m^*_{part}Pe\frac{\partial {T_s}^*}{\partial t^*}$	10^4
Diffusivity portion of solid phase energy equation	$\big(1-\varphi\big)\big(\nabla^2 {T_s}^*\big)$	10^{-1}
Source term portion of solid phase energy equation	$Bi_{int}\big(T^*_s - T^*_f\big)$	10^3
Transient portion of fluid phase energy equation	$\varphi m^*_{part}u^*_z\frac{\partial {T_f}^*}{\partial t^*}$	10^1
Advective transport portion of fluid phase energy equation	$\big(\mathbf{u}^*.\nabla\big){T_f}^*$	10^2
Diffusivity portion of fluid phase energy equation	$\varphi\frac{1}{Pr}\big(\nabla^2 {T_f}^*\big)$	10^0
Source term portion of fluid phase energy equation	$\frac{Nu_{int}}{Pr}\big(T^*_s - T^*_f\big)$	10^4
Heat loss of the solid phase in the reactor wall	$Bi_{ext}T^*_s$	10^1
Heat loss of the solid phase through in the reactor top	$Bi_{ext}T^*_s$	10^1
Heat loss of the solid phase through in the reactor bottom	$Bi_{ext}T^*_s$	10^0
Heat loss of the fluid phase through the reactor wall	$\frac{Nu_{ext}}{Pr}T^*_f$	10^{-2}

4. CONCLUSIONS

This work developed and validated a numerical model able to simulate the cooling process in a porous bed. The results from the simulation matched the experimental temperatures well at the top parts of the reactor. However, in the middle and lower region, there were some noticeable differences. To improve the match between the model and the real data, some portions of the equations and boundary condition of flux were adjusted. The changes helped the model better follow the cooling behavior seen in the experiment and allowed the visualization of how each portion of some equations affects the behavior of cooling curves. Even though the model used some simplifications, like ignoring moisture evaporation and treating the mixture as pure sand, it still had good results. The model is now better suited for future studies of smoldering combustion and other heat transfer processes in porous materials. Adding effects like evaporation will make it even more accurate in the future.

5. ACKNOWLEDGEMENTS

We gratefully acknowledge Prof. Márcio Ferreria Martins for providing the laboratory facilities and equipment used in this study at Federal University of Espirito Santo. We also thank Prof. Flávio Lopes Francisco Bittercourt from Federal Institute of Espirito Santo for assistance with the numerical simulations. The authors declare no conflict of interest related to this work.

6. REFERENCES

Bittencourt, F.L.F., 2023. *TOWARD A SAFE AND CIRCULAR THERMOCHEMICAL PROCESS TO SANITIZE HUMAN FECES IN RESOURCE-POOR ENVIRONMENTS*. Ph.D. thesis, Universidade Federal do Espírito Santo.

Bittencourt, Flávio Lopes Francisco, G.D. and Martins., M.F., 2022. "Free convection development caused by bed shrinkage in a vacuum-induced smoldering reactor". *Chemical Engineering Journal*, Vol. 430, p. 132847.

Callister Jr, W.D. and Rethwisch, D.G., 2020. *Materials science and engineering: an introduction*. John wiley & sons.

Fan, Z., Hu, C., Zhu, Q., Jia, Y., Zuo, D. and Duan, Z., 2021. "Three-dimensional pore characteristics and permeability properties of calcareous sand with different particle sizes".

Ferreira Martins, M., 2008. *Structure d'un front de combustion propagé en co-courant dans un lit fixe de schiste bitumineux broyé*. Ph.D. thesis, Diss. Toulouse.

Gan, Z., Zhao, C., Li, Y., Chen, G., Song, Z., Zhang, Z. and Ran, W., 2022. "Experimental investigation on smoldering combustion for oil sludge treatment: Influence of key parameters and product analysis". *Fuel*, Vol. 316, p. 123354. ISSN 0016-2361. doi:https://doi.org/10.1016/j.fuel.2022.123354. URL https://www.sciencedirect.com/science/article/pii/S001623612200223X.

Incropera, F.P. and De Witt, D.P., 1985. "Fundamentals of heat and mass transfer".

Miry, S.Z., Zanoni, M.A., Rashwan, T.L., Torero, J.L. and Gerhard, J.I., 2022. "Investigation of multi-dimensional transfer effects in applied smouldering systems: A 2d numerical modelling approach". *Combustion and Flame*, Vol. 246, p. 112385. ISSN 0010-2180. doi:https://doi.org/10.1016/j.combustflame.2022.112385. URL https://www.sciencedirect.com/science/article/pii/S001021802200400X.

Nield, D.A., Bejan, A. *et al.*, 2006. *Convection in porous media*, Vol. 3. Springer.

Pallares, J. and Grau, F., 2010. "A modification of a nusselt number correlation for forced convection in porous media". *International Communications in Heat and Mass Transfer*, Vol. 37, No. 9, pp. 1187–1190. ISSN 0735-1933. doi:https://doi.org/10.1016/j.icheatmasstransfer.2010.07.014. URL https://www.sciencedirect.com/science/article/pii/S0735193310001788.

Torero, José L., e.a., 2020. "Processes defining smouldering combustion: Integrated review and synthesis". *Progress in Energy and Combustion Science*, Vol. 81, p. 100869.

Wakao, S. Kaguei, N., 1982. "Heat and mass transfer in packed beds". *Gordon and Breach Science Publishers*, p. 292–294. ISSN 0017-9310. doi:https://doi.org/10.1002/aic.690010211. URL https://aiche.onlinelibrary.wiley.com/doi/abs/10.1002/aic.690010211.

Zanoni, M.A., Torero, J.L. and Gerhard, J.I., 2019. "Delineating and explaining the limits of self-sustained smouldering combustion". *Combustion and Flame*, Vol. 201, pp. 78–92. ISSN 0010-2180. doi:https://doi.org/10.1016/j.combustflame.2018.12.004. URL https://www.sciencedirect.com/science/article/pii/S0010218018305212.

Zhao, C., Li, Y., Gan, Z. and Nie, M., 2021. "Method of smoldering combustion for refinery oil sludge treatment". *Journal of Hazardous Materials*, Vol. 409, p. 124995. ISSN 0304-3894. doi:https://doi.org/10.1016/j.jhazmat.2020.124995. URL https://www.sciencedirect.com/science/article/pii/S0304389420329861.

Çengel, Y.A. e Cimbala, J., 2007. *Mecânica dos Fluidos - Fundamentos e Aplicações*. McGraw-Hill Interamericana do Brasil Ltda, Brazil.

7. RESPONSIBILITY NOTICE

The authors declares that they are solely responsible for the content and accuracy of the information presented in this paper. The authors also affirms that the work complies with ethical standards and that any necessary permissions for data or material usage have been obtained.

A.3 Technical visit at The Open University

My academic trip to Milton Keynes, United Kingdom, provided an important opportunity to get to know the scientific environment of The Open University (OU), an institution internationally recognized for its excellence in teaching and research. I arrived on April 29, 2025, and, after settling in, began my activities at the university the next day.

Figure A.1: Main entrance of The Open University.

The first academic contact was with Professor Tarek Rashwan and his PhD student Fatemah, who welcomed me and introduced the main research directions of their group and important necessary procedures at The Open University and bureaucracies. This initial meeting allowed us to exchange ideas, outline possibilities for future scientific collaboration, and share social experiences while mixing cultures between Brazil and England.

Figure A.2: First contact and casual discussion.

The next day, i made a presentation of my master's research project developed at the Federal University of Espírito Santo (UFES), Vitória, Brazil. The presentation highlighted the theoretical and methodological aspects of my work, especially the numerical simulations focused on smoldering combustion. This was an important moment of scientific exchange, as it allowed me not only to share the progress achieved so far but also to receive critical feedback and valuable suggestions for improvement.

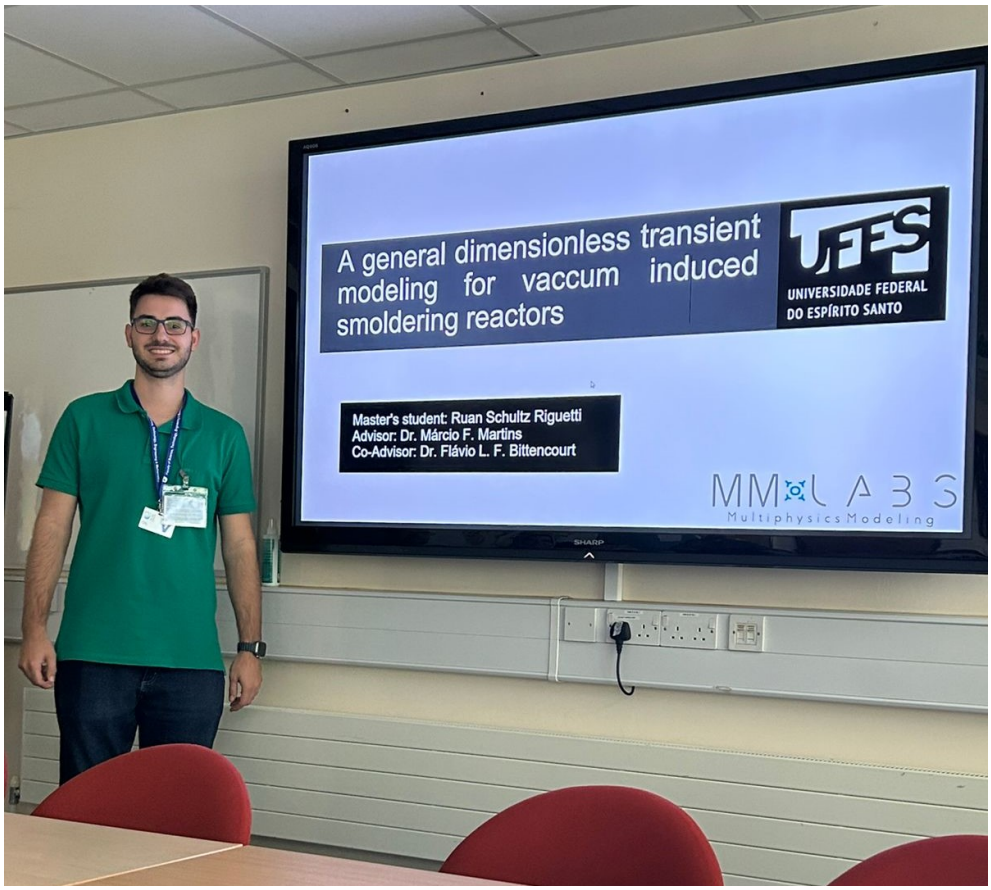

Figure A.3: Presentation of my dissertation theme.

In the following days, technical and scientific meetings were held dedicated to discussions on computational physical modeling applied to my study

area. These meetings were productive, focusing on the numerical methods employed, the potential limitations of the current approach, and the possible considerations adopted that could affect the simulations. The discussions helped me identify aspects that required adjustments and also pointed to alternative strategies that could improve the quality of the results.

Figure A.4: Focused technical meetings on smoldering combustion.

Working with Tarek Rashwan also enabled me to make concrete progress in numerical simulation. This was a key step in strengthening the scientific consistency of my research and my understanding of the topic.

Figure A.5: Particular technical meetings focused on smoldering combustion with Tarek Rashwan.

During my stay, I was also able to experience daily common life at The Open University, including the use of casual spaces and meals at the university restaurant. These simple experiences contributed to a better connection with the academic community and created opportunities for more informal interactions. In general, my stay at The Open University was an enriching academic experience. It combined scientific exchange, practical learning opportunities, and cultural integration. This experience confirmed the importance of academic mobility as a fundamental element in the formation of researchers, opening new institutional perspectives for the development of my master's research.

Figure A.6: Engineering Department – location of meetings and study activities.